AN ABSTRACT OF THE THESIS OF

ROBERTA CONARD for the degree of MASTER OF SCIENCE

in Chemistry presented on July 16, 1976

Title: A STUDY OF THE CHEMICAL COMPOSITION OF CA-AL-RICH INCLUSIONS FROM THE ALLENDE METEORITE

Abstract approved: Redacted for Privacy
Roman A. Schmitt

Nine Ca-Al-rich inclusions and one olivine inclusion from Allende meteorite were studied for Ti, Al, Fe, Mg, Ca, Na, Cl, K, Sc, V, Cr, Mn, Co, Ni, Zn, Hf, W, Ir, Au, Ta, and Re via INAA (instrumental neutron activation analysis) and REE, Ba, Sr via RNAA (radiochemical NAA). The inclusions were classified according to the scheme of Martin and Mason (1974). It was found that Group I inclusions have lower volatile element content (Na, K, Zn, Cl, Mn and Fe) and light REE and higher refractory element content than Group II inclusions. Group III inclusions are intermediate between Group I and Group II. The siderophile elements Ir and Re are correlated; W does not correlate with Ir and from thermodynamic calculations, W is predicted to condense as WO_2 at 1380°K instead of the metallic form at higher temperatures.

The Ca-Al-rich inclusions exhibit the REE patterns defined by Martin and Mason (1974). Group I is flat and

10-12X chondrites. Also classified in this group is an inclusion (A-2) with depleted Gd to Er and Lu relative to the rest of the REE. Group II contains patterns with flat light REE and severely fractionated heavy REE with positive Tm and Yb anomalies relative to their neighboring Er and Lu but normal Tm relative to La-Sm. The element Tm correlates with Ta along the line defined by cosmic ratios. Group III shows flat REE patterns with negative Eu and Yb anomalies. A new REE pattern has been found with a negative Ce anomaly in an inclusion, tentatively classified as a Group I inclusion. The approximate character of the REE patterns of Group II and III may be predicted from thermodynamic calculations.

All of the inclusions studied have covariant Eu and Sr abundances which are nearly equal on a chondritic normalized basis, suggesting extensive divalent behavior of Eu. All the fractionated patterns observed have nearly equal chondritic normalized Eu and Yb which is unexpected and not predicted from thermodynamic calculations. The REE patterns observed appear to support gaseous condensation models and demonstrate the complex nature of their origin.

A Study of the Chemical Composition of Ca-Al-rich Inclusions from the Allende Meteorite

by

Roberta Conard

A THESIS

submitted to

Oregon State University

in partial fulfillment of
the requirements for the
degree of

Master of Science

Completed July 16, 1976

Commencement June, 1977

APPROVED:

Redacted for Privacy

Professor of Chemistry
in charge of major

Redacted for Privacy

Chairman of the Department of Chemistry

Redacted for Privacy

Dean of Graduate School

Date thesis is presented July 16, 1976

Typed by Deanna L. Cramer for Roberta Conard

Dedicated to my parents, who taught
"there is no such word as can't."

ACKNOWLEDGEMENTS

I wish to express my appreciation to my major professor, Dr. R. A. Schmitt, for his encouragement and financial support without which I could never have completed this work. The many discussions with him and with Dr. W.V. Boynton greatly improved the quality of this manuscript.

I am grateful to Prof. G.J. Wasserburg for providing precious Allende inclusions for analysis.

Dr. Patricia Starzyk and Dr. J.C. Laul provided great assistance in the radiochemical separations. The reactor personnel, particularly T.V. Anderson and Bill Carpenter, spent hours at the console during sample irradiations; Steve Bennett and the rest of the radiation safety staff provided assistance in the safety aspects of the work. I am also grateful to Vern Smith who always knows where to find anything that's missing and to Doyle Woodrow who spent many hours keeping the temperamental ND 3300 in working condition.

I especially want to thank Andy Ungerer for his sense of humor and for all the assistance he provided during the course of this work.

TABLE OF CONTENTS

LIST OF TABLES

LIST OF FIGURES

A STUDY OF THE CHEMICAL COMPOSITION OF CA-AL-RICH INCLUSIONS FROM THE ALLENDE METEORITE

INTRODUCTION

The Allende meteorite has attracted considerable attention since its spectacular fall in February, 1969. Recovery of about two tons of meteorite pieces established Allende as the largest stony meteorite shower ever recorded (Clarke et al., 1970).

The large amount of material available prompted the suggestion that bulk Allende would be a good interlab comparison standard when powdered and homogenized (Morgan et al., 1969). In hindsight, the wisdom of this idea could be questioned because the meteorite is particularly heterogeneous: about 57 percent matrix (mostly Fe rich olivine), about 34 percent chondrules (Mg or Ca-Al-rich), and about 9 percent aggregates (also Ca-Al-rich) with very little Fe in the free metallic state (Clarke et al., 1970). Interest in the Allende inclusions, particularly the Ca-Al-rich chondrules and aggregates, was sparked by the observation of Marvin et al. (1970) that they possessed a mineralogy and chemistry remarkably similar to that postulated for an early high temperature condensate from a gas of solar composition (Lord, 1965; Larimer, 1967). Recently, more complete thermodynamic condensation sequences have been

published (Grossman, 1972, 1973; Boynton, 1975), as have numerous chemical and mineralogical analyses of the Ca-Al-rich inclusions.

Since each author devised his own classification scheme, it is worthwhile to review their nomenclature in order to understand when each is discussing the same type of inclusion.

Allende has four major components (matrix, chondrules, irregular aggregates, and dark inclusions) according to Clarke et al. (1970). Chondrules are spherical and either Mg-rich or Ca-Al-rich in chemical composition. The Mg-rich chondrules have different textures of olivine or pyroxene.[1] The Ca-Al-rich chondrules' mineralogy is a) gehlenite-fassaite-anorthite-spinel, b) anorthite-forsterite-spinel, and c) nepheline-sodalite-fassaite-olivine. The Ca-Al-rich chondrules Type a and b are coarse-grained; the Type c chondrules are very fine-grained. The aggregates are also Ca-Al-rich with compositions similar to Type a chondrules but with occasional nepheline and sodalite.

Gray et al. (1973) also classified the inclusions into chondrules and aggregates. The chondrules are relatively rare, discrete objects of rounded or subrounded form, 3-20 mm in size. The aggregates are more abundant, irregular shaped with variable dimensions (microscopic to 10 mm) and

---

[1]Chemical formulae of the minerals mentioned are given in Table 1.

Table 1. Chemical composition of minerals referred to in text.[a]

Clinopyroxene	
Ti-pyroxene	$CaTiAl_2O_6$
Ca-Al pyroxene	$CaAl_2SiO_6$
Diopside	$CaMgSi_2O_6$
Fassaite	$Ca(Mg,Al,Ti)(Al,Si)_2O_6$
Melilite	
Gehlenite	$Ca_2Al_2SiO_7$
Åkermanite	$Ca_2MgSi_2O_7$
Sodamelilite	$NaCaAlSi_2O_7$
Olivine	
Forsterite	Mg_2SiO_4
Fayalite	Fe_2SiO_4
Plagioclase	
Anorthite	$CaAl_2Si_2O_8$
Albite	$NaAlSi_3O_8$
Grossular	$Ca_3Al_2Si_3O_{12}$
Hibonite	$CaAl_{12}O_{19}$
Nepheline	$NaAlSiO_4$
Perovskite	$CaTiO_3$
Sodalite	$Na_4Al_3Si_3O_7Cl$
Spinel	$MgAl_2O_4$
Wollastonite	$CaSiO_3$

[a]Based on Table 1 in Grossman and Clark (1973).

a pasty appearance. The chondrules contain millimeter size crystals while the aggregates are very fine grained. The chondrules are subdivided into Ca-Al-rich or pyroxene or olivine with mineralogies to match. The Ca-Al-rich chondrules are composed of high temperature minerals: melilite, fassaite, anorthite, and spinel or just melilite. The olivine chondrules range from Fo_{67} to Fo_{98}. In contrast, the aggregates' mineralogy is spinel, hibonite, pervoskite, gehlenite, anorthite, wollastonite (high temperature phases) joined with sodalite and nepheline. The aggregates are further divided into low-Rb (~1 ppm) or high-Rb (~10 ppm). The low-Rb aggregates have lower Na, K, Fe, and higher Al contents and although fine-grained, are not as fine-grained as the high-Rb aggregates.

Martin and Mason (1974) recognized four distinct groups of inclusions: Group I, melilite-rich chondrules with a mineralogy of melilite, Ti-rich fassaite, spinel, and anorthite; Group II, Ca-Al-rich aggregates with fractionated chondritic-normalized rare earth element (REE) patterns; Group III, Ca-Al-rich aggregates with negative Eu and Yb anomalies in the REE patterns; Group IV, olivine-rich chondrules and aggregates. Groups II and III have similar mineralogies (spinel, fassaite, melilite, occasionally grossular, minor amounts of nepheline and sodalite) and are divided on the basis of trace element abundances.

Instead of chondrules and aggregates, Grossman and Ganapathy (1975) divided the Ca-Al-rich inclusions into coarse and fine-grained inclusions. The coarse-grained inclusions have a mineralogy of melilite, spinel, perovskite, Ti-pyroxene, and anorthite which is roughly equivalent to Gray's chondrules. The mineralogy of the fine-grained inclusions of nepheline, sodalite, grossular, spinel, and pyroxene also roughly corresponds to Gray's aggregates. Unfortunately, at this point Grossman and Ganapathy compared their classification scheme with that of Gray and decided that Gray's low-Rb aggregate is coarse-grained instead of the fine-grained classification expected if chondrules correspond to coarse-grained and aggregates correspond to fine-grained. Thus, it appears that there are some intermediate inclusions which could belong in either category. Grossman (1975) further classifies the coarse-grained inclusions into Type A or Type B in which the "fundamental difference is in the abundance, morphology, and composition of the clinopyroxene." The pyroxene in Type B inclusions contains >15 percent Al_2O_3 and >1.8 percent TiO_2 while the Type A inclusions have <9 percent Al_2O_3 and <0.7 percent TiO_2. Type B pyroxenes are coarse crystals; Type A pyroxenes occur in bands 1.5 μm wide. These Ti-rich pyroxenes are termed fassaite in Gray et al. (1973) and Martin and Mason (1974). The major mineralogy of Type A inclusions is 80-85 percent melilite, 15-20

percent spinel, and 1-2 percent perovskite, while Type B is 30-60 percent clinopyroxene, 15-30 percent spinel, 5-25 percent plagioclase, and 5-20 percent melilite.

A classification based on mineralogy was proposed by Blander and Fuchs (1975). They designated the inclusions containing hibonite as h, those without olivine or hibonite but containing fassaite as f, those with both olivine and fassaite as o, and those with nepheline or other feldspathoids as n.

It appears that Ca-Al-rich chondrules (excluding Type c of Clarke et al., 1970), Type A and B coarse-grained inclusions and h and f type inclusions are subspecies all of which are included in Group I chondrules. Aggregates, fine-grained inclusions, or n type inclusions all appear to be synonyms of a general category for Group II or Group III and high- or low-Rb aggregates. However, a Group II aggregate does not necessarily imply that it is also a high-Rb aggregate or that a Group III aggregate in a low-Rb aggregate. Group IV, olivine chondrules and aggregates and o type inclusions are the same and are referred to by Grossman and Steele (1976) who also designated the Type c chondrules of Clarke et al. (1970) as olivine aggregates. Grossman and Steele (1976) distinguished between olivine chondrules and aggregates; here no distinction will be made between them. In this paper coarse-grained inclusions and chondrules will be used interchangeably as will fine-

grained inclusions and aggregates. A summary of the various names for each type of inclusion is provided in Table 2.

At first, it was postulated that all of the Ca-Al-rich inclusions were the high-temperature condensates that could have originally condensed from a solar nebula. As more of the inclusions were studied, it became apparent that their mineralogies and trace element distributions differed, falling into two broad categories (chondrules or aggregates). The Type A inclusions are the only inclusions which possess the same mineralogy as the theoretical high temperature condensate (Grossman, 1975), while the other chondrules and aggregates of Allende appear to have a more complex history (e.g., Grossman and Ganapathy, 1976a).

Rb-Sr dating of the Bulk Allende gives a model age of $4.56 \pm 0.03 \times 10^9$ y (Gray et al., 1973). The high Rb/Sr ratio of Allende bulk is similar to that of ordinary chondrites, but some of the Allende Rb-poor aggregates have the most primitive $^{87}Sr/^{86}Sr$ ratios yet observed. Therefore, they are inferred to be some of the oldest objects available for study. The Rb-Sr isotope data are variable from inclusion to inclusion; within an inclusion two different samples will also give different initial $^{87}Sr/^{86}Sr$ ratios. The inclusions do not define an isochron, thus showing the Rb-Sr isotopic system has been

Table 2. Summary of classifications of Allende inclusions.

Gray et al. (1973)	Olivine	Chondrules: Pyroxene	Chondrules: Ca-Al rich	Aggregates: Low-Rb	Aggregates: High-Rb
Grossman (1975)	Olivine Aggregates	Coarse-Grained Inclusions		Fine-Grained Inclusions	
Grossman and Ganapathy (1975)		Type B	Type A		
Grossman and Steele (1976)					
Martin and Mason (1974)	Group IV	Chondrules:	Group I	Aggregates: Group II	Group III
Clarke et al. (1970)	Mg-Rich Type c	Chondrules: Type a	Type b	Aggregates	
Blander and Fuchs (1975)	o	f	h	n	

disturbed sometime between the present and 3.59×10^9 y ago (Gray et al., 1973). That this disturbance would have had to be mild is attested to by the narrow range of oxygen isotopic variations found by Clayton et al. (1973).

Understanding how these ancient inclusions formed should lead to new understanding of the chemical history of the early solar nebula. Many models have been introduced to explain their formation: chondrules are solidified liquid droplets (e.g., Blander and Fuchs, 1976); inclusions (especially aggregates) condensed directly from gas to solid (Grossman et al., 1975); chondrules are early high temperature solar condensates, while aggregates condensed at a lower temperature and include residual high temperature elements (Grossman and Ganapathy, 1976b); and chondrules and aggregates are evaporation residues (Chou et al., 1976).

One of the models which appears to have much promise is that envisioned by Martin (1976). He suggests that a collision between two large bodies (one of them a comet) will release enough energy to vaporize substantial amounts of material to form a gas of solar composition. Rapid cooling under higher pressures causes the chondrules to condense from gas to liquid to crystalline solids. The fine-grained inclusions would then condense in regions of lower pressure directly from the gaseous to solid state.

The model must be constrained to fit the oxygen isotopic anomalies found in mineral separates of coarse-grained inclusions (Onuma, et al., 1974). The complete melting (or vaporization) of the colliding bodies cannot take place or the oxygen isotopes will be homogonized. Nagasawa et al. (1976) suggest that pre-existing spinel and pyroxene with oxygen isotope anomalies condensed with melilite in a cooling sequence too fast for isotope equilibration.

The purpose of this work is to determine the major and trace elemental compositions, particularly the REE, of some chondrules and aggregates that have already been dated in order to search for correlations between unique chemical fractionation patterns and their ages and to search for any new and unique REE patterns whose interpretation might lead to insights into the very early history of condensation in the primeval solar nebula. A side interest in the REE determinations is to look for significant Sm/Nd fractionations relative to chondrites. If such fractionations are observed, then it may be possible to use the reaction

$$^{147}Sm \dashrightarrow \alpha + {}^{143}Nd \quad (t_{1/2} = 1.08 \times 10^{11}\ y)$$

as a new geochronometer for estimating lithophile element fractionation times (Lugmair, 1974; Lugmair et al., 1975).

EXPERIMENTAL

The Allende inclusions (except I-3 and I-8) were obtained from Prof. G. J. Wasserburg of the Division of Geological and Planetary Sciences, California Institute of Technology. Sample designations in this work correspond to those in Gray et al. (1973) who analyzed portions of the same inclusions. With the exception of B-32, the inclusions were transferred and sealed into small clean polyethylene vials and not handled further. Minimum handling and transfer was dictated by the extremely small sample sizes which ranged from 6 to 40 mg and averaged 15 mg. Two hand separations of B-32 into light and dark portions were made after lightly crushing in an agate mortar. Estimates of cross-contamination in the first separate of less than five percent light in the dark portion and less than one percent dark in the light portion were determined by inspection under a microscope. Cross-contamination estimates for the second separate are ten percent light in dark and five percent dark in white. Thus the first separate appears to be of better quality. The pink aggregates, I-3 and I-8, were obtained by and analyzed with Dr. W. V. Boynton who obtained them from Dr. T. W. Osborn III. The Allende bulk samples were from NMNH #3496 which had been crushed by Dr. H. Wakita some years before. The Melilite sample was separated by Dr. Nagasawa of Gakushuin

University, Tokyo, for trace element analysis. In addition to the Allende samples, the U.S.G.S. standard rocks BCR-1, PCC-1, and CRB-1 (in house standard BCR basalt) were analyzed to provide internal checks. The chondritic normalization abundances were checked using duplicate analyses of the L-6 chondrite, Leedey.

The Allende samples were divided into two sets to be analyzed via neutron activation analysis (NAA). The INAA (instrumental neutron activation analysis) procedure is a modification of that used by Curtis (1974). The first analysis was an activation for short-lived radionuclides (Table 3). The samples were individually loaded into the Oregon State University TRIGA Reactor (Flux = 5×10^{12} n/cm^2/sec--500 kW) via the pneumatic terminal (rabbit system) for four minutes each. After a fifteen minute decay period, each sample was counted for 400 seconds using a high resolution Ge(Li) detector coupled to a 4096 channel analyzer. The long decay period was necessary to allow the large amount of 2.3 m ^{28}Al to decay away so that other radionuclides could be measured.

Table 3 also lists interferences caused by the fast neutron flux of the TRIGA reactor. Corrections are as follows:

$$100\%\ SiO_2 \equiv 0.56\%\ Al_2O_3$$

$$100\%\ Al_2O_3 \equiv 26\%\ MgO$$

Table 3. Elements obtained from the short activations ("rabbit run").

Radionuclide	Half-life[a]	Gamma-ray Energy (keV)	Interferences
^{28}Al	2.31 m	1778.7	$^{28}Si(n,p)^{28}Al$
^{52}V	3.75 m	1434.3	
^{51}Ti	5.79 m	320.0	
^{49}Ca	8.8 m	3084.4	
^{27}Mg	9.46 m	1014.5	$^{27}Al(n,p)^{27}Mg$
^{38}Cl	37.3 m	1642.7	
^{59}Mn	2.58 h	1811.1	
^{24}Na	15.0 h	1368.7	$^{27}Al(n,\alpha)^{24}Na$; $^{24}Mg(n,p)^{24}Na$

[a]Half-lives and energies of radionuclides were taken from Filby et al. (1970).

$$100\%\ Al_2O_3 \equiv 400\ ppm\ Na_2O$$

$$100\%\ MgO \equiv 530\ ppm\ Na_2O$$

Importance of the correction varies; in cases of high Al and low Mg, the correction may be as high as 60 percent. Generally, the Si contribution to Al in the Allende inclusions was estimated to be less than one percent; for the bulk sample, Si contributed about six percent of the ^{28}Al. Correction for Al contributed to Mg varied from three percent in the whole rock to sixty percent in the Melilite sample with the inclusions averaging fifty percent. The contribution of Mg to Na was small, from one to three percent. Contribution of Al to Na was significant in some cases, i.e. twenty percent in Melilite. Generally, however, the correction was less than five percent.

Chlorine was measured in the second rabbit run only, since the first set of samples had been destroyed (radiochemical neutron activation analysis) before it was realized that Cl was present in measurable concentrations.

Following the short-lived activations, the samples and appropriate standards were placed in the rotating rack of the OSU TRIGA Reactor for a six hour activation at a flux of 3×10^{12} $n/cm^2/sec$. Samples and standards were allowed to decay overnight before sequential counting was commenced for the various radionuclides listed in Table 4. A 4096 channel analyzer coupled to a high resolution right angle Ge(Li) detector was used which was calibrated at

Table 4. Elements obtained from the long activations.

Radionuclide	Half-life	Gamma-ray Energy (keV)	Interference
Count #1. 1-2 days decay. Count length about 160 minutes.			
^{152m}Eu	9.3 h	121.8	^{152}Eu (121.8 keV)
^{42}K	12.4 h	1524.7	
^{69m}Zn	14.1 h	439.1	
^{24}Na	15.0 h	1368.4	
^{188}Re	16.7 h	155.0	
Count #2. 3-4 days decay. Count length 200-400 minutes.			
^{187}W	23.9 h	685.7	
^{140}La	40.2 h	1596.6	
^{153}Sm	46.8 h	103.2	
^{198}Au	64.7 h	411.8	
Count #3. Approximately 1 week decay. Count length 400-800 minutes.			
^{175}Yb	101 h	396.1	
^{47}Ca	4.54 d	1297.1	

Table 4 (continued)

Radionuclide	Half-life	Gamma-ray Energy (keV)	Interference
		Count #3 (continued)	
^{177}Lu	6.74 d	208.3	$^{176}Yb(n,\gamma)1.9h\ ^{177}Yb\ \beta^{-}\rightarrow\ ^{177}Lu$
Count #4. Two weeks-one month decay. Count length 800-1600 minutes.			
^{51}Cr	27.8 d	320.0	^{192}Ir (316.5 keV)
^{181}Hf	42.5 d	133.1 482.2	^{192}Ir (136.4 keV)
^{59}Fe	45.6 d	1291.5	^{192}Ir (484.7 keV)
^{58}Co (Ni)	71.3 d	811.1	
^{192}Ir	74.2 d	468.1	
^{46}Sc	83.9 d	889.3	
^{182}Ta	115 d	1221.3	
^{65}Zn	243 d	1115.5	^{46}Sc (1120.5 keV)
^{60}Co	5.26 y	1173.2	
^{152}Eu	12.7 y	121.8	

0.4 keV/channel in order to minimize interferences. Each radionuclide in Table 4 is listed under the count where the best abundance with the lowest statistical counting error is obtained. Obviously, most elemental abundances may be calculated from more than the one count they are listed under. Successive counts also provide half-life checks for most radionuclides. Abundances calculated from successive counts usually agreed within the statistical counting error.

Important interferences with the radionuclides of interest are also listed in Table 4. Because of the short half-life of ^{152m}Eu compared to ^{152}Eu, after 90 hours decay ^{152}Eu is about 13 percent of the 121.8 keV peak; therefore, ^{152m}Eu can no longer be used to calculate Eu abundances accurately unless the samples and standards are counted close in time.

If the heavy rare earth element (REE) pattern is sharply fractionated, the correction ^{176}Yb (n,γ) 1.9 h $^{177}Yb \xrightarrow{\beta^-} {}^{177}Lu$ becomes important. Experimental determination of this interference shows that 1 ppm Yb is equivalent to 0.004 ppm Lu. The correction was ignored in the INAA determinations because of the poor counting statistics for Lu ($\geq$ 10%) and because the REE would be redetermined by using RNAA. For a normal chondritic ratio the contribution of Yb to Lu is <3 percent. For the

fractionated patterns of some of these inclusions the contribution of Yb to Lu may be as high as 20 percent.

The ^{192}Ir 316.5 keV peak interferes with the 320 keV peak of ^{51}Cr. Since Ir abundances are very high in the inclusions and Cr abundances are rather low, the samples were recounted for Cr with the calibration spread to 0.13 keV/channel which completely resolved the Ir and Cr peaks.

Since both the ^{192}Ir and the ^{181}Hf peaks at 133 keV are small and of the same intensity, the 0.4 keV/channel calibration resolved them. At 480 keV the ^{192}Ir peak is much larger than the ^{181}Hf peak so that the peak from ^{192}Ir overwhelmed that of ^{181}Hf and resolution was impossible. The same thing happens with ^{65}Zn and ^{46}Sc (1115 and 1120 keV). The five keV difference between the two peaks should be enough to resolve them using 0.4 keV/channel and a high resolution Ge(Li), but since ^{46}Sc is so much more intense than ^{65}Zn, the result is a large peak due to ^{46}Sc with a little blip perched on the left side of the peak due to ^{65}Zn. Since Zn abundances obtained from ^{65}Zn would be expected to have large errors from the necessary ^{46}Sc correction, more reliance is placed in the abundances obtained by using ^{69m}Zn.

Reproducible counting geometry was essential since the samples were placed as close to the detector as possible for counting due to their low count rates. Hence, the small cone polyvials (maximum volume 0.05 ml) were secured

inside a larger polyvial which fit in a special holder on the face of the detector. Care was taken to always orient the cone polyvials parallel to the detector face. With these precautions, most duplicate counts gave elemental abundances within counting statistics of each other.

Major and trace element abundances of the Allende samples and standard rocks obtained via the INAA procedures are given in Table 5. The major elements are customarily reported as oxides as is done in this work. However, elemental abundances and not the mineralogical form of the element are measured when activation analysis is used, so the element must be assumed to be present in the valence state of the reported oxide. This procedure is not entirely satisfactory for Ti which is probably present in both +3 and +4 states (Grossman, 1975), or for other elements which exhibit variable valence states.

The final analytical procedure was the RNAA of the inclusions for K, Sr, Ba and the REE abundances. The techniques used are those of Boynton et al. (1976). Details of the RNAA separation and yield determinations are given in the appendix.

When the samples were removed from the polyvials for RNAA, it was expected that some loss would occur from incomplete transfer of samples. Therefore, the empty polyvials were saved and counted later for Sc. From the amount of Sc left in the polyvial, it could be determined how much

Table 5. Major and trace element analysis of Allende whole rock, chondrules and aggregates by INAA. Errors reflect 1σ counting statistics.

Sample	Weight (mg)	SiO_2 % by difference	TiO_2 %	Al_2O_3 %	FeO %	MgO %	CaO %	Na_2O %	Cl ppm	K ppm	Sc ppm	V ppm	Cr ppm	Mn ppm	Co ppm	Ni ppm	Zn ppm	Hf ppm	Ta ppm	W ppm	Re ppm	Ir ppm	Au ppm
Ca-rich chondrules (Group I)[a]																							
A-2 (1)[b,c]	19.46	33	1.08 ±0.04	25.8 ±0.3	0.84 ±0.02	14.5 ±0.4	24.3 ±0.5	0.134 ±0.005	--[f]	42 ±7	18.8 ±0.2	802 ±6	451 ±5	35.8 ±0.8	40.0 ±0.3	880 ±15	48 ±5	0.29 ±0.03	0.24 ±0.03	0.35 ±0.04	0.018 ±0.006	0.417 ±0.004	0.076 ±0.001
B-28 (1)	22.25	34	1.65 ±0.04	25.6 ±0.3	1.08 ±0.01	10.7 ±0.3	26.5 ±0.4	0.25 ±0.01	--	93 ±11	133 ±2	814 ±6	415 ±4	28.1 ±0.8	86 ±1	2100 ±40	53 ±17	2.1 ±0.2	0.33 ±0.07	1.90 ±0.09	0.46 ±0.05	7.4 ±0.1	0.106 ±0.002
D-7 (NM3898xa) (2)[c,d]	10.30	24	1.21 ±0.04	31.5 ±0.4	0.30 ±0.03	5.7 ±0.4	36.7 ±0.7	0.063 ±0.001	250 ±80	25 ±3	83 ±1	554 ±8	141 ±4	23.2 ±0.8	9.9 ±0.4	250 ±50	34 ±4	1.8 ±0.2	0.12 ±0.05	1.75 ±0.05	0.34 ±0.01	4.8 ±0.1	0.025 ±0.001
-(NM3529yc) (2)[e]	31.55	31	1.21 ±0.02	27.8 ±0.4	0.74 ±0.02	11.1 ±0.2	28.1 ±0.5	0.24 ±0.01	720 ±40	100 ±17	74 ±2	295 ±6	420 ±10	49 ±1	21 ±1	450 ±50	53 ±9	1.5 ±0.2	0.22 ±0.02	1.25 ±0.06	0.42 ±0.03	5.9 ±0.1	0.140 ±0.002
Cl-S2	11.97	31	1.03 ±0.04	29.6 ±0.4	1.97 ±0.05	13.8 ±0.4	21 ±1	1.65 ±0.02	4800 ±160	280 ±60	87 ±2	52 ±4	685 ±12	135 ±3	8.1 ±0.3	86 ±20	260 ±45	1.7 ±0.2	0.16 ±0.05	(14.6)[g] ±0.5)	<0.5	7.8 ±0.1	0.030 ±0.001
Ca-rich aggregate (Group III)[a]																							
B-30 (1)	13.13	20	0.78 ±0.06	52.2 ±0.5	1.56 ±0.02	9.7 ±0.5	15 ±1	0.99 ±0.01	--	380 ±33	111 ±2	180 ±5	323 ±20	70 ±1	4.5 ±0.2	85 ±46	580 ±40	1.6 ±0.2	0.50 ±0.06	2.2 ±0.2	1.44 ±0.07	20.2 ±0.2	0.081 ±0.002
Ca-rich aggregates (Group II)[a]																							
B29-S1	6.72	37	0.20 ±0.03	28.9 ±0.4	7.0 ±0.1	4.0 ±0.5	12.1 ±0.5	7.9 ±0.1	22600 ±460	1080 ±250	40 ±1	34 ±4	870 ±10	470 ±10	20 ±1	190 ±20	1150 ±230	<0.3	0.28 ±0.06	<4	<2	0.16 ±0.01	0.013 ±0.002
I-3[e,h]	14.09	--	--	--	7.9 ±0.2	--	10.4 ±0.5	3.88 ±0.05	--	3300 ±500	12.0 ±0.1	--	1100 ±50	--	30 ±1	215 ±50	1140 ±70	--	--	--	--	0.30 ±0.02	0.016 ±0.002
B-32 (white)[i] (1)	11.20	31	0.34 ±0.08	37.2 ±0.4	5.2 ±0.1	7.5 ±0.5	11.4 ±0.4	6.8 ±0.1	--	2640 ±330	51 ±1	90 ±6	337 ±4	207 ±4	27.4 ±0.3	260 ±20	820 ±20	<0.3	0.85 ±0.08	<1.4	<3	0.024 ±0.004	0.015 ±0.001
B-32 (white) (2)	5.48		0.38 ±0.06	34.7 ±0.5	7.0 ±0.1	5.9 ±0.5	14.9 ±0.7	5.1 ±0.1	9500 ±300	1740 ±180	51.5 ±0.5	209 ±7	392 ±4	410 ±7	32.9 ±0.6	200 ±20	970 ±140	--	0.76 ±0.09	<3	<1.4	0.057 ±0.006	0.043 ±0.002
Ca-poor aggregates																							
B-32 (dark)[i] (1)	13.92	35	0.26 ±0.06	3.7 ±0.1	28.1 ±0.3	29.8 ±0.5	2.8 ±0.2	0.52 ±0.01	--	290 ±42	61 ±1	110 ±4	3700 ±200	1260 ±13	807 ±2	16400 ±400	130 ±20	0.15 ±0.09	0.14 ±0.07	0.6 ±0.1	<0.2	1.21 ±0.01	0.227 ±0.003
B-32 (dark) (2)	23.27	--	0.14 ±0.03	4.28 ±0.08	27.8 ±0.4	28.1 ±0.4	3.2 ±0.2	0.82 ±0.01	740 ±80	590 ±42	10.3 ±0.1	92 ±3	3330 ±40	1170 ±12	680 ±7	14000 ±140	120 ±20	--	--	1.5 ±0.2	<0.3	0.624 ±0.006	0.23 ±0.01
I-8[e,h]	12.00	--	--	--	23.1 ±0.4	--	3.7 ±0.3	1.06 ±0.02	--	1000 ±200	12.4 ±0.1	--	2300 ±100	--	385 ±10	10200 ±600	35 ±10	--	--	--	--	0.84 ±0.05	0.57 ±0.03
Allende bulk and a melilite separate																							
Bulk (1)[j]	10.25 27.19	37	0.20 ±0.06	2.85 ±0.05	31.3 ±0.3	26 ±1	2.3 ±0.2	0.44 ±0.03	--	280 ±25	11.1 ±0.1	104 ±5	3740 ±40	1420 ±50	706 ±8	14200 ±150	105 ±15	0.16 ±0.07	<0.16	0.6 ±0.1	<0.14	0.85 ±0.01	0.125 ±0.001
Bulk (2)[j]	10.25 18.48	36	0.15 ±0.04	3.06 ±0.06	31.2 ±0.4	26.6 ±0.4	2.3 ±0.2	0.47 ±0.01	310 ±60	270 ±20	10.2 ±0.1	90 ±4	3360 ±40	1370 ±50	656 ±8	13200 ±200	111 ±10	0.21 ±0.06	0.14 ±0.04	0.24 ±0.08	<0.2	0.71 ±0.01	0.112 ±0.001
C3 chondrites[k]		33	0.15	2.60	31.8	24.1	2.4	0.47	250-420	230-280	9.1	88	3500	1490	620	14000	120	0.25	--	0.31	--	0.73	0.18
Melilite (1)	29.44	29	0.37 ±0.03	26.4 ±0.3	0.089 ±0.004	4.2 ±0.2	40.0 ±0.4	0.043 ±0.001	--	30 ±5	31 ±1	184 ±4	48 ±3	11.0 ±0.2	33 ±1	890 ±40	22 ±5	0.49 ±0.06	0.11 ±0.02	0.85 ±0.03	0.20 ±0.01	2.8 ±0.1	0.012 ±0.001
Standard Rocks																							
BCR-1 (1)[j]	27.84 15.09	57	2.40 ±0.06	13.4 ±0.1	12.2 ±0.1	2.9 ±0.2	6.8 ±0.2	3.15 ±0.05	--	13400 ±750	31.2 ±0.5	442 ±4	11 ±1	1320 ±20	40 ±1	--	--	4.9 ±0.2	0.60 ±0.07	--	--	--	--
BCR-1 (2)[j]	16.38 16.01	57	2.08 ±0.05	13.2 ±0.2	12.4 ±0.2	3.4 ±0.3	6.9 ±0.3	3.37 ±0.04	--	14000 ±400	32.0 ±0.3	428 ±6	12 ±1	1290 ±30	39 ±1	--	--	4.7 ±0.2	0.4 ±0.1	--	--	--	--
CRB (2)[j,l]	21.27 19.71	57	2.20 ±0.05	13.6 ±0.2	12.2 ±0.2	3.1 ±0.2	6.9 ±0.3	3.20 ±0.04	--	13200 ±470	31.0 ±0.4	431 ±6	11 ±1	1290 ±30	37 ±1	--	--	4.9 ±0.2	0.72 ±0.06	--	--	--	--
PCC-1 (1)	17.94	--	--	0.60 ±0.03	--	44.6 ±0.4	0.62 ±0.06	0.007 ±0.001	--	--	--	32 ±2	--	870 ±10	--	--	--	--	--	--	--	--	--
PCC-1 (2)	17.94	46	--	0.72 ±0.04	7.5 ±0.1	46.7 ±0.5	0.67 ±0.07	0.005 ±0.001	--	--	8.0 ±0.1	31 ±2	2610 ±30	820 ±10	121 ±2	2210 ±40	--	--	--	--	--	--	--

Footnotes - Table 5.

[a]Groups I, II and III denote inclusion classification system of Martin and Mason (1974).

[b]Sample notation follows that of Gray et al. (1973) who analyzed portions of the same inclusions.

[c]Numbers in parentheses denote different INAA runs.

[d]NM3898xa is not D-7 but comes from the same chondrule as D-7.

[e]Not analyzed by Gray et al. (1973).

[f]Dashes denote elements not analyzed for.

[g]Suspected W contamination with tools used to separate the chondrule from the matrix.

[h]Pink inclusions obtained by and analyzed with W.V. Boynton. Incomplete INAA is due to lack of time before RNAA.

[i]White and dark are separates of B-32.

[j]TiO_2, Al_2O_3, MgO, CaO, Na_2O, V and Mn are averages of duplicate analyses. All values reported for BCR-1(1) are duplicate analyses.

[k]Average values for C-3 chondrites from Mason (1971) and Schmitt et al. (1972).

[l]CRB is in-house standard basalt taken from the same quarry as BCR-1.

of the samples remained in the polyvial. (It must be assumed that Sc is homogeneously distributed in the sample.) Losses ranged from one to five percent.

Since the REE were separated as a group, they were counted several times to obtain abundances for all the fourteen REE (Table 6). From the table, it can be seen that most elements are determined from more than one count; some (ex. La, Sm, Yb) can be obtained from counts even though they are not listed under that count. When an element is not listed under a certain count, it doesn't necessarily mean that it cannot be obtained there, but that there is another more optimum counting time. An abbreviated counting sequence can also be used by counting only three times: the day of RNAA, the day after RNAA and two weeks after RNAA. When this system is used, duplicate counts for half life checks are not available. This sequence will also encounter more interference problems because the decay before counting for certain elements is not optimized. A composite REE standard (concentrations given in the Appendix) was used, insuring similar backgrounds in sample and standard counts.

The Ce abundance in Inclusion C1-S2 was a factor of three lower than expected when a smooth line was drawn from La and Nd (normalized to chondrites). The abundance was calculated using ^{143}Ce and two counts of ^{141}Ce taken about a month apart; the numbers obtained from all three

Table 6. Counting sequence for the RNAA of the Rare Earth Elements.

Radionuclide	Half-life	Gamma-ray energy (keV)	Calibration	Interferences
		Count #1. Day of RNAA. Repeated if time permits.		
^{165}Dy	2.32 h	94.5	0.4 keV/channel	
^{171}Er	7.52 h	295.9 308.3		^{169}Yb (307.5 keV)
^{152m}Eu	9.3 h	841.6 121.8		^{152}Eu (121.8 keV)
^{142}Pr	19.2 h	1575.6		
		Count #2. Day after RNAA.		
^{171}Er	7.52 h	295.9 308.3	0.4 keV/channel	^{169}Yb (307.5 keV)
^{152m}Eu	9.3 h	841.6 121.8		^{152}Eu (121.8 keV)
^{159}Gd	18.0 h	363.3		
^{142}Pr	19.2 h	1575.6		
^{166}Ho	26.8 h	80.6		
		Count #3. About three days after RNAA.		
^{166}Ho	26.8 h	80.6	0.4 keV/channel	
^{143}Ce	33.7 h	293.3		

Table 6 (continued)

Radionuclide	Half-life	Gamma-ray energy (keV)	Calibration	Interferences
		Count #3 (continued)		
^{140}La	40.2 h	487.0		
^{153}Sm	46.8 h	103.2		
^{175}Yb	4.2 d	396.1		
^{177}Lu	6.74 d	208.3		$^{176}Yb(n,\gamma)1.9\ h\ ^{177}Yb\ \beta^-\rightarrow\ ^{177}Lu$
		Count #4. About one week after RNAA.		
^{140}La	40.2 h	487.0	0.13 keV/channel 200 channel zero suppression	
^{153}Sm	46.8	103.2		
^{175}Yb	4.2 d	396.1		
^{177}Lu	6.7 d	208.3		$^{176}Yb(n,\gamma)1.9\ h\ ^{177}Yb\ \beta^-\rightarrow\ ^{177}Lu$
^{147}Nd	11.1 d	91.1		
^{160}Tb	72.1 d	298.5		
^{170}Tm	129 d	84.5		
		Count #5. Third week after RNAA or later.		
^{147}Nd	11.1 d	91.1	0.13 keV/channel 200 channel zero suppression	
^{169}Yb	31.8 d	177.0		
^{141}Ce	32.5 d	145.4		^{175}Yb (144.7 keV)

Table 6 (continued)

Radionuclide	Half-life	Gamma-ray energy (keV)	Calibration	Interferences
		Count #5 (continued)		
^{160}Tb	72.1 d	298.5		
^{170}Tm	129 d	84.5		
^{153}Gd	242 d	97.5		
^{152}Eu	12.7 y	344.2		
	Yields. Count #1 -- Immediately after reactivation.			
^{149}Nd	1.73 h	211.4	0.13 keV/channel 200 channel zero suppression	
^{177}Yb	1.90 h	150.3		
^{165}Dy	2.32 h	94.5		
^{176m}Lu	3.69 h	88.3		
^{171}Er	7.52 h	308.3		
^{152m}Eu	9.3 h	121.8		^{177}Yb (121.6 keV)
^{166}Ho	26.8 h	80.6		
^{140}La	40.2 h	487.0		
^{153}Sm	46.8 h	103.2		
	Yields. Count #2 -- Day after reactivation.			
^{143}Ce	33.7 h	293.3		

counts were similar. The same standard used to calculate Ce in C1-S2 was also used to calculate a normal BCR-1 Ce abundance (57±2 ppm). Therefore, the depleted Ce in C1-S2 is considered real and not due to experimental procedures. Note that most of the gamma-ray energies used are of very low energy; for example ^{166}Ho at 80.6 keV, ^{170}Tm at 84.4 keV, or ^{147}Nd at 91.1 keV. Because of absorption effects, it is important that the matrix solution of sample and standard be of the same density. A minimum amount of concentrated HNO_3 is used to dissolve the final $REE(OH)_3$ precipitate which is then diluted to 1 ml with H_2O. The standard is diluted with 2N HNO_3 to 1 ml to make the matrix densities equivalent.

Although the chemistry appears straightforward, occasionally problems were encountered such as with the third set of RNAA. Barium for C1-S2 and Bulk(3) and Sr for D-7, Bulk(3), and BCR(3) were lost. The losses appear to be compounded from several steps, beginning with the extra fine crystalline precipitate of $(Ba,Sr)SO_4$ which was difficult to centrifuge.

The K yields from Run 3 were also unreasonable. The yields for Bulk(3), BCR(3), NM3529yc, and D-7, although less than 20 percent, were still a factor of two larger than expected when comparing the K abundances obtained by RNAA with those from the INAA (see K values in Tables 5 and 7). Conversely, the yields of approximately 50 percent

for B29-S1 and C1-S2 seemed about 30 percent low. Apparently, the ^{137}Cs tracer and the K were fractionated, possibly through a difference in pH characteristics or solubilities of the precipitate. The solubility of $CsPh_4B$ (cesium tetraphenyl boron) is 0.430 mg Cs/100 ml H_2O, while that of KPh_4B is 0.578 mg K/100 ml H_2O (Geilman and Gebauhr, 1953). Since the Ph_4B precipitates very thoroughly washed with H_2O to help remove ^{24}Na, it is probable that more KPh_4B was dissolved and washed away than was $CsPh_4B$. This would cause the yields to seem too large as is the case for Bulk(3), BCR(3), NM3529yc, and D-7. This difficulty could be avoided by washing the precipitates with a Ph_4B solution rather than with water. An alternate possibility for causing fractionations is incomplete precipitation caused if insufficient $NaPh_4B$ was added (Keays et al., 1974). Variable K impurities in the fusion material (Na_2O_2 and NaOH) could add more K carrier to the solution than the amount of $NaPh_4B$ could precipitate. Thus the yield would be too large and the sample concentrations too small. Limited confidence is placed in the K abundances from Run 3 obtained by RNAA.

Tables 7 and 8 list the K, Ba, Sr, and REE abundances obtained via RNAA for the samples analyzed. The abundances for the melilite separate are INAA since RNAA was not performed on this sample.

Table 7. Analysis of REE, Ba, Sr, K in Allende whole rock, aggregates, and chondrules. All values obtained by RNAA except as noted. All numbers given in ppm. Errors reflect 1σ counting statistics.

Sample	Weight (mg)	$\Delta^{26}Mg$[a] (‰)	K	Rb (Gray et al.)[b]	Sr	Sr (Gray et al.)[b]	Ba	La	Ce	Pr	Nd	Sm	Eu	Gd	Tb	Dy	Ho	Er	Tm	Yb	Lu
Ca-rich chondrules (Group I)[c]																					
A-2 (2)[d]	19.46	+0.02	42 ±2	0.38	153 ±3	141	63.7 ±0.6	3.03 ±0.06	10.1 ±0.4	1.5 ±0.2	5.3 ±0.2	2.11 ±0.02	1.17 ±0.01	1.1 ±0.1	0.222 ±0.009	1.28 ±0.04	0.23 ±0.01	0.70 ±0.06	0.42 ±0.02	2.70 ±0.03	0.122 ±0.002
B-28 (2)	22.25	nd	91 ±2	0.29	185 ±4	203	46.8 ±0.4	4.74 ±0.07	13.7 ±0.4	1.6 ±0.2	8.0 ±0.2	3.03 ±0.03	1.37 ±0.01	4.2 ±0.2	0.91 ±0.03	6.40 ±0.06	1.48 ±0.01	4.4 ±0.1	0.54 ±0.02	4.07 ±0.04	0.63 ±0.01
D-7 (NM3898xa) (3)[d,e]	10.30	nd +1.9	(10)[f] (±1)	0.014	1.c.[g]	627	48 ±3	4.51 ±0.07	10.4 ±0.3	1.9 ±0.4	7.0 ±0.6	2.48 ±0.03	1.36 ±0.01	3.6 ±0.3	0.62 ±.01	4.35 ±0.06	0.87 ±0.02	2.8 ±0.2	0.40 ±0.02	2.42 ±0.05	0.387 ±0.007
-(NM3529yc) (3)[h]	31.55		(58) (±3)		138 ±3		26.5 ±0.5	4.61 ±0.06	11.8 ±0.4	2.2 ±0.3	8.3 ±0.6	2.75 ±0.03	1.28 ±0.01	3.6 ±0.2	0.62 ±0.03	4.41 ±0.06	1.01 ±0.03	3.1 ±0.1	0.46 ±0.02	4.02 ±0.05	0.40 ±0.01
C1-S2 (3)	11.97	-1.7	(420) (±20)	2.36	100 ±10	131	1.c.	4.15 ±0.06	3.7 ±0.2	1.7 ±0.3	6.3 ±0.3	2.54 ±0.05	1.19 ±0.02	3.2 ±0.2	0.57 ±0.04	4.41 ±0.07	0.93 ±0.03	3.0 ±0.2	0.37 ±0.03	2.87 ±0.06	0.40 ±0.01
Ca-rich aggregate (Group III)[c]																					
B-30 (1)[d]	13.13	+3.0	295 ±7	1.19	41.7 ±0.7	37.8	5.0 ±0.2	4.6 ±0.1	10.1 ±0.3	2.0 ±0.3	8.6 ±0.4	2.99 ±0.05	0.388 ±0.005	4.9 ±0.1	0.87 ±0.01	5.25 ±0.09	1.26 ±0.01	3.95 ±0.08	0.62 ±0.02	0.89 ±0.02	0.68 ±0.01
Ca-rich aggregates (Group II)[c]																					
B29-S1 (3)	6.72	+2.7	(1370) (±30)	9.6	<15	36	<2	7.9 ±0.2	18.8 ±0.6	4.0 ±0.6	14.2 ±0.6	4.49 ±0.06	0.215 ±0.003	3.6 ±0.3	0.64 ±0.02	3.14 ±0.05	0.24 ±0.03	0.49 ±0.06	0.78 ±0.04	0.31 ±0.01	0.022 ±0.001
I-3[h,i]	13.88		3300 ±500		36.8 ±0.5			4.65 ±0.05	18.3 ±0.6	2.2 ±0.3	8.1 ±0.3	3.60 ±0.04	0.187 ±0.002	0.8 ±0.1	0.110 ±0.005	0.67 ±0.02	0.050 ±0.007	0.13 ±0.07	0.54 ±0.03	0.86 ±0.01	0.015 ±0.001
B-32 (white) (1)[j]	11.20	+1.4[k]	2900 ±60	8.6[k]	28.6 ±0.6	33.4[k]	4.9 ±0.8	15.1 ±0.3	37 ±1	6.0 ±0.5	29 ±1	9.1 ±0.1	0.193 ±0.005	8.1 ±0.2	1.23 ±0.03	4.98 ±0.05	0.33 ±0.01	0.42 ±0.03	1.36 ±0.04	0.41 ±0.01	0.014 ±0.001
Ca-poor aggregates																					
B-32 (dark) (1)[j]	13.92		274 ±8		16.2 ±0.3		5.7 ±0.3	0.48 ±0.02	1.2 ±0.1	0.23 ±0.07	1.1 ±0.2	0.306 ±0.008	0.105 ±0.003	2.4 ±0.1	0.49 ±0.01	3.20 ±0.03	0.511 ±0.005	0.90 ±0.03	0.08 ±0.01	0.334 ±0.008	0.089 ±0.002
I-8[h,i]	11.97		1000 ±200		18.6 ±0.6			0.51 ±0.03	1.4 ±0.3	<0.25	1.0 ±0.2	0.296 ±0.003	0.124 ±0.003	0.3 ±0.1	0.079 ±0.006	0.55 ±0.01	0.121 ±0.005	0.37 ±0.07	0.09 ±0.02	0.34 ±0.01	0.050 ±0.001
Allende bulk and a Melilite separate																					
Bulk (2)[l]	18.48		235 ±6	1.01	15.0 ±0.4	13.8	6 ±2	0.78 ±0.02	2.0 ±0.1	0.35 ±0.07	1.2 ±0.1	0.370 ±0.003	0.123 ±0.002	0.46 ±0.07	0.088 ±0.004	0.563 ±0.003	0.140 ±0.003	0.43 ±0.03	0.072 ±0.007	0.395 ±0.007	0.055 ±0.001
Bulk (3)	27.19		(118) (±5)		1.c.		1.c.	0.48 ±0.02	1.16 ±0.06	0.09 ±0.07	0.71 ±0.09	0.286 ±.004	0.110 ±0.002	0.33 ±0.06	0.077 ±0.004	0.46 ±0.01	0.101 ±0.003	0.29 ±0.04	0.051 ±0.004	0.315 ±0.009	0.046 ±0.001
C3 Chondrites[m]			230-280		14.5		5	0.46	1.1	0.17	0.85	0.33	0.10	0.46	0.071	0.46	0.10	0.28	0.043	0.28	0.042
Melilite[n]	29.44		30 ±5					3.9 ±0.1				2.37 ±0.03	1.63 ±0.01							2.02 ±0.02	0.36 ±0.01
Standard Rocks																					
BCR-1 (1)	27.84		14000 ±330		323 ±3		573 ±6	27.5 ±0.4	59 ±1	8 ±1	29 ±1	6.87 ±0.07	1.96 ±0.05	6.9 ±0.2	1.12 ±0.02	6.20 ±0.07	1.29 ±0.04	3.5 ±0.2	0.54 ±0.02	3.62 ±0.07	0.534 ±0.007
BCR-1 (2)	15.09		14100 ±250		340 ±7		588 ±5	25.8 ±0.4	53 ±1	7.8 ±0.8	27.5 ±0.6	6.67 ±0.06	1.99 ±0.02	5.6 ±0.3	1.07 ±0.03	6.40 ±0.04	1.26 ±0.02	3.3 ±0.3	0.46 ±0.03	3.55 ±0.04	0.506 ±0.006
BCR-1 (3)	16.38		(5860) (±180)		1.c.		670 ±40	26.7 ±0.3	57 ±2	9 ±1	29 ±1	6.74 ±0.07	2.02 ±0.02	6.8 ±0.4	1.09 ±0.02	6.7 ±0.1	1.24 ±0.04	3.5 ±0.4	0.49 ±0.04	3.48 ±0.07	0.51 ±0.01

Footnotes - Table 7.

[a]Mg isotopic anomalies from Lee and Papanastassiou (1974).

[b]Rb and Sr averages from Gray et al. (1973).

[c]Group I, II, and III denote inclusion classification system of Martin and Mason (1974).

[d]Sample notation is that used in Gray et al. (1973). Numbers in parentheses denote different RNAA runs.

[e]NM3898xa is not D-7 but comes from the same chondrule as D-7.

[f]K values in parentheses are of questionable accuracy. See text.

[g]l.c. denotes lost during chemical procedure.

[h]Not analyzed by Gray et al. (1973).

[i]Pink inclusions obtained by and analyzed with W.V. Boynton. K values are INAA.

[j]White and dark are separates of inclusion B-32.

[k]Values determined on entire aggregate, not a separate.

[ℓ]REE values are systematically about 25% high.

[m]Averages taken from Clarke et al. (1970) and Haskin et al. (1966).

[n]Values for melilite are INAA.

Table 8. RNAA duplicate analyses of REE in the L-6 chondrite, Leedey and in BCR-1. All numbers are given in ppm. Errors reflect 1σ counting statistics.

Element	Leedey-a (267.0 mg)	Leedey-b (286.9 mg)	BCR-1 (102.5 mg)
La	0.30 ±0.01	0.33 ±0.01	25.1 ±0.5
Ce	0.79 ±0.02	0.78 ±0.02	54 ±1
Pr	0.102±0.009	0.120±0.009	6.6 ±0.4
Nd	0.54 ±0.02	0.61 ±0.03	29.1 ±0.7
Sm	0.18 ±0.01	0.204±0.003	6.5 ±0.2
Eu	0.081±0.002	0.077±0.001	2.04±0.04
Gd	0.31 ±0.02	0.27 ±0.02	6.8 ±0.4
Tb	0.049±0.003	0.049±0.004	1.05±0.02
Dy	0.320±0.004	0.339±0.004	6.63±0.07
Ho	0.083±0.002	0.079±0.002	1.49±0.06
Er	0.28 ±0.03	0.25 ±0.02	4.0 ±0.3
Tm	0.034±0.002	0.031±0.005	0.55±0.02
Yb	0.224±0.007	0.227±0.005	3.43±0.07
Lu	0.0331±0.0008	0.0338±0.0005	0.49±0.01

RESULTS AND DISCUSSION

Comparison of Standard Rock Values

The elements determined via INAA for BCR-1 and PCC-1 are given in Table 5. Agreement between BCR-1 values from different runs is good, within counting statistics except for TiO_2, MgO, Na_2O, Sc and V. For MgO and Sc the individual analyses are within counting statistics of their average; for Na_2O and V they are <5 percent outside counting statistics; for MgO and TiO_2 they are about 10 percent outside counting statistics. The in-house standard basalt, CRB-1, also agrees with the BCR-1 values. Thus, it appears that the analyses from the different runs are systematically coherent.

Table 9 is a comparison of BCR-1 and PCC-1 values with those of Flanagan (1973) and more recent work. Errors listed for this work are standard deviations which are comparable to the counting statistics. Agreement between the different analyses of BCR-1 is in general, very good. The value of Cr obtained here is the lowest listed, but the absolute abundance of Cr is so low that agreement is still reasonable. It may be significant that Mn is low in both BCR-1 and PCC-1; this would indicate a possible systematic error in the Mn standard that was used. The Ta value of 0.66 ppm for BCR-1 is in agreement with that of Grossman

Table 9. Comparison of BCR-1 and PCC-1 elemental abundances.

	BCR-1				PCC-1	
	This work[a]	Flanagan (1973)[b]	Grossman and Ganapathy (1976a)[c]	Laul and Schmitt (1975)[d]	This work[e]	Flanagan (1973)
TiO_2%	2.2±0.2	2.20 (1)				
Al_2O_3	13.4±0.2	13.61 (1)		13.7	0.66±0.08	0.74 (2)
FeO	12.3±0.1	12.05 (1)	12.24±0.08	12.3	7.5±0.1	7.51 (2)
MgO	3.1±0.3	3.46 (1)			45.7±1.5	43.18 (2)
CaO	6.9±0.06	6.92 (1)		6.9	0.65±0.04	0.51 (2)
Na_2O	3.24±0.1	3.27 (1)		3.20	0.006±0.001	0.006 (3)
K	1.41±0.01[f,g]	1.41 (1)		1.41[f]		
Sc ppm	31.4±0.5	33 (3)	34.7±0.3	32	8.0±0.1	6.9 (2)
V	434±7	399 (2)		420	31±0.7	30 (2)
Cr	11±0.6	17.6 (2)	14±3		2610±30	2730 (2)
Mn	1300±17	1406 (2)		1350	845±35	959 (2)
Co	39±2	38 (3)	37.5±0.2	36	121±2	112 (2)
Ni					2210±40	2339 (2)
Hf	4.8±0.1	4.7 (2)	5.0±0.2	4.7		
Ta	0.66±0.08[h]	0.91 (1)	0.67±0.04			
Ba	610±52[f]	675 (1)		650[f]		
Sr	330±12[f,g]	330 (1)		330[f]		

[a] Average of two BCR-1 and one CRB-1 (in-house standard basalt). Errors denote standard deviations of the mean.

Table 9 (continued)

[b](1) recommended
(2) average
(3) magnitude

[c]Average of three BCR-1, error is standard deviation of mean.

[d]Average of six BCR-1.

[e]Average of two PCC-1: Al_2O_3, MgO, CaO, Na_2O, V, Mn; error is standard deviation of mean. Single determination: FeO, Sc, Cr, Co, Ni; error is counting statistics.

[f]Obtained via RNAA.

[g]Average of two BCR-1.

[h]Average of one BCR-1 and one CRB-1. Third value was not used in the average because of the large error in counting statistics.

and Ganapathy (1976a) which supports their contention that the Ta value in Flanagan (1973) may be too high.

The abundances of PCC-1 from this work and that compiled by Flanagan (1973) do not agree as well as the BCR-1 numbers do. This is partially due to the fact that the elemental abundances of PCC-1 are not known as well as that of BCR-1 (note that most of the PCC-1 numbers given by Flanagan are averages and thus are not considered well enough known to be "recommended" numbers). Even so, agreement is either within counting statistics or better than ten percent for all elements except Ca (25 percent high), Sc (16 percent high), and Mn (12 percent low). Although the discrepancy noted for Mn may be attributed to the standard as previously discussed, the discrepancies noted for Ca and Sc are not expected to be due to the standards because of the agreement of BCR-1 analyses. Rather it is thought that heterogeneities in the small PCC-1 samples are the likely causes of disagreement.

REE values obtained by RNAA for BCR-1 in this work are compared to other values in Table 10. The errors listed are standard deviations of the mean and in all cases (except Nd) are larger than the counting statistics for individual analyses. Within these errors, all of the REE in BCR-1 agree with other analyses. The Tm value of 0.51 ppm agrees with Laul and Schmitt (1975) but is less than the 0.6 ppm of Flanagan (1973). The Yb value of 3.52 ppm is

Table 10. Comparison of REE abundances in BCR-1. All numbers given in ppm.

	This work[a]	Laul and Schmitt (1975)[b]	Nakamura (1974)[c]	Grossman and Ganapathy (1976a)[d]	Flanagan (1973)[e]
La	26.3 ±1.1	25.0	24.4	25.2	26 (2)
Ce	56 ±3	53	54.2	54	53.9 (1)
Pr	8 ±1				7 (3)
Nd	28.7 ±0.8	29	28.8		29 (1)
Sm	6.70±0.15	6.70	6.72	6.73	6.6 (2)
Eu	2.00±0.04	1.90	1.98	1.97	1.94(1)
Gd	6.5 ±0.6		6.67		6.6 (1)
Tb	1.08±0.03	1.1			1.0 (1)
Dy	6.48±0.23	6.30	6.36		6.3 (1)
Ho	1.32±0.12	1.2			1.2 (3)
Er	3.6 ±0.3		3.70		3.59(1)
Tm	0.51±0.04	0.52			0.6 (1)
Yb	3.52±0.08	3.40	3.40	3.4	3.36(2)
Lu	0.51±0.02	0.42	0.503		0.55(1)

[a] RNAA, average of 4. Error listed is standard deviation of the mean.
[b] RNAA
[c] Mass spectrometric isotope dilution
[d] INAA, average of 3
[e] (1) recommended; (2) average; (3) magnitude

about four percent higher than the average of 3.4 ppm; Lu is greater than Laul and Schmitt's value, but less than that of Flanagan.

Judging from the reproducibility of the REE in BCR-1 from here and other work, the REE analyses for the Allende inclusions are estimated to be accurate to about 5 percent.

Comparison of Chondritic Normalization Factors

Since small differences between adjacent REE are of interest, the REE chondritic normalization factors were re-determined using the L-6 chondrite, Leedey (see Table 8). Ordinary chondritic REE abundances were used rather than the primitive C-1 chondrites for normalization because the REE abundances are better known in ordinary chondrites and it is the relative and not the absolute differences between the REE in the inclusions which is of interest. The average value of Leedey for this work is compared with the average chondritic abundances used by other workers (Table 11).

In general, excepting Ce, the agreement is excellent among this work, Wakita et al. (1970), and Wakita and Zellmer (1970). The numbers obtained by Masuda et al. (1973) are systematically high by 15-20 percent so they were not included in the overall average. The overall average used for the normalization values gives equal weight to the REE abundances by Wakita et al. (1970),

Table 11. Comparison of chondritic normalization factors. All numbers given in ppm.

	Leedey[a] (This work)	Wakita and Zellmer (1970)[b]	Wakita et al. (1970)[c]	Masuda et al. (1973)[d]	Overall average[e]
La	0.32 ±0.01	0.34	0.32	0.378	0.33
Ce	0.78 ±0.02	0.91	0.86	0.976	0.85
Pr	0.111 ±0.009	0.121	0.11		0.114
Nd	0.57 ±0.02	0.64	0.59	0.716	0.60
Sm	0.194 ±0.008	0.195	0.196	0.230	0.195
Eu	0.079 ±0.002	0.073	0.071	0.0866	0.074
Gd	0.29 ±0.02	0.26	0.25	0.311	0.27
Tb	0.049 ±0.003	0.047	0.048		0.048
Dy	0.329 ±0.004	0.30	0.31	0.390	0.31
Ho	0.081 ±0.002	0.078	0.071		0.077
Er	0.26 ±0.02	0.20	0.20	0.255	0.22
Tm	0.032 ±0.002	0.032	0.031		0.032
Yb	0.225 ±0.005	0.22	0.19	0.249	0.21
Lu	0.0334±0.0005	0.034	0.033	0.0387	0.033

[a]Average of two determinations (RNAA)

[b]Composite of 12 chondrites (RNAA)

[c]Average of 29 chondrites (RNAA)

[d]One determination (mass-spectrometric isotope dilution)

[e]Work of Masuda et al. (1973) not included in the overall average.

Wakita and Zellmer (1970) and this work, even though fewer measurements were made here. It is felt that this is justified because of the agreement between the determinations and because systematic errors in the standard used for both Leedey and the Allende inclusions would be minimized. The same REE standard was used for the Leedey and Allende analyses thereby eliminating any systematic errors introduced by standards. However, some of the Leedey REE values have large errors associated with them due to counting statistics, so it was felt that the overall values would be more accurate if they were averaged with other determinations.

Comparison of Bulk Allende

The results of Allende whole rock analysis for major, minor and trace elements are listed in Tables 5 and 7. The average abundances obtained from this work are compared to other workers' values in Tables 12 and 14.

Duplicate analyses of the bulk sample were made with generally good agreement between them, although not as good as the counting statistics imply. In general, the values for Bulk(2) are less than those for Bulk(1). Especially note that Ni and Co are about six percent lower, Cr is eleven percent lower, and Ir and Au are about fifteen percent lower which could be attributed to slightly more metal phase in Bulk(1) compared to Bulk(2). The discrepancies

Table 12. Comparison of Allende bulk analyses for major, minor and trace elements, except REE.

	This work (avg. of 2)	C-3 (Mason, 1971)	Emery et al. (1967)	King et al. (1969)	Morgan et al. (1969)	Clarke et al. (1970)	Wakita and Schmitt (1970)	Showalter et al. (1971)	Martin and Mason (1974)	Grossman and Ganapathy (1976a)	Chou et al. (1976)	Range	Average
TiO_2 (%)	0.17±0.03	0.15		0.18		0.15			0.15			0.15-0.18	0.16
Al_2O_3	2.9±0.1	2.60	2.55	3.31		3.27	3.23±0.09	3.25±0.04	3.29			2.55-3.31	3.15
FeO	31.3±0.3	31.8	35.8	30.4	31.4±0.5	30.7	28.2±0.5	33.8±0.6	27.15	30.4		27.15-35.8	31.0
MgO	26.6±0.4	24.1	21.7	24.0		24.6			24.63			21.7-24.63	23.7
CaO	2.3±0.2	2.4	2.63	2.52		2.62	2.8±0.3	2.5±0.4	2.59			2.5-2.8	2.61
Na_2O	0.46±0.01	0.47		0.40	0.44±0.01	0.44	0.45±0.1	0.44±0.01	0.46			0.40-0.46	.44
Cl (ppm)	310±60[a]	250-420				224[b]							
K	235±5[c]	230-280		250		200		220±10	250			200-250	230
Sc	10.7±0.5	9.1	10		12.2±0.2	11	11.0±0.5	12.0±0.2		11.69		10-12.2	11.3
V	97±7	88		170		70	130±10	112±3				70-170	120
Cr	3550±200	3500	4200	4200	3900±100	3600	3680±100	4230±80		3770		3600-4230	3940
Mn	1400±40	1490	1700	1300		1400	1450±40	1400±10				1300-1700	1450
Co	680±20	620	600	700	684±17	600	640±20	738±13		650		600-738	660
Ni	13,700±500	14,000	11,500	14,100	14,300±900	13,900					14,400	11,500-14,400	13,600
Zn	108±8	120				25					114	25-114	
Ba	6±2[c]	5		10		5			4.1			4.1-10	6
Sr	15.0±0.4[a]	14.5				13			12			12-13	12.5
W	0.4±0.1	0.31			0.15±0.02								
Ir	0.78±0.06	0.73			0.71±0.03					0.773	0.81	0.71-0.81	0.76
Au	0.118±0.006	0.18			0.26±0.01					0.162	0.16	0.16-0.26	0.19
Hf	0.19±0.05	0.25	<0.7		0.16±0.020				0.2			0.16-0.2	0.17
Ta	0.13±0.04[a]	0.017[d]											

[a]Single determination. [b]Published by Clarke et al. (1970); determined by M. Quijana-Rico, Max-Planck-Institute, Mainz. [c]Single determination, RNAA. [d]C2 meteorite (Ochansk).

between the analyses can be mainly attributed to the small masses (20-30 mg) of the analyzed aliquants. When comparing the average bulk composition obtained in this work with other analyses, it is seen that most of the values fall within the ranges reported by other workers and near the values for other C-3 meteorites. The exceptions are MgO (7 percent high) and Au (25 percent low). The differences are probably due to heterogenieties in the bulk samples which were analyzed, since Allende is a heterogeneous meteorite. A suspected error in the content of Au in the Au standard was ruled out after the standard ^{198}Au specific activity had been checked against two other Au standards, one of which was freshly prepared for the test. The explanation of less metal in the bulk sample used in this work (as compared to other bulk samples that have been analyzed) also doesn't hold because Ir values determined in this work agree with those measured by other workers.

The W value is 2.6 times larger than that reported by Morgan et al. (1969), but is close to that given for other C-3 chondrites (Mason, 1971). No other Ta value has been reported; the Ta value of 0.13 ppm given here is nearly a factor of ten larger than Mason's value for C-2 chondrites.

A comparison of the REE abundances obtained for the bulk samples by both RNAA and INAA is given in Table 13. Within errors, the INAA values for Bulk(2) and Bulk(3) agree with each other. In general, INAA values are lower

Table 13. Comparison of REE abundances in Allende bulk obtained via INAA and RNAA. All numbers given in ppm.

	Bulk (2)		Bulk (3)	
	RNAA	INAA	RNAA	INAA
La	0.78 ±0.02	0.47 ±0.03	0.48 ±0.02	0.44 ±0.03
Sm	0.370 ±0.002	0.296 ±0.002	0.286 ±0.004	0.25 ±0.03
Eu	0.123 ±0.002	0.116 ±0.009	0.110 ±0.002	0.110 ±0.005
Yb	0.395 ±0.007	0.35 ±0.04	0.315 ±0.009	0.27 ±0.03
Lu	0.055 ±0.001	0.050 ±0.005	0.046 ±0.001	0.035 ±0.004

than the RNAA but still agree within error ranges listed. Exceptions to this are La and Sm of Bulk(2) and Lu of Bulk(3). Because of fewer interferences, RNAA abundances are usually considered to be superior. However, the RNAA results of Bulk(2) and Bulk(3) show Bulk(2) consistently higher than Bulk(3) by about 20 percent. Since the INAA results of both samples agreed with the RNAA results of Bulk(3) and since the Bulk(3) results agreed better with those of other workers, the error was attributed to the Bulk(2) analysis.

Since all the REE are consistently high in Bulk(2), the yield determination was suspected to be in error. The yield reactivation and analysis was carried out twice with identical results, so systematic errors in yield may be eliminated as the source of error. The following hypothesis concerning the error in Bulk(2) is suggested: The sample is liquid and was sealed only in a 0.4 dram polyvial before counting. If the heat seal on this polyvial was of poor quality and the polyvial tipped over between the final count and the reactivation for yield determination (a delay of ten days), some of the REE solution could have leaked out. If this happened, the yields would appear too low and the final REE abundances of Bulk(2) would be too high. In reality, this would seem unlikely, but inspection of the heat seal on this polyvial revealed a poor quality seal

which did leak into the two dram polyvial that it was encased in for yield determinations.

Thus, Bulk(3) is considered more accurate than Bulk(2) for the REE abundances. Only Pr, Nd, and Gd of Bulk(3) are less than the reported ranges given for the REE in bulk Allende (Table 14) and these three elements all have large errors associated with them. It is obvious from Table 14 that there are large variations between different analytical groups. The REE were determined on different portions and pieces of the meteorite and probably reflect the inherent heterogeneities of Allende, although systematic differences between various laboratories could also contribute to the scatter.

Mineralogy of Inclusions

As discussed in the introduction, Gray et al. (1973) divided the inclusions into chondrules and aggregates on the basis of morphology and mineralogy. The inclusions analyzed here were classified as Ca-Al chondrules (D-7, B-28, A-2, Cl-S2), Ca-Al aggregates-low Rb (B-30), or Ca-Al aggregates-high Rb (B29-S1, B-32). The inclusion NM3529yc was not analyzed by Gray but appears to be a Ca-Al chondrule. The inclusion I-3 corresponds to the Ca-Al aggregates-high Rb. The inclusion I-8 has major and trace element chemistry similar to the bulk composition and could be an olivine aggregate. Although Mg was not analyzed in

Table 14. Comparison of REE abundances of Allende bulk samples. All abundances given in ppm.

	This work		C-3 (Mason, 1971)	Clark et al. (1970)	Wakita and Schmitt (1970)	Showalter et al. (1971)	Masuda et al. (1973)	Tanaka and Masuda (1973)	Grossman (1973)	Martin and Mason (1974)	Nakamura (1974)	Range reported and average[b]
	Bulk (2)[a]	Bulk (3)										
La	0.47±0.03	0.48±0.02	0.46	0.7	0.44±0.02	0.50±0.02	0.586	0.663	0.48	0.51	0.507	0.44-0.7 0.53
Ce		1.16±0.06	1.1	1	1.25±0.06	1.39±0.05	1.527	1.69		1.3	1.325	1-1.69 1.4
Pr		0.09±0.07	0.17	0.2	0.20±0.01	0.21±0.005				0.21		0.2-0.21 0.21
Nd		0.71±0.09	0.85	0.9	0.91±0.05	1.05±0.10	1.146	1.03		0.97	1.007	0.9-1.146 1.02
Sm	0.296±0.002	0.286±0.004	0.33	0.5	0.29±0.01	0.347±0.015	0.368	0.313	0.24	0.34	0.330	0.24-0.368 0.32
Eu	0.116±0.009	0.110±0.001	0.10	0.1	0.107±0.005	0.116±0.001	0.1401	0.110	0.12	0.10	0.113	0.1-0.1401 0.11
Gd		0.33±0.06	0.46	0.6	0.43±0.02	0.44±0.01	0.445	0.384		0.42	0.414	0.384-0.6 0.42
Tb		0.077±0.004	0.071	0.09	0.074±0.005	0.081±0.004				0.08		0.074-0.09 0.078
Dy		0.46±0.01	0.46	0.6	0.42±0.02	0.44±0.02	0.535	0.451		0.42	0.504	0.42-0.6 0.46
Ho		0.101±0.003	0.10	0.1	0.12±0.01	0.113±0.001	0.356	0.301		0.10		0.10-0.356 0.20
Er		0.29±0.04	0.28	0.3	0.31±0.02	0.295±0.006				0.29	0.303	0.29-0.31 0.30
Tm		0.051±0.004	0.043		0.049±0.001	0.055±0.003				0.05		0.049-0.055 0.051
Yb	0.35±0.04	0.315±0.009	0.28	0.4	0.32±0.02	0.300±0.005		0.330	0.47	0.31	0.315	0.30-0.47 0.34
Lu	0.050±0.005	0.046±0.001	0.042		0.058±0.002	0.049±0.001		0.0495			0.0465	0.0465-0.058 0.051

[a] Excluding Clarke et al. (1970).

[b] INAA.

I-8, if all the iron is calculated as fayalite, then the olivine composition is 67 percent Fo (forsterite) which agrees with the olivine compositions given by Grossman and Steele (1976) for amoeboid olivine aggregates. As described in the experimental section, B-32 was separated into white and dark portions. The chemical analysis of the white separate shows that it corresponds to the Ca-Al aggregates-high Rb. The dark separate, probably a combination of reaction rim and matrix, appears to be mainly composed of olivine (60 percent Fo) assuming all Fe is present as olivine.

If the classification scheme of Grossman and Ganapathy (1975) is used, the aggregates become fine-grained inclusions and the chondrules become coarse-grained inclusions. The chondrules are further classified as Type A or Type B on the basis of the Ti and Al content of the fassaite or Ti-pyroxene (see introduction).

Using electron microprobe analyses, Gray et al. (1973) established average chemical compositions for major phases (fassaite, melilite, spinel, and anorthite) in the Allende chondrules A-2, B-28, D-7 and Cl-S2. Table 15 is adapted from their data and also includes the major element data for the melilite separate analyzed here via INAA.

The composition of the fassaite determines whether the chondrules are classified as Type A or Type B. From Table 15, fassaite in A-2, B-28, and Cl-S2 averages 20.1 percent Al_2O_3 and 5.3 percent TiO_2. Fassaite in D-7 is much more

Table 15. Average major mineral compositions in Allende chondrules.[a]

	Melilite			Fassaite		Spinel	Anorthite
	M[b]	D-7	Separate[c]	M[b]	D-7	C-1	M[b]
SiO_2 %	33.8	27.1	29[d]	39.5	32.8	0.6	43.3
TiO_2	na[e]	f	0.37	5.3	17.3	0.4	na
Al_2O_3	17.1	27.7	26.4	20.1	18.3	71.3	35.6
FeO	0.1	f	0.09	0.1	f	0.1	0.1
MgO	7.2	3.7	4.2	10.5	7.1	28.1	0.1
CaO	39.8	40.8	40.0	24.2	25.2	0.2	19.6
Na_2O	0.1	f	0.04	f	f	f	0.1

[a]Average of A-2, B-28 and C-1.
[b]Based on Table II, Gray et al. (1973).
[c]This work.
[d]Obtained by difference.
[e]Not analyzed.
[f]Less than 0.05%.

titaniferous, containing 18.3 percent Al_2O_3 and 17.3 percent TiO_2. These chondrules are thus well within the specifications for Type B coarse-grained inclusions (Grossman, 1975).

If the melilite separate is considered a solid solution of gehlenite and akermanite, then it is composed of 71 percent gehlenite and 28 percent akermanite. Similarly, the melilite in D-7 is 75 percent gehlenite and 25 percent akermanite. The average composition of melilite in A-2, B-28 and C1-S2 differs from the above, being 46 percent gehlenite and 49 percent akermanite. Both compositions are similar to previously reported melilites in Type B inclusions (Grossman, 1975). From equilibrium thermodynamic calculations melilite is the first Si containing condensate from a gas of solar composition (T_{cond} = 1675°K). As such it does not contain sodamelilite, contrasting the usual terrestrial melilite (Grossman and Clark, 1973).

The minor phases in the chondrules are also somewhat unusual: the spinel is nearly pure $MgAl_2O_4$; the anorthite is approximately An_{98} in composition.

The aggregates are so fine grained that microprobe analyses cannot be performed. Using major element chemistry and X-ray powder diffraction, Clarke et al. (1970) determined gehlenite, anorthite, fassaite, spinel, grossular, nepheline, and sodalite. Thus, except for nepheline and

sodalite, the aggregates' mineralogy is similar to that of the chondrules.

Rare Earth Elements

The rare earth elements (REE) in these inclusions present a wide variety of patterns when normalized to ordinary chondrites (Fig. 1, 2 and 3). The inclusions B-28, D-7 and NM3529yc have REE patterns that average 12X chondrites (Fig. 1) and are similar to those observed for Group I in the classification scheme of Martin and Mason (1974). The patterns appear nearly flat or slightly enriched in the heavy REE (B-28) with a small positive Eu enrichment. There may be a small positive Yb enrichment in NM3529yc in addition to the Eu enrichment. These patterns approximate that of the mineral melilite: both are flat and about 12X chondrites but melilite has a stronger Eu enrichment than do the Group I inclusions. The light REE, La through Eu, of inclusion A-2 resemble those of the other Group I inclusions. The intermediate REE, Gd through Er, and the heavy REE Lu are depleted by a factor of two relative to the light REE and to Yb and Tm. Thus, relative to their neighbors Er and Lu, Yb and Tm present a large positive anomaly. Conversely, since Yb and Tm and the light REE are enriched to similar degrees, it is evident that Yb and Tm are normal and Gd through Er and Lu are the anomalous REE.

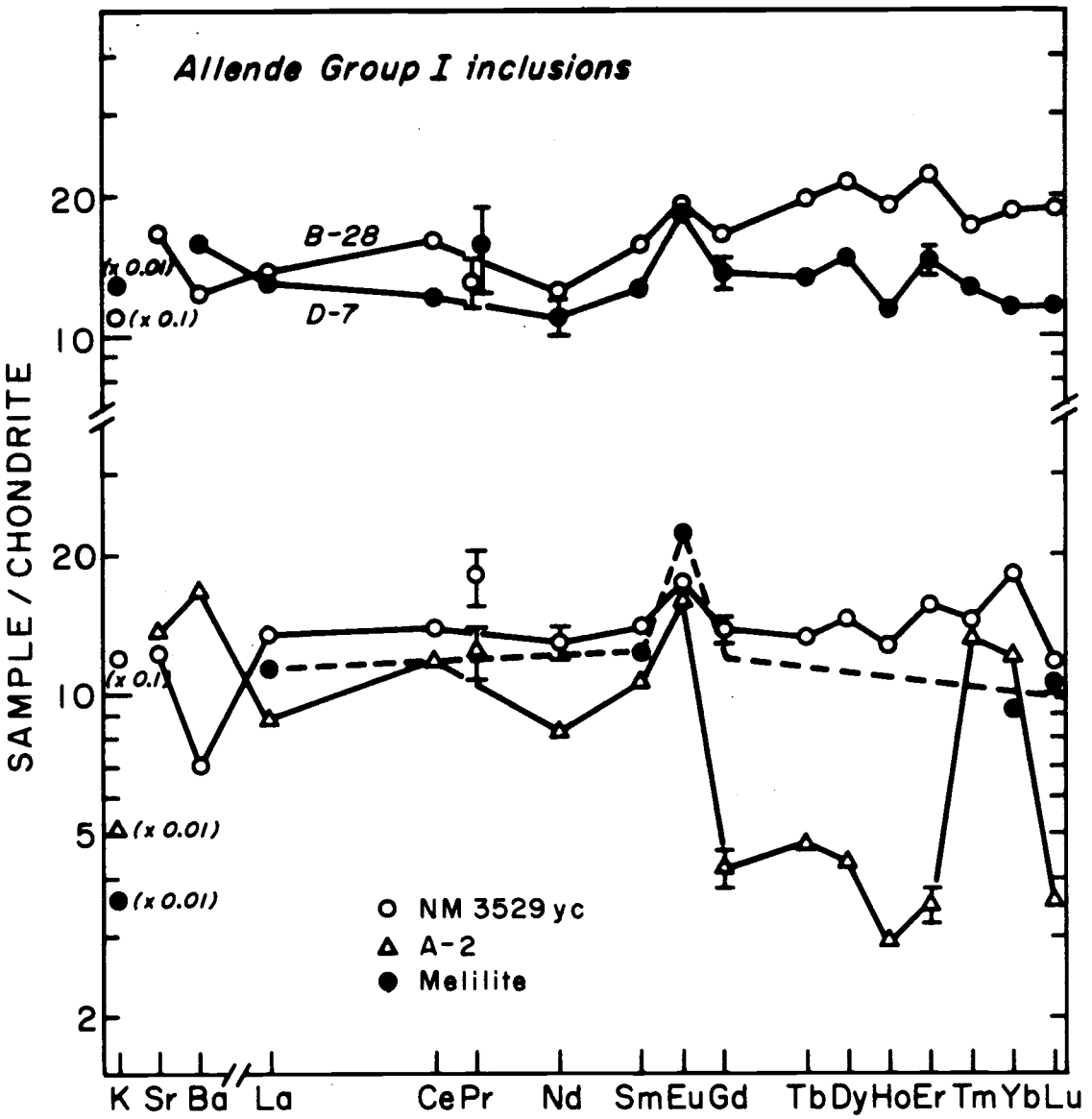

Figure 1. REE in Ca-Al-rich Group I inclusions and a melilite separate. Error bars denote 1σ counting statistics.

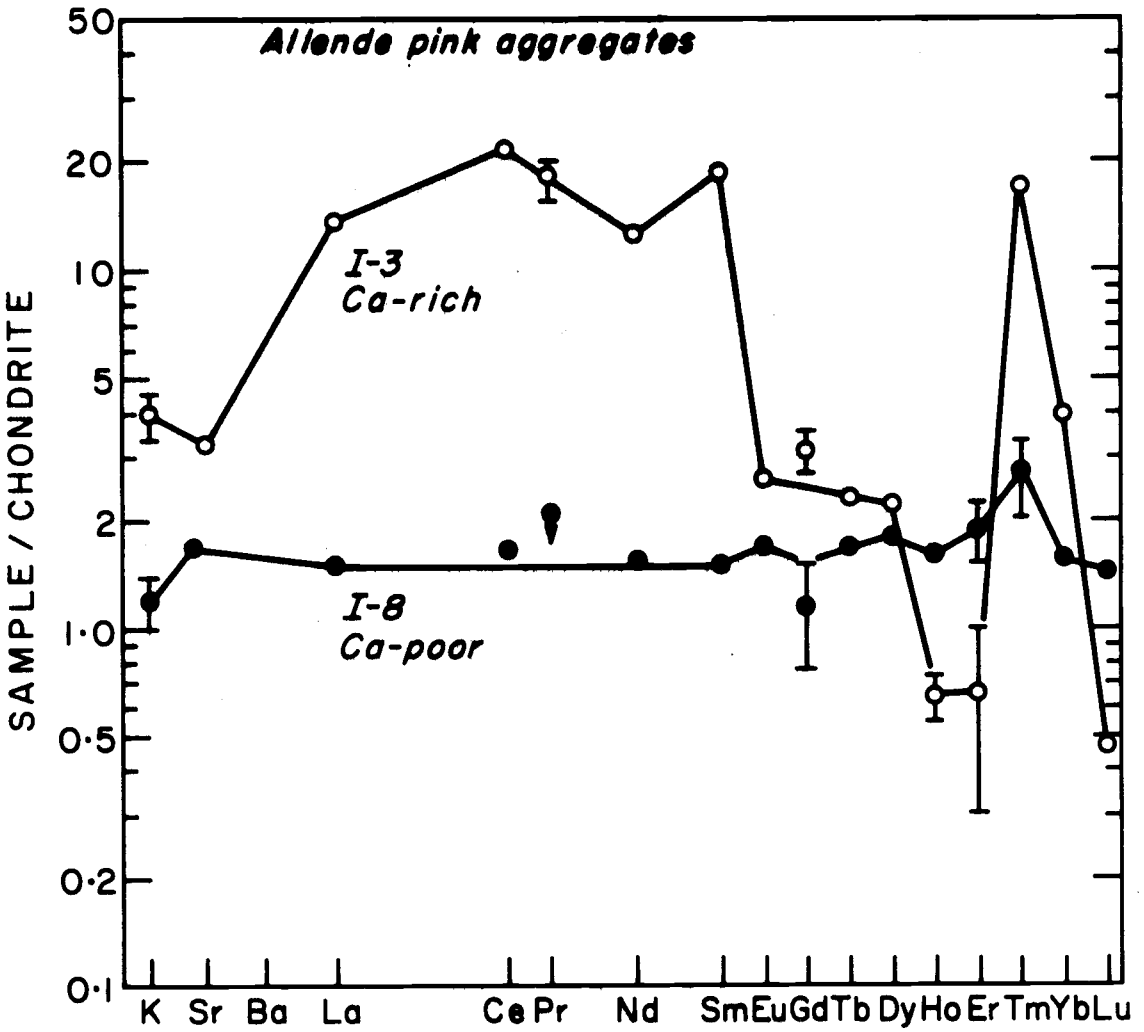

Figure 2. REE patterns of bulk Allende, Allende Ca-Al-rich aggregates (Groups II and III) and a Ca-Al-rich chondrule. Error bars denote 1σ counting statistics.

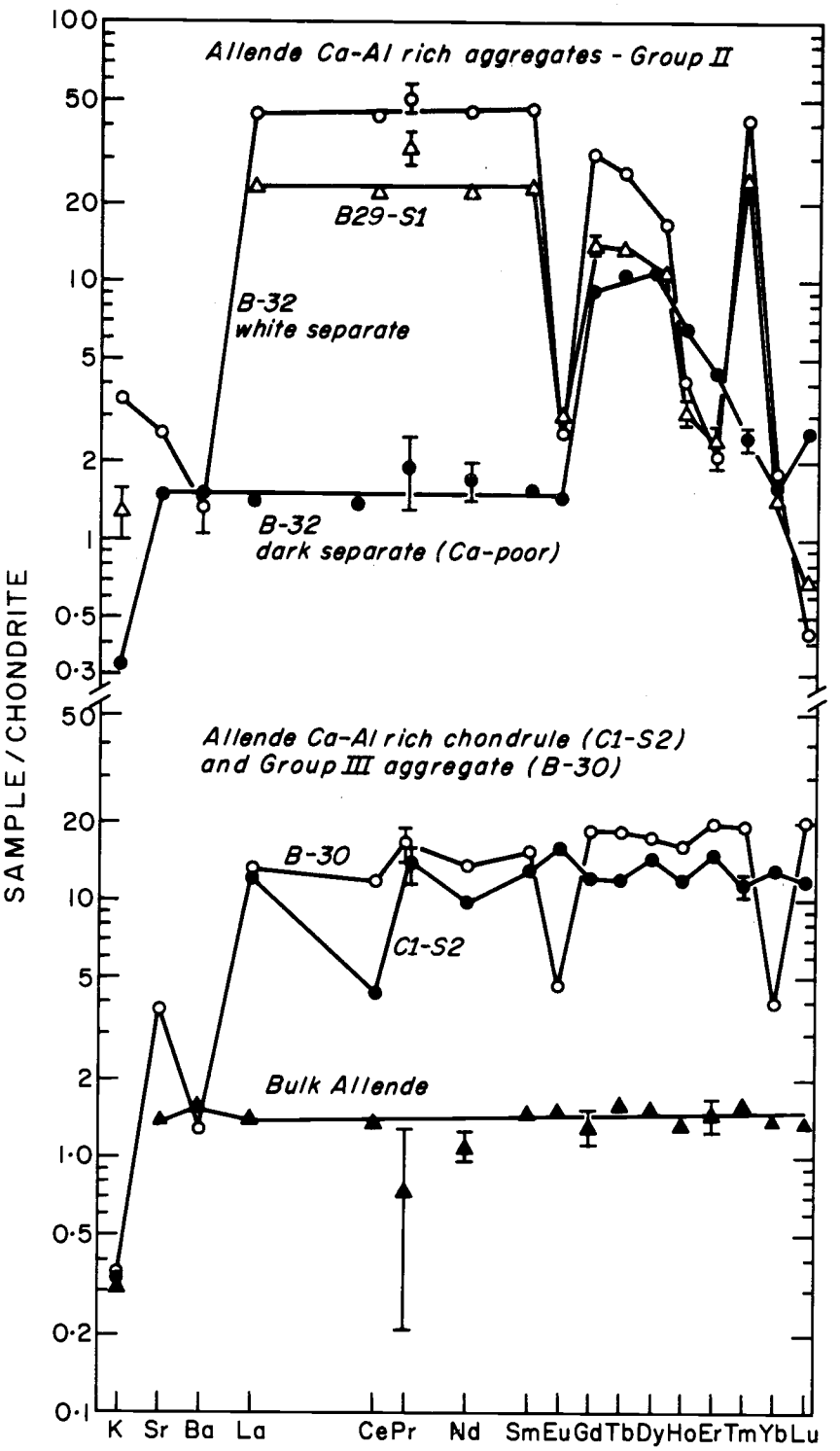

Figure 3. REE patterns of Allende pink aggregates. One aggregate is Ca-rich and high alkali (similar to Group II); the other is Ca-poor and olivine. Error bars denote 1σ counting statistics.

The intermediate alkali inclusions (Fig. 2) present two other patterns. In inclusion B-30, Yb and Eu are depleted similar to the Group III inclusions (Martin and Mason, 1974) or Inclusion O of Tanaka and Masuda (1973). In inclusion Cl-S2, the pattern looks like that observed in Group I inclusions except for the substantial Ce depletion. Note that the Ce of Cl-S2 and the Eu and Yb of B-30 have normalized values of 4.4, 4.6, and 4.0 respectively. Although interesting, it is probably coincidental that they are depleted to the same degree.

Gray et al. (1973) classified B-30 as a low Rb aggregate. Interestingly, the inclusions from Martin and Mason (1974) with similar REE patterns also have similar Rb abundances (about 1.1 ppm) and similar Na_2O percentages (about 1.5 percent). Unfortunately, this comparison cannot be carried further. Either the REE were not analyzed in great enough detail to identify the pattern (Grossman and Ganapathy, 1976b) or neither Rb nor Na was measured (Tanaka and Masuda, 1973).

The Ce depletion in Cl-S2 is considered real and not an experimental artifact and may presently be the only reported negative Ce anomaly in Allende inclusions. Inclusion 8 analyzed by Grossman and Ganapathy (1976a) possibly also exhibits this same pattern.

Also plotted in Fig. 2 are the REE patterns for the inclusions B29-S1 and B-32. The patterns of B29-S1 and

B-32 white are very similar qualitatively; quantitatively B-32 white is nearly 2X higher than B29-S1. Both have flat light REE, Eu depletions, and extremely fractionated heavy REE. The Tm is anomalously high (by a factor of 20) relative to its neighbors Eu and Yb but appears normal when compared to the light REE. This pattern is quite common for Ca-Al rich aggregates and has been observed by a number of other workers (Tanaka and Masuda, 1973; Martin and Mason, 1974; Grossman and Ganapathy, 1976b). Tm is generally not analyzed, so their patterns do not show the Tm enrichment.

The dark separate of B-32 is much lower in REE content than the white separate with its light REE comparable to that of the bulk sample. The Tm enrichment does not appear in B-32 dark but Gd, Tb, Dy, and Ho are enriched about 6X relative to the light REE. Thus, this could be considered a two-component system: one part being composed of bulk-like material and the other part consisting of a pattern of heavy REE.

The Allende pink aggregates (Fig. 3) are of two types. One, I-3, is a Ca-rich aggregate with a REE pattern intermediate between B29-S1 or B-32 white, and A-2. The light REE are enriched about 20X chondrites, Eu is depleted and Tm is normal compared to B-32 white or B29-S1. The intermediate REE, Gd to Er, do not form a smooth depletion pattern as seen in B29-S1 or B-32 white but appear more like

the pattern of A-2. The other inclusion, I-8, has a pattern much like the bulk Allende (Fig. 2) except for the small Tm enrichment. Since there is a large counting statistics error (~20 percent) associated with Tm, the enrichment may only be an artifact of the graph. If the enrichment is real, then inclusion I-8 is remarkable because it is the only inclusion that has a Tm anomaly in the conventional sense. A case can be made for all the other inclusions for normal Tm relative to the light REE but in I-8, Tm is enriched by almost a factor of two over La and the other light REE.

Classification of Inclusions

The four divisions of inclusions defined by Martin and Mason (1974) and reproduced in Table 2 appear to fit the available data very well. The Ca-Al-rich inclusions are included in Groups I, II, and III; the olivine inclusions are Group IV. Major differences between Group I and Groups II or III are mineralogical and trace element data, especially the REE patterns. The major difference between Groups II and III is trace element data, again specifically the REE patterns. Stylized drawings of the REE patterns in Groups I, II and III are shown in Fig. 4 which is taken from Boynton (1976). Also included is one REE pattern discovered in this work (inclusion I-3) that is different from the defined patterns; for discussion purposes it will be

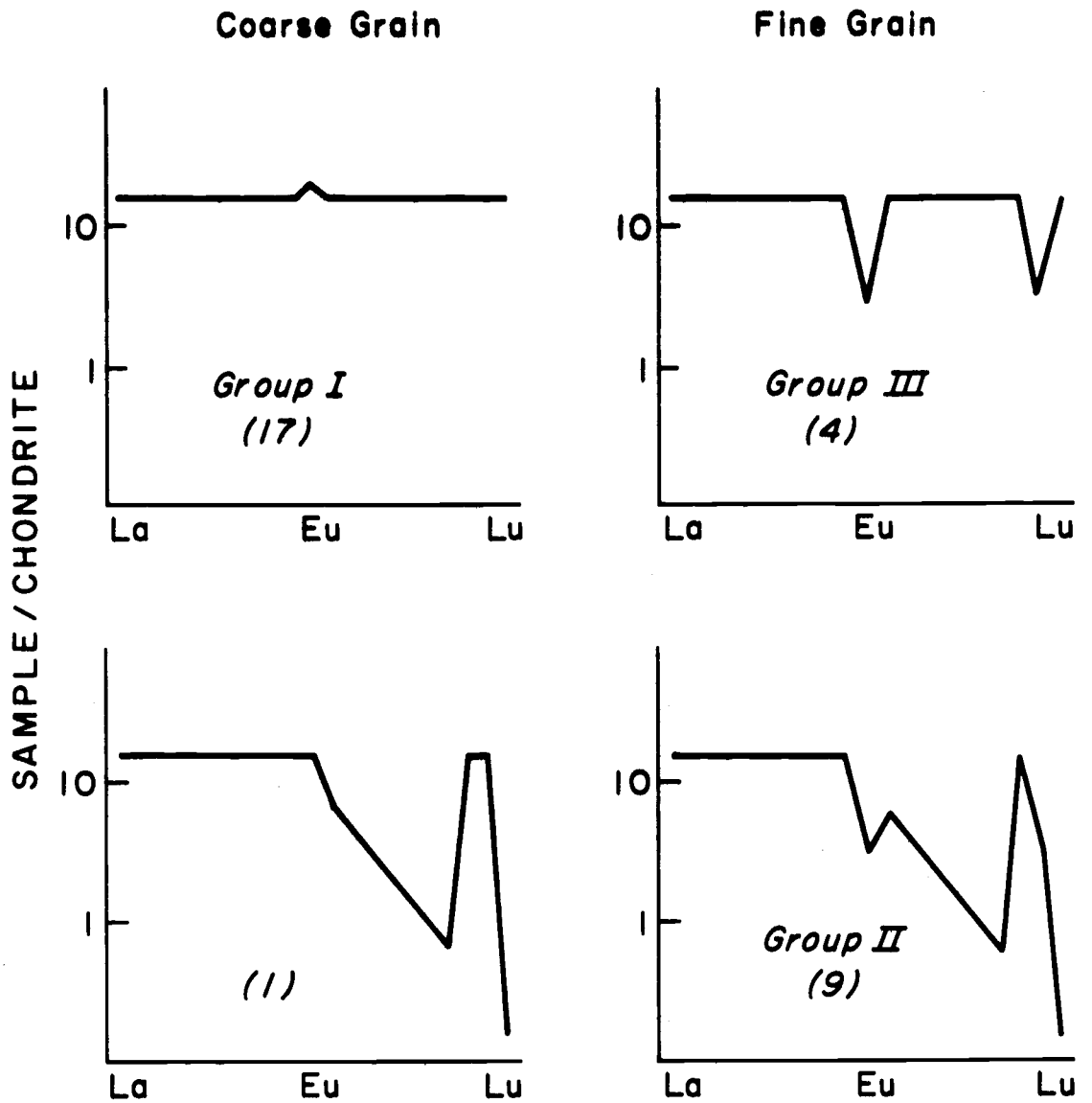

Figure 4. Stylistic drawings of REE patterns in Allende inclusions. Coarse and fine-grained refer to the classification of Grossman (1975); Groups I, II and III refer to the classification of Martin and Mason (1974). Numbers in parentheses denote number of inclusions of each type for which detailed REE analyses have been made. From Boynton (1976).

included in Group II. The numbers in parentheses indicate the number of detailed REE analyses of each type of inclusion that have been reported by Conard et al. (1975), Tanaka and Masuda (1973), Martin and Mason (1974) and this work. The REE data reported by Grossman and Ganapathy (1976a, 1976b) has not been included since they classify the inclusions differently and also have not analyzed enough REE in order to define detailed REE patterns. Even so, some of their REE patterns do seem defined enough for tentative classification by the above scheme. The coarse- and fine-grained classification of Grossman and Ganapathy roughly corresponds to Group I and to the combined Groups II and III defined here.

The REE pattern defined in Group I is essentially flat (10-15X chondrites) and generally has a small positive Eu anomaly. This pattern is shown by B-28, D-7, and NM3529yc. The inclusion A-2 which has depleted intermediate REE (Gd to Er) is also included in this group because it is unfractionated with respect to Eu and Yb.

Group III which has negative Eu and Yb anomalies describes inclusion B-30. Inclusions B29-S1 and B-32 white are represented in Group II.

Inclusion C1-S2 looks like a Group I chondrule except for the negative Ce anomaly. As previously mentioned, the Ce is depleted to the same extent as the Eu and Yb in inclusion B-30, but in inclusion C1-S2, Eu and Yb are not

depleted. Thus Cl-S2 doesn't appear to fit in either Group I or Group III, but since it looks more like a Group I inclusion than a Group III, it will be classified in Group I. If future studies reveal that Ca-Al rich inclusions with REE patterns similar to Cl-S2 are relatively common, then a Group V may have to be defined to encompass these inclusions.

Interelement Comparisons

From the limited number of Ca-Al rich samples analyzed in this work, a few general conclusions concerning elemental compositions have been drawn. If the geometric mean is calculated for each element in Groups I and II and compared with the elemental abundances of the single inclusion in Group III (Table 16), some trends are immediately obvious. Decreasing in content from Group I to Group III (Inclusion B-30) to Group II are Ti, Mg, Ca, Sr, Ba, Eu, Yb, V; the elements Fe, Na, K, Ce, Pr, Nd, Sm, Tm, Mn, Zn, and Cl are increasing in abundance from Group I to Group III to Group II. For the REE these trends are probably not meaningful since the REE contents of the inclusions are variable within each group. No clear trends are shown by Al, Ta, Ir, Co, Ni, Au and Cr. If only the variations between Groups I and II are considered, it is apparent that Group I has less Al, Ta, and Cr, more Ir, Ni and Au, and similar Co abundances than does Group II.

Table 16. Geometric means of elemental abundances in Group I, Group II, and Group III inclusions compared to abundances in C-1 chondrites.

	Group I			Group III			Group II						
	This work	All[a]	Number samples used	This work	All[c]	Number samples used	This work	All[d]	Number samples used	C-1[e]	I/C-1	III/C-1	II/C-1
Ti (%)	0.73	0.75	8	0.47	0.49	3	0.16	0.23	4	0.041 (2)	18	12	5.6
Al	14.8	13.9	9	27.6	21.6	4	17	17	5	0.84 (2)	17	26	20
Fe	0.64	0.63	10	1.2	2.2	3	5.1	4.4	11	17.8 (2)	0.035	0.12	0.25
Mg	6.4	6.2	7	5.8	7.6	3	3.3	5.1	4	9.4 (3)	0.66	0.81	0.54
Ca	19.2	19.2	11	11	10.5	4	8.1	7.2	12	0.98 (1)	19.6	11	7.3
Na	0.18	0.19	10	0.73	0.97	3	4.4	2.2	11	0.48 (2)	0.40	2.0	4.6
Cl	0.095	0.096	4	-	-	-	2.3	1.0	6	0.053 (2)	1.8	-	19
K (ppm)	77	121	7	300	340	3	2180	1350	5	480 (2)	0.25	0.71	2.8
Sc	67	82	8	111[f]	-	-	29	34	9	6.4 (1)	13	17	5.3
V	350	390	6	180[f]	-	-	55	-	2	49 (2)	8.0	3.7	1.1
Cr	377	348	8	320[f]	-	-	690	940	9	2300 (2)	0.15	0.14	0.41
Mn	43	43	8	70[f]	-	-	310	290	8	1720 (2)	0.025	0.041	0.17
Co	23	21	8	4.5[f]	-	-	25	22	9	470 (2)	0.045	0.010	0.047
Ni	450	500	6	85[f]	-	-	220	-	3	9500 (2)	0.053	0.0090	0.023
Zn	65	68	6	580[f]	-	-	1020	1020	8	350 (2)	0.19	1.6	2.9
Sr	142	142	7	42	49	4	32	23	5	8.6 (5)	16.5	5.7	2.7
Ba	44	46	6	5	15	4	4.9	9.8	4	2.2 (3)	21	6.8	4.5
La	4.2	4.3	11	4.6	6.0	4	8.2	8.6	12	0.19 (4)	23	32	45
Ce	5.9	8.5	11	10.1	13.4	4	23	23	12	0.66 (4)	13	20	35
Pr	1.8	1.7	8	2.0	2.1	3	3.8	3.3	5	0.097 (4)	17.6	22	34
Nd	6.9	7.2	8	8.6	10.9	4	15	14	6	0.44 (4)	16.4	25	32
Sm	2.6	2.7	11	3.0	3.5	4	5.3	5.3	12	0.131 (4)	21	27	40
Eu	1.3	1.2	11	0.39	0.45	4	0.20	0.29	12	0.050 (4)	24	9.0	5.8
Gd	2.9	3.0	9	4.9	5.0	4	2.9	2.3	6	0.20 (2)	15	25	12
Tb	0.54	0.57	9	0.87	0.83	3	0.44	0.54	11	0.039(1)	15	21	14
Dy	3.7	4.2	11	5.3	6.4	4	2.2	2.0	12	0.22 (4)	19	29	9.1
Ho	0.77	0.80	8	1.3	1.7	3	0.16	0.14	5	0.054 (4)	15	31	2.6
Er	2.4	2.7	9	4.0	4.9	4	0.30	0.25	6	0.11 (4)	24.5	45	2.3
Tm	0.43	0.42	7	0.62	0.69	3	0.83	-	3	0.022 (4)	19	31	38
Yb	3.1	2.9	11	0.89	1.5	4	0.48	0.50	12	0.16 (4)	18	9.4	3.1
Lu	0.34	0.39	7	0.68	0.71	2	0.016	0.012	4	0.022 (4)	18	32	0.55
Hf	1.2	1.4	10	1.6[f]	-	-	-	-	-	0.10 (1)	14	16	-
Ta	0.20	0.21	8	0.50[f]	-	-	0.49	0.52	8	0.0134 (2)	16	37	39
W	1.10	1.22	7	2.2[f]	-	-	-	-	-	0.088 (2)	14	25	-
Re	0.23	0.27	6	1.44[f]	-	-	-	-	-	0.035 (6)	7.7	41	-
Ir	3.7	4.9	8	20.2[f]	-	-	0.10	0.039	9	0.51 (6)	9.6	40	0.076
Au	0.061	0.065	8	0.081[f]	-	-	0.015	0.009	9	0.14 (2)	0.46	0.59	0.064

[a] Five samples from this work; one sample from Wänke et al. (1974); high and low extremes of range of ten samples given by Martin and Mason (1974); one sample from Tanaka and Masuda (1973); two samples from Grossman and Ganapathy (1975, 1976a).

[b] Number of samples used for overall mean.

[c] One sample from this work; one sample from Tanaka and Masuda (1974); two from Martin and Mason (1974).

[d] Three from this work; one from Tanaka and Masuda (1974); high and low extremes of range of five samples as given by Martin and Mason (1974); six from Grossman and Ganapathy (1975, 1976a, 1976b).

[e] Values from (1) Grossman and Ganapathy (1976a); (2) Wänke et al. (1974); (3) Nakamura (1974); (4) Schmitt et al. (1964); (5) Mason (1971); (6) Krahenbühl et al. (1973).

[f] Single determination (inclusion B-30).

The overall geometric means using data from this work, Tanaka and Masuda (1973), Martin and Mason (1974), Wänke et al. (1974) and Grossman and Ganapathy (1975, 1976a, 1976b) are also given in Table 16. Martin and Mason (1974) listed their data as ranges for ten Group I inclusions and five Group II inclusions. Because of this, in the calculated geometric means their Group I inclusions were treated as two inclusions which represent respectively the high and low elemental abundances (range) of the ten analyzed chondrules. Group II inclusions were treated similarly. The inclusions used in the means from Grossman and Ganapathy (1975, 1976a, 1976b) represent only a portion of the inclusions that they analyzed. These inclusions were the ones that could be tentatively identified as belonging to either Group I (inclusions 1 and 3) or Group II (inclusions 5, 12, 13, 14, 17, 18). Since they did not analyze enough REE to define the REE patterns, particularly the heavy REE, most of their REE patterns are too ambiguous for an unambiguous classification. In particular, this is the reason none were classified as Group III.

The variable elemental compositions within Groups I, II and III are demonstrated by comparing the overall geometric means with those of this work. For most samples, the absolute means change very little. Even when absolute means differ, the general trends between groups do not. A work of caution must be included here. Many of the

elemental abundances in Group III are represented by only a single analysis; these elements are Hf, Sc, V, Ta, W, Re, Ir, Co, Ni, Au, Mn, Cr, Zn, and Cl. For comparative purposes it has been assumed that Inclusion B-30 is representative of all Group III inclusions. For some elements, particularly Ir, this is likely to be a poor assumption since the Ir abundance in B-30 is unusually high at 20.2 ± 0.2 ppm which is 5X that observed in Group I inclusions.

Refractory Elements

The Allende Ca-rich inclusions (coarse-grained) are thought to be high temperature condensates (for example, see Marvin et al., 1970) or evaporation residues (Kurat, 1970; Chou et al., 1976); as such they should be enriched in the refractory trace elements which condense (or evaporate) in the same temperature range as the major refractory minerals. These elements and their condensation temperatures, as given by Grossman and Larimer (1974), are reproduced in Table 17 along with a few low temperature minerals. If the refractory elements are normalized to their abundances in C-1 chondrites, then enrichments or depletions are readily observed. C-1 chondrites have been described as the least disturbed or most primitive objects available for study, i.e. their chemical composition is thought to be nearest to the original solar nebula composition which is the reason their elemental abundances are

Table 17. Relationships between the condensation temperatures and the refractory trace elements and those of the major high temperature and some low temperature minerals. From Grossman and Larimer (1974) and Grossman (1972).

Gaseous species	Crystalline phases	Condensation temperature °K	
		10^{-3} atm	10^{-4} atm
Os	Os[a]	1925	1840
WO, W	W	1885	1798
ZrO, ZrO_2, Zr	ZrO_2	1840	1789
Re	Re	1839	1759
	Corundum (Al_2O_3)	1758	1679
HfO, HfO_2, Hf	HfO_2	1719	1652
YO, Y	Y_2O_3	1719	1646
ScO, Sc	Sc_2O_3	1715	1644
Mo, MoO	Mo	1684	1603
	Perovskite ($CaTiO_3$)	1647	1571
REO, RE[b]	RE_2O_3	1647	1571
Ir	Ir	1629	1555
	Gehlenite ($Ca_2Al_2SiO_7$)	1625	1544
Ru	Ru	1614	1441
VO, V	V_2O_3	1534	1458
	Spinel ($MgAl_2O_4$)	1513	1444
TaO, Ta	Ta_2O_5	1499	1452
ThO_2, ThO, Th	ThO_2	1496	1429
	(Fe,Ni)	1473	
	Diopside ($CaMgSi_2O_6$)	1450	
	Forsterite (Mg_2SiO_4)	1440	
	Anorthite ($CaAl_2Si_2O_8$)	1362	
	Enstatite ($MgSiO_3$)	1349	

[a]Highest condensing crystalline phase.

[b]Rare earths condensing in solid solution with perovskite.

used for normalization (Anders, 1971). The ratios of refractory elements normalized to C-1 chondrites for Groups I, II and III are shown in Fig. 5. (The concentrations of elemental abundances in C-1 chondrites used for normalizations are given in Table 16).

The refractory elements in the Group I inclusions are rather uniformly enriched except for Mg whose main mineral source is forsterite (Grossman, 1972) which is a low temperature mineral at 1440°K (Table 17). The average enrichment for 26 elements is 16.7; if only the lithophile elements are considered, the average becomes 17.5. This enrichment factor is similar to the 18.6 reported by Grossman and Ganapathy (1976a) for 15 elements in 10 coarse grained inclusions.

The Group III refractory elements do not present the same uniform enrichment as does Group I. Especially, note that Eu and Yb are depleted relative to their REE neighbors. Excluding Eu and Yb, the average enrichment of the refractory elements is 24.2; if the siderophile elements Ir, Re and W are omitted, the average decreases slightly to 22.7. Thus, the average refractory element content (dominated in these averages by REE) is higher for Group III than Group I.

The behavior of the refractory elements in Group II inclusions is even more unusual than that of Group III. Enrichments ranging from 20 to 45 are seen for Al, La, Ce,

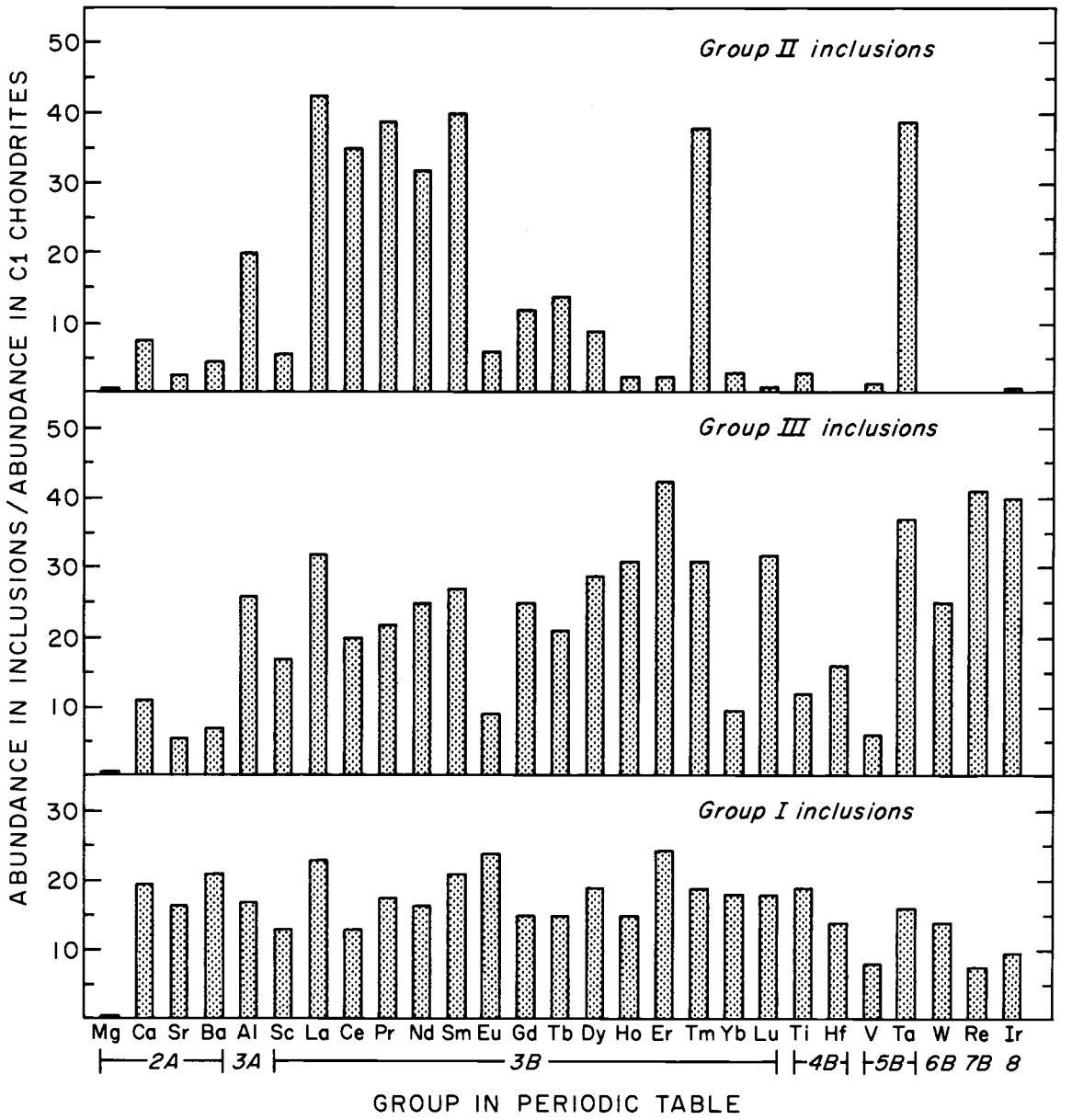

Figure 5. Comparison of the refractory element enrichments relative to C-1 chondrites in Allende inclusions, Groups I, II and III.

Pr, Nd, Sm, Tm and Ta. The intermediate REE (Gd, Tb and Dy) have enrichments of 10 to 15. The remaining refractories are enriched by factors of seven or less.

The uniform enrichment of lithophile elements observed in the Group I inclusions is not seen in the Group II inclusions. Instead there appear to be three enrichment groups with enrichments of 3.4, 12 and 35.

The metallic elements W and Re were not observable in the Group II aggregates via INAA and Ir is severely depleted compared to C-1 chondrites. Thus the depletion of siderophile elements in fine-grained inclusions reported by Grossman and Ganapathy (1976b) is also observed in this work for Group II inclusions.

Rather striking is the similarity of enrichments of the light REE (La-Sm), Tm, and Ta for each group of inclusions. Particularly interesting is Fig. 6, a correlation of Tm and Ta. Using the method of least squares, a correlation coefficient $r = 0.92$ is calculated at the 99 percent confidence level. The Ta-Tm data points plot along the line defined by the cosmic ratio of Ta/Tm = 0.61 indicating that Tm behaves normally relative to Ta and to the light REE. This suggests that the light REE, Tm, and Ta may reside in the same phase.

Of the 24 refractory lithophile elements studied, 14 of them are REE. Since the REE usually behave as a coherent group and since Ta correlated with Tm indicating it

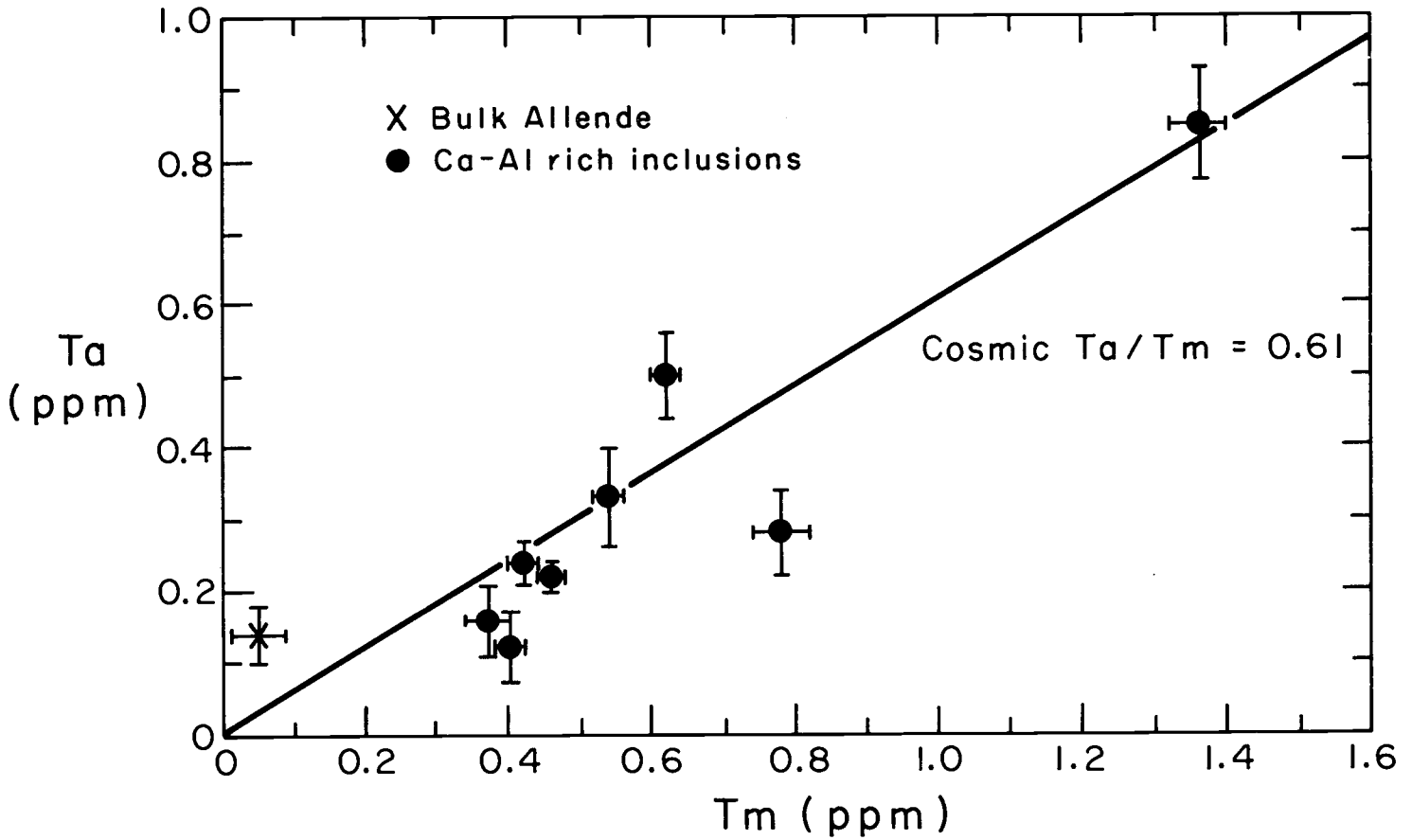

Figure 6. Correlation of Ta and Tm in Allende inclusions. Error bars denote 1σ counting statistics.

is also following the REE, the averages were recalculated without the REE and Ta to obtain the enrichment of the remaining nine lithophile refractory elements. The enrichment factors dropped from 17.5 to 15.9 for Group I and from 24.2 to 12.3 for Group III. The enrichment using the same elements in Group II is 6.7. An interesting pattern now emerges. The light REE and Tm increase in abundance from Group I to III to II while the average of the other lithophile refractory elements (excluding the heavy REE) decreases from Group I to III to II. Thus the light REE and Ta do not behave in the same manner as the other refractory lithophile elements.

Comparing the enrichment of Ta versus V (Group 5B), the Ta has an enrichment in Group III of 37 (39 in Group II) while V has an enrichment of only 4 (Group III) or 1.1 (Group II). In Group I, Ta is decreased to 16 while V has increased to 14. According to thermodynamic calculations, V_2O_3 condenses only 35° before Ta_2O_5 (Table 17) so it would be expected that their enrichments would be similar as observed in Group I unless some other effect was also taking place to fractionate them. This could possibly be a crystal control effect involving spinel which condenses at a temperature intermediate between V and Ta. The V^{+3} ion is well known for its tendency to substitute for Al^{+3} in spinel (Mason and Berry, 1968); in this case the V_2O_3 may even have served as a nucleating agent for the spinel

condensation. A similar effect would be expected for Ta^{+5} which has the same ionic radii (r = 72Å) and co-ordination number (VI) as the V^{+3} (Whittaker and Muntus, 1970). However, the large charge difference between V^{+3} and Ta^{+5} has a greater influence on the ion's entry into the spinel lattice than does size or co-ordination number. Thus the Ta^{+5} would be prevented from substituting for Al^{+3} due to its greater ionic charge and less Ta relative to V is expected to be present in spinel. Spinel is observed in coarse-grained inclusions in quantities of 15-30 percent (Grossman, 1975), but there have been no quantitative estimates of spinel content in fine-grained inclusions. An upper limit of spinel content can be calculated using the mean Mg content for Group II inclusions. If all the Mg (3.3 percent) is calculated as spinel, then 19 percent of the inclusion is spinel. It is highly unlikely that all Mg is in spinel since other Mg bearing minerals have also been identified in aggregates (Grossman et al., 1975; Marvin et al., 1970). Thus there is probably less spinel in fine-grained inclusions than in coarse-grained so that V can be correlated with spinel. The mean V concentration in Group I inclusions is a factor of 10 higher than the concentration in Group II inclusions. The element Ta must be in a different phase than V; a phase which is common to all inclusions.

A better comparison of the refractories results if the ratios of the elements in Group II or III versus those in Group I are plotted (Fig. 7). About half of the refractories are enriched relative to Group I inclusions and about half are depleted. The Group II inclusions have enriched Al, La, Ce, Pr, Nd, Sm, Tm, and Ta; the Group III inclusions have the above elements enriched and also Mg, Gd, Tb, Dy, Ho, Hf and W. Since the Re and Ir means for Group III inclusions are probably not representative, Re and Ir were not included in Fig. 7. Hafnium and W were not determined for Group II, so no comparison between Group II and Group I is possible for these elements.

Group II inclusions have a higher concentration of the light REE and Tm than do the Group I inclusions; similar types of enrichments are observed for the Group III inclusions for all REE except Eu and Yb. The depletions or enrichments of REE and other elements in Group II are more pronounced than those of Group III inclusions.

Volatile Elements

Elements considered nonrefractory or volatile are those which do not condense, either as pure oxide or metal or in solid solution with a major mineral phase, at higher condensation temperatures than that for Ni Fe which condenses at 1453°K (Grossman, 1972). In Group I inclusions the volatile elements are depleted relative to C-1

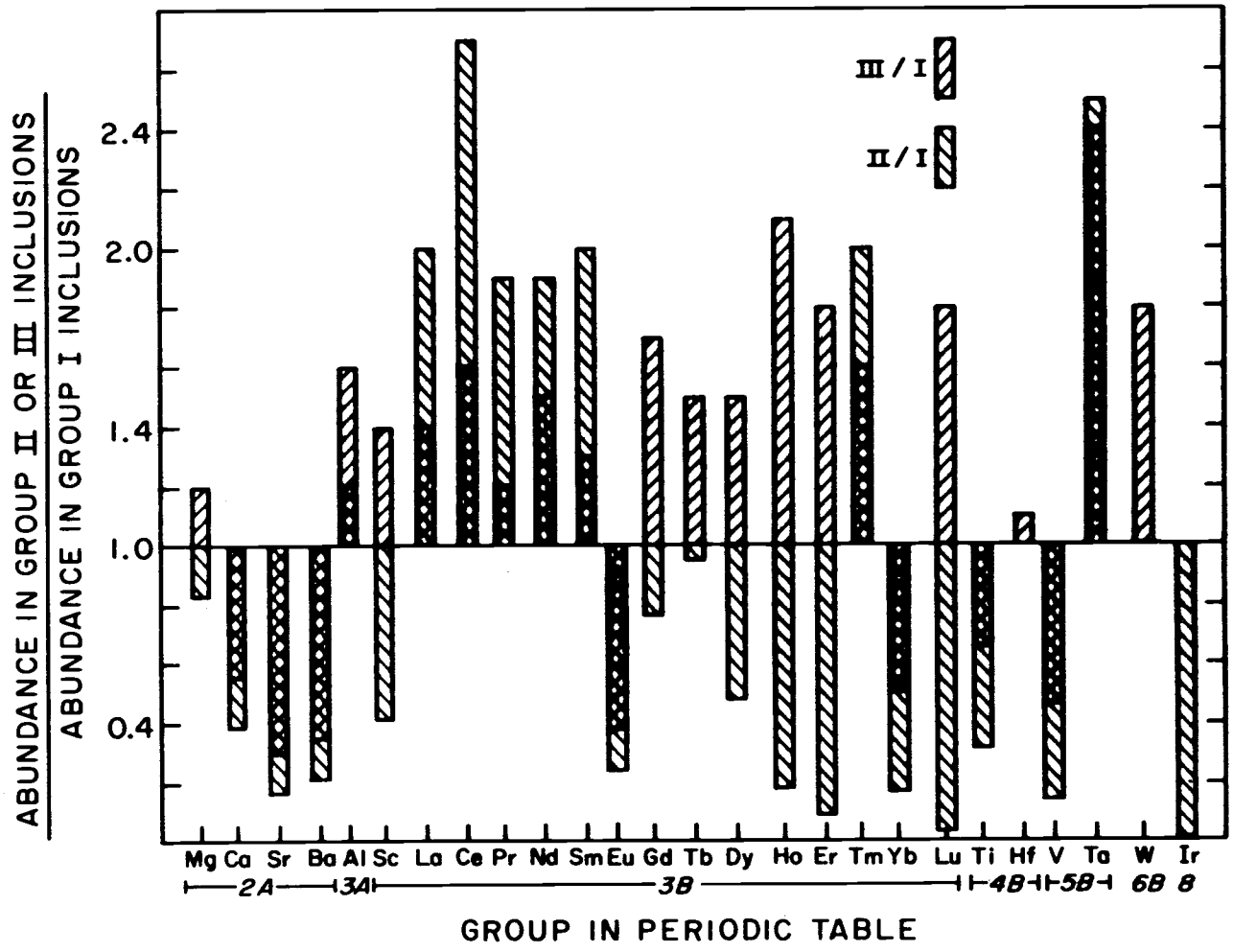

Figure 7. Relative abundances of refractory elements in Allende Group I, II, and III inclusions.

chondrites (except Cℓ) as shown in Fig. 8. Sodium, K, Zn and Cr are depleted to similar extents; their average ratio relative to C-1 chondrites is 0.25. The elements Mn, Fe, Co and Ni have ratios less than 0.06. They exhibit a depletion trend with Mn more depleted than Fe than Co than Ni. Gold and Mg have similar depletion ratios of about 0.6.

An increased concentration of volatiles in the Group III inclusions as compared to the Group I inclusions is shown. Now Na and Zn are enriched relative to C-1 chondrites, but K and Cr are still depleted. The Ni to Mn depletion trend has nearly reversed itself, so that Ni is most depleted followed by Co, then Fe and Mn. No Cℓ abundances in Group III inclusions are available for comparison. Gold and Mg are less depleted than in Group I.

In the Group II inclusions Na, K, Zn, and Cℓ are enriched relative to C-1 chondrites. Chromium, Mn, and Fe have similar depletion ratios (average = 0.28). The same depletion trend of Mn, Fe, Co and Ni observed in Group III inclusions is also observed in Group II inclusions but to a lesser extent. Gold is depleted to a similar extent as Ni and Co.

The ratios of abundances in the Group II or III inclusions to the Group I inclusions for the volatile elements are shown in Fig. 9. The values for Rb were taken from Gray et al. (1973). For Group I, Rb is the average of

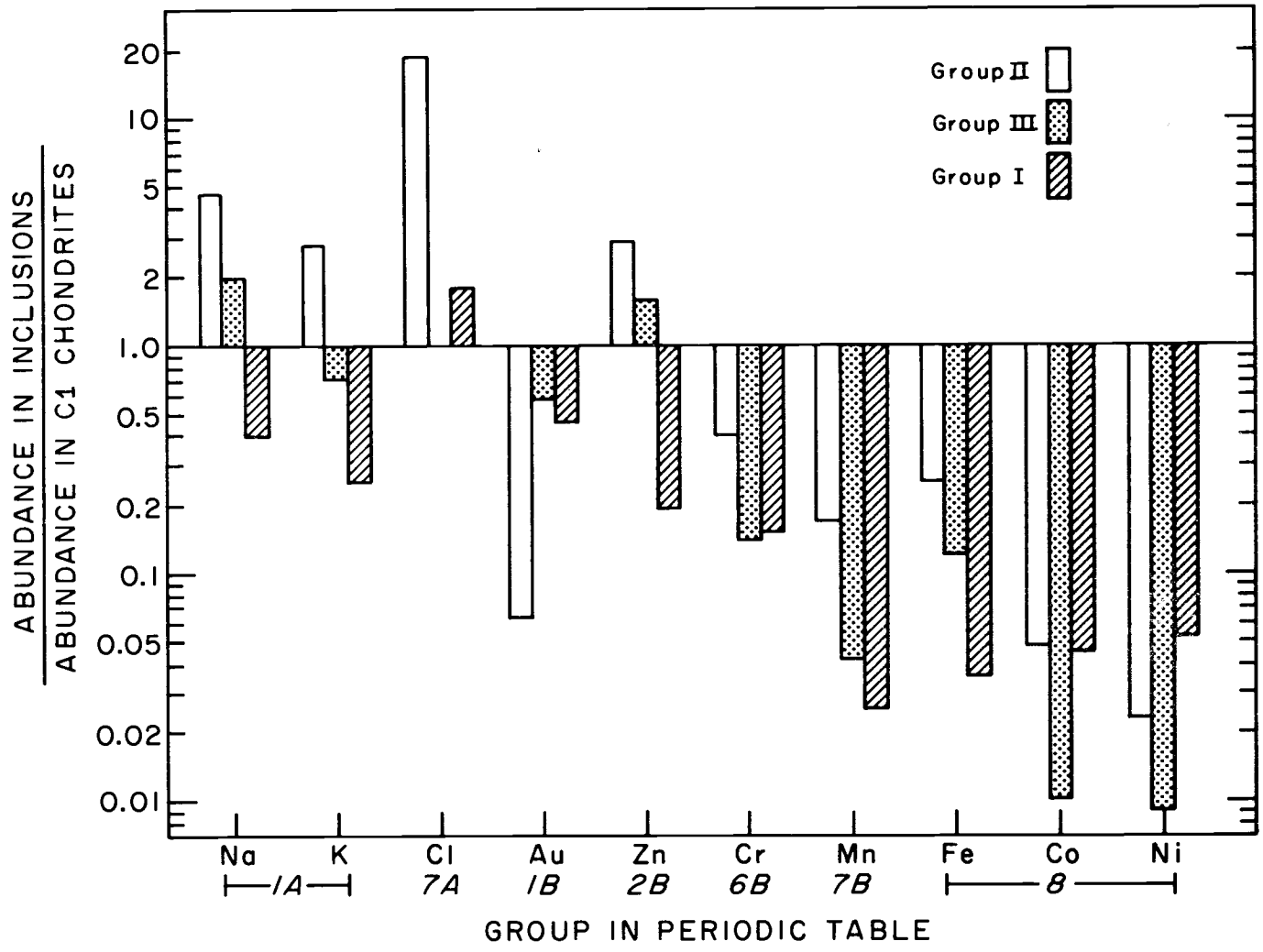

Figure 8. Relative abundances of volatile elements in Allende Group I, II and III inclusions compared to C-1 chondrites.

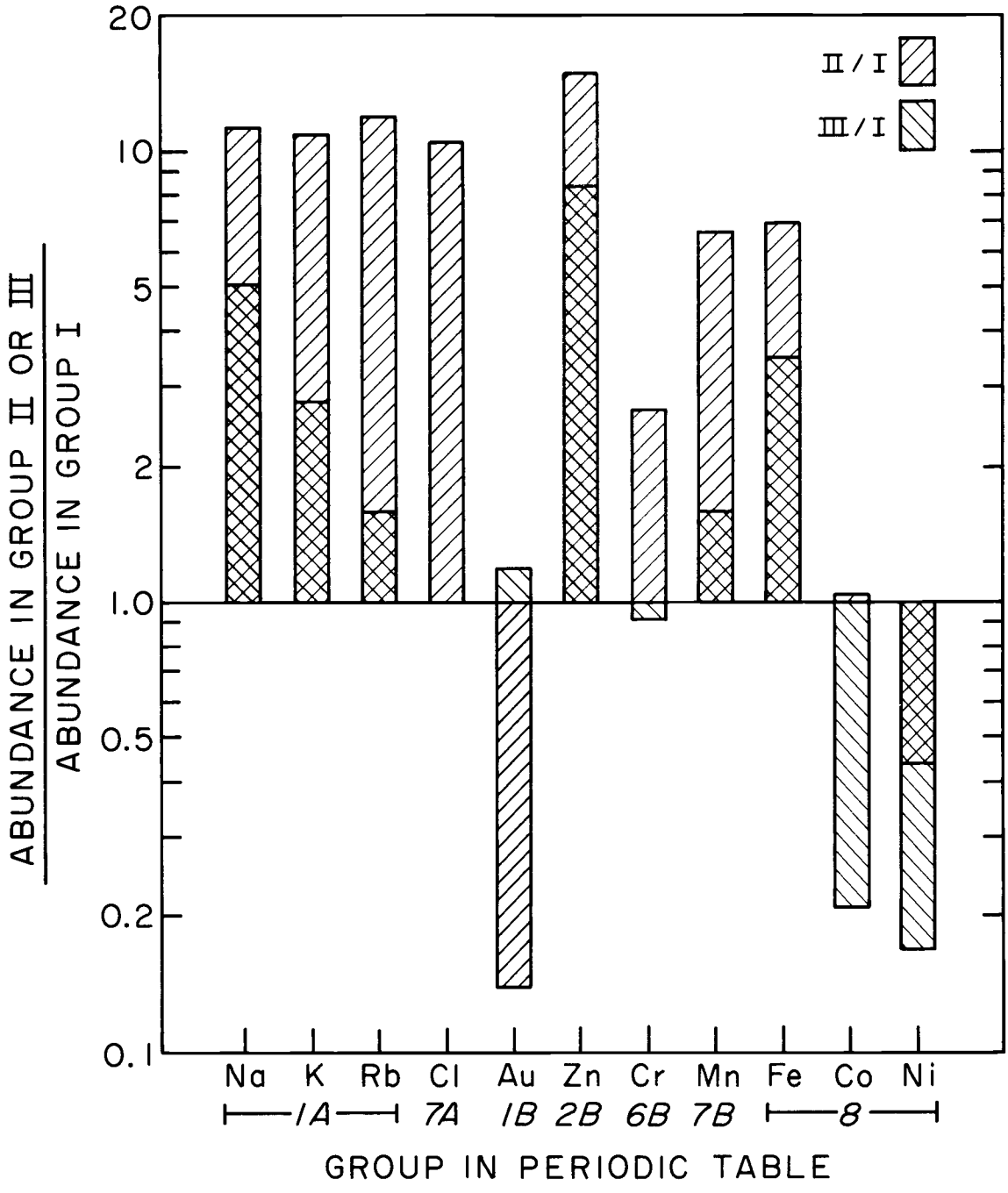

Figure 9. Abundances of volatile elements in Allende inclusions Groups II and III relative to Group I.

B-28, A-2, D-7, and Cl-S2; for Group II Rb is the average of B-29 and B-32; for Group III Rb abundance is that determined in B-30.

Similar enrichments (10-15X) of Group II over Group I are noted for the alkalis (K, Rb, and Na) and also for Cℓ and Zn. The alkalis in Group III compared to Group I are decreasing in enrichment as ionic size is increased. This could possibly be due to a transport effect; the smaller ions of Na should diffuse into the inclusion at a faster rate than the larger K or even larger Rb. The uniform enrichment noted in Group II may then indicate alkalis of primary origin, and not acquired by secondary processes. This idea is further supported by the euhedral cavernous intergrowths of alkali bearing minerals with high temperature minerals such as melilite and grossular (Grossman et al., 1975).

Grossman and Ganapathy (1975) noted low Na, Mn and Cℓ concentrations for coarse-grained inclusions and high Na, Mn, and Cℓ concentrations for fine-grained inclusions. This same pattern is observed here for Group I and II inclusions and is extended to K, Rb, and Zn. The Group III inclusions have concentrations of the above elements intermediate between Group I and II.

What are some implications of the trends between the Groups of refractory and volatile elements?

Fig. 10 is a plot of Ca versus Fe abundances for all the Allende Ca-Al rich inclusions found in the literature, including those which are not classified as Group I, II or III. Although there is scatter, the general trend is decreasing Ca with increasing Fe. Group I inclusions are higher in Ca and lower in Fe than Group II, Group III inclusions are intermediate. Ca minerals condense at higher temperatures than do Fe minerals (Grossman, 1972), implying a larger complement of high temperature minerals in those inclusions with high Ca than those with lower Ca. At the lower temperature implied by greater Fe content most of the Ca was already condensed, leaving a smaller proportion of Ca for condensation into Group II.

The increasing trend from Group I to III to II is demonstrated only by "volatile" elements, the light REE and Ta while those elements that decrease from Group I to III to II are all considered refractory elements. The positive correlations of Na with the other volatiles K, Mn, Cℓ and Zn are shown in Figs. 11 and 12. For Na versus Cℓ, K, or Zn the points fall very nearly on a straight line; Mn versus Na exhibits much more scatter but still shows the same positive straight line trend. The inclusion Cl-S2, which was only tentatively classified as part of Group I, has the highest Na, Zn, and Mn abundances of all the inclusions in Group I and is actually much closer to Group III or II abundances. This suggests that Cl-S2

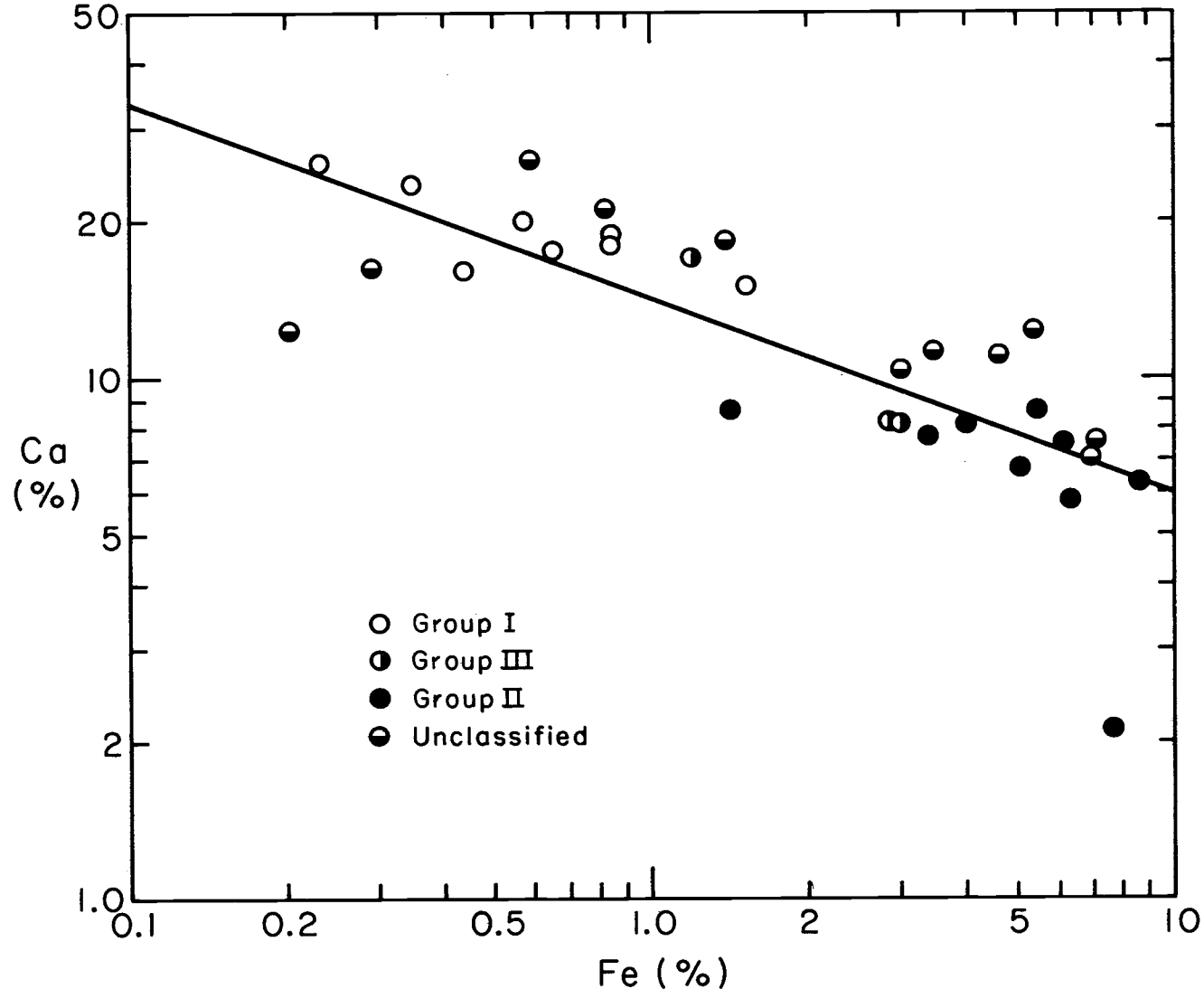

Figure 10. Ca is inversely correlated with Fe in Allende Ca-Al-rich inclusions.

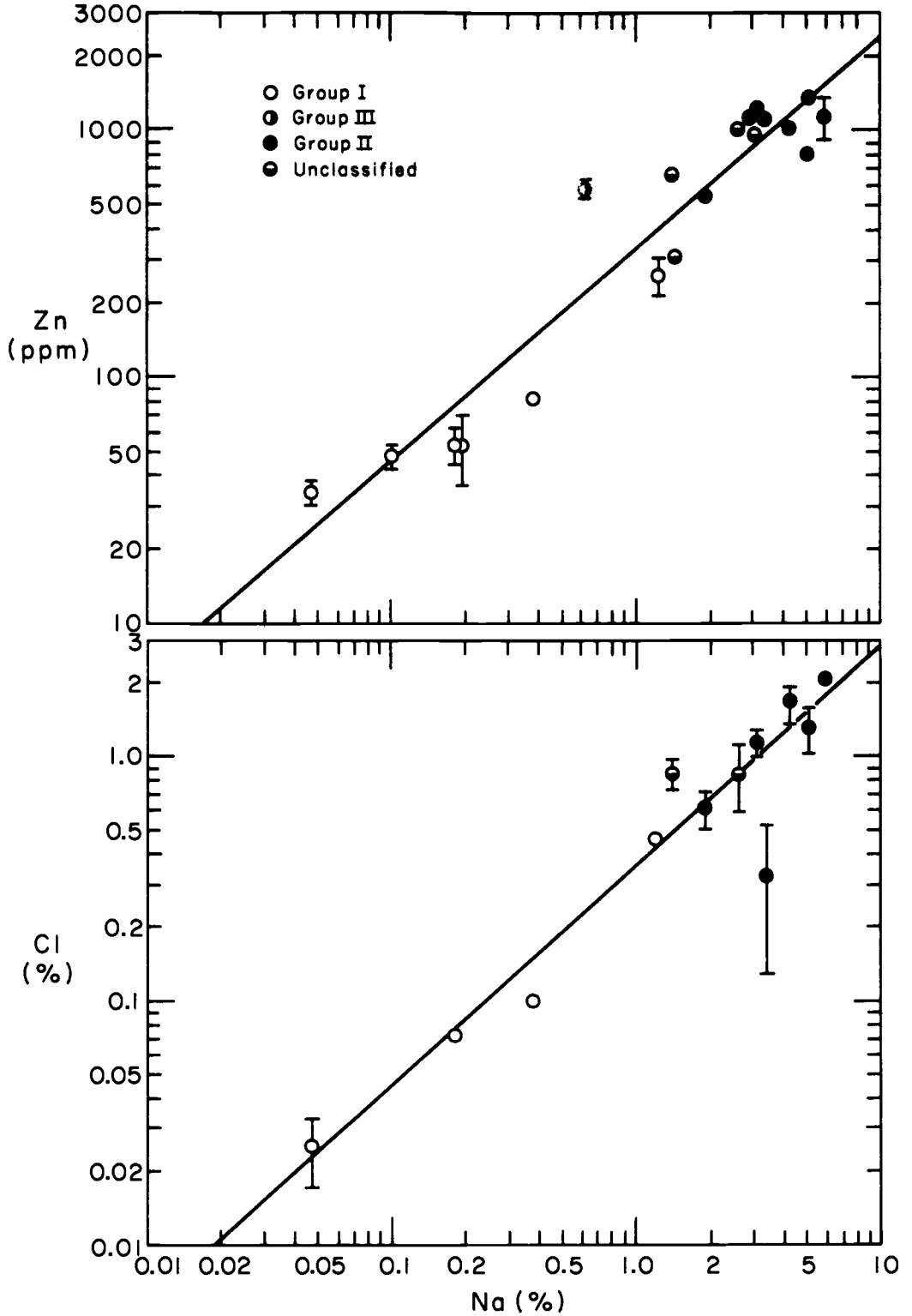

Figure 11. Cℓ and Zn are correlated with Na in Allende Ca-Al-rich inclusions. Error bars denote 1σ counting statistics.

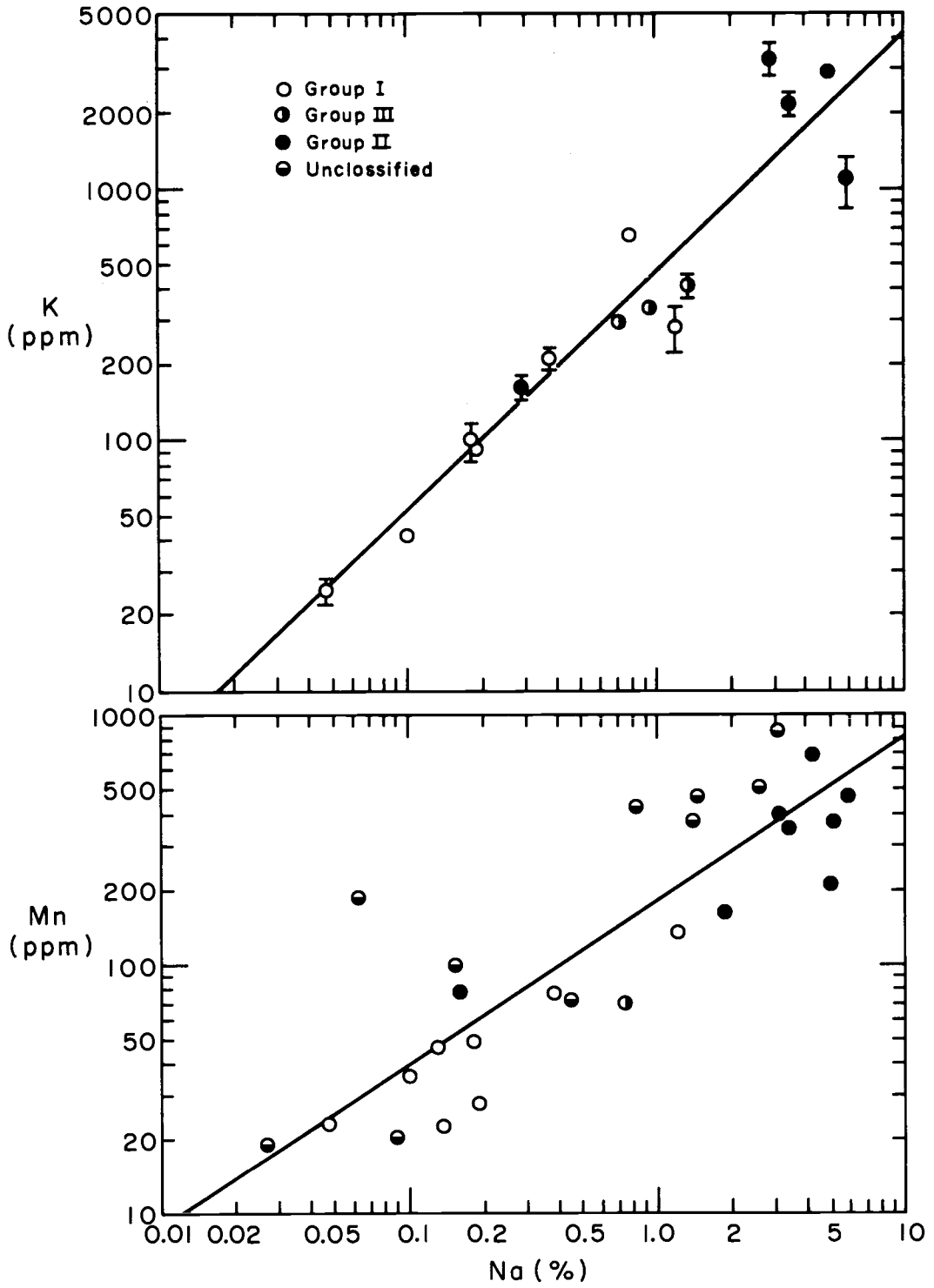

Figure 12. K and Mn are correlated with Na in Allende Ca-Al-rich inclusions. Error bars denote 1σ counting statistics.

should be reclassified. In all cases the Group I inclusions contain the fewest volatiles. Since each correlation is plotted on log-log paper, the relationship is not linear but one corresponding to an exponential relationship of $y = ax^b$.

Siderophile Elements

Grossman and Ganapathy (1976a) demonstrated a positive correlation for the siderophile elements Ir, Os and Ru in Allende coarse-grained inclusions and showed that the ratio Os/Ir was identical to the cosmic ratio. A similar correlation pattern is also observed for Ir-Re (Fig. 13) and is further confirmed by Ganapathy and Grossman (1976). The Ir and Re abundances in the inclusions are correlated along the line defined by the cosmic Ir/Re ratio which was determined from C-1 chondritic analyses by Krahenbühl *et al.* (1973).

Referring to Table 17, it is noted that the predicted condensation sequence of elements condensing as metals is Os, W, Re and Ir. Of these elements, both Os and Re are correlated with Ir. Figure 14 is a plot of W versus Ir using data from this work and that of Grossman and Ganapathy (1976a). Obviously, W is not correlated, which seems to contradict the characterization of W as exclusively siderophile (Amiruddin and Ehmann, 1962).

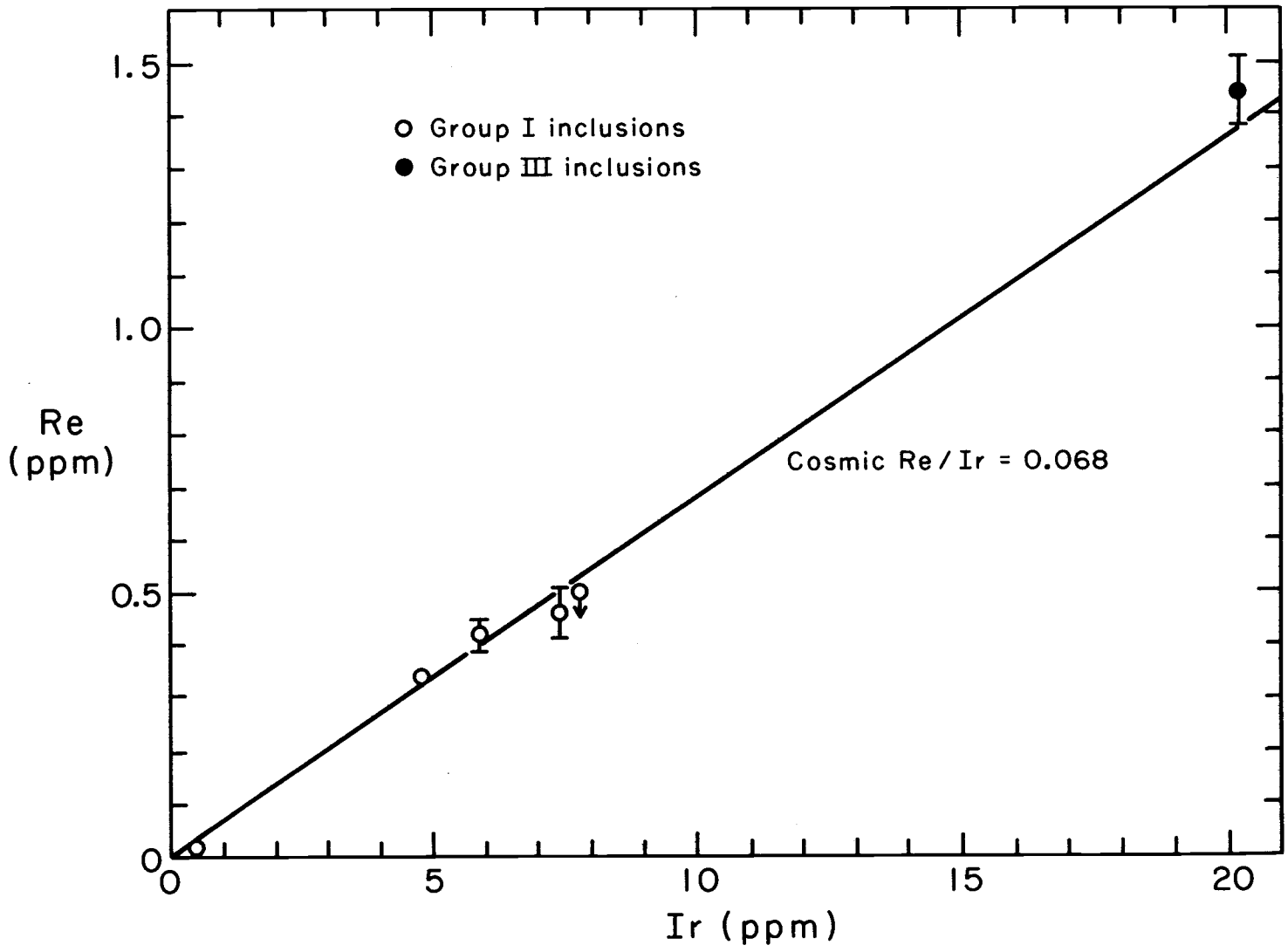

Figure 13. Correlation of the siderophile elements, Re and Ir. Error bars denote 1σ counting statistics.

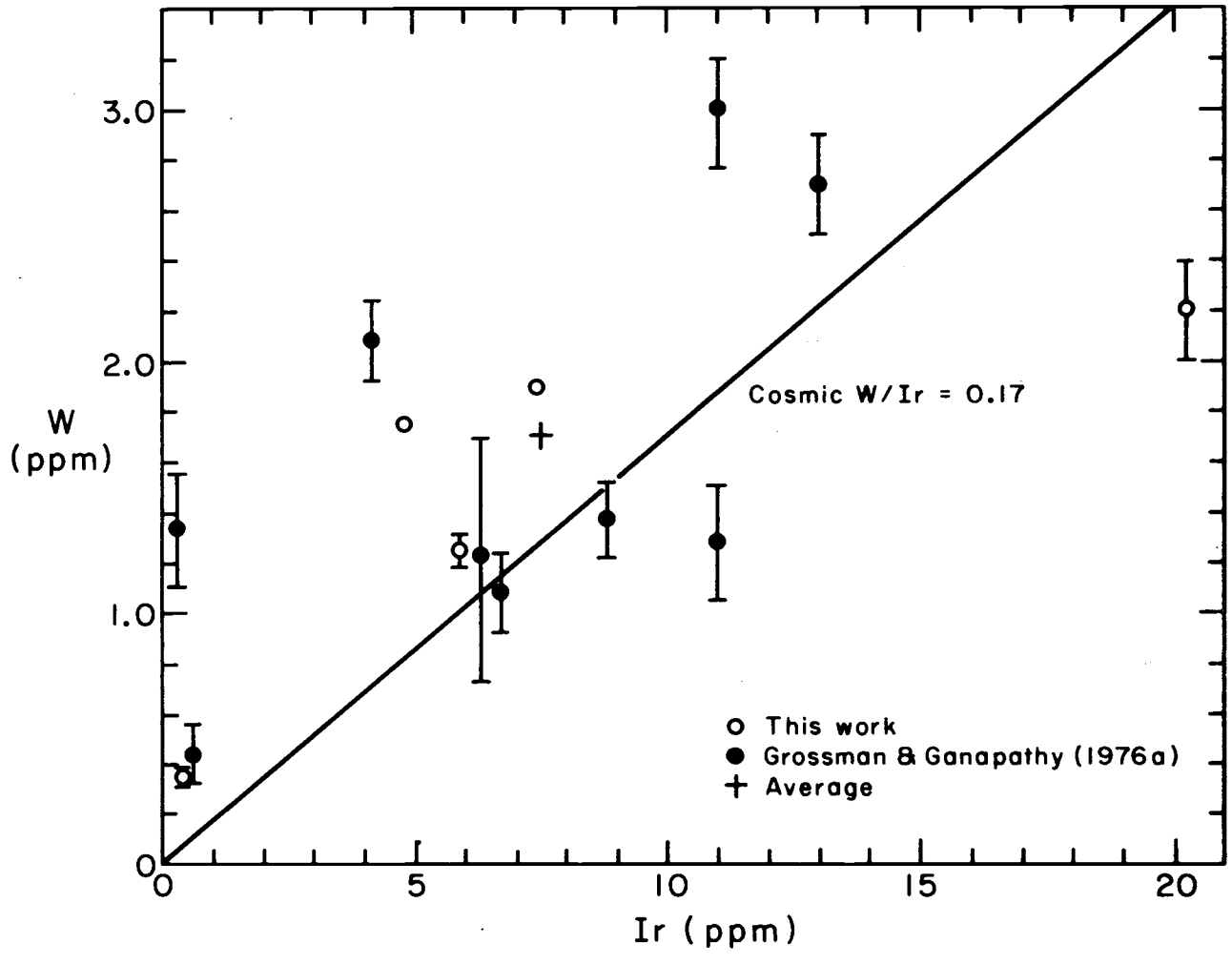

Figure 14. Siderophile elements W and Ir are not correlated. Error bars denote 1σ counting statistics.

The W value of 14.6 ppm in the C1-S2 inclusion was eliminated as being unreasonably high. Since tungsten tools were used to separate the matrix from the inclusions in this work (private communication, Prof. G. J. Wasserburg), it was thought that a minute metal chip from the tools had been included in C1-S2. Thus it is possible that lab contamination could also account for the W scatter observed in this work. However, the data of Grossman and Ganapathy (1976a) also exhibit the same type of scatter and approximately the same abundances of 1-2 ppm which leads to the conclusion that the scatter is real and not laboratory induced.

Using thermodynamic data (JANAF tables, 1967), the free energy of formation can be calculated for the reaction

$$WO_{(g)} + H_2 \rightarrow W_{(g)} + H_2O_{(g)}$$

The equilibrium constant at any given temperature is therefore

$$K_{eq} = \exp(-\Delta G/RT) = \frac{(p_{H_2O})(p_W)}{(p_{WO})(p_{H_2})}$$

The partial pressure of H_2 and H_2O can be calculated for an assumed total pressure (10^{-3} atm) and solar elemental abundances taken from Cameron (1968). Using this information, the fraction of W gas may be estimated from the method of Boynton (1975). At 1900°K and 10^{-3}atm only about one percent of the W is present as metallic gas, while the

rest is WO. A similar calculation was also attempted in order to confirm the assignment of Os, Re and Ir to the metallic state at the condensation temperatures given by Grossman (1973). No $\Delta H^{o}_{f(298)}$ values could be found for OsO or ReO; for IrO the $\Delta H^{o}_{f(298)} \geq 126$ kcal/mol (Brewer and Rosenblatt, 1969). Thus the oxides of Os and Re do not form; the ratio of Ir/IrO $\simeq 10^{7}$ so essentially no IrO forms either.

The W gas condenses to metal at 1885°K (Grossman, 1973) which should shift the equilibrium so that WO will dissociate into $W_{(g)}$ which in turn may condense to $W_{(s)}$ when the p_w equals the W vapor pressure. If cooling is rapid and equilibrium is not maintained, then WO will condense, probably as the oxide WO_2 or WO_3. From thermodynamic calculations (after Grossman, 1973), it is found that WO_2 condenses at 1380°K as the pure oxide, ~170° before WO_3. Therefore it is concluded that W is fractionated between the metal and nonmetal phases of the inclusions and no correlation between W and the metallic Ir should be expected.

It appears that the coarse grained inclusions contain a metallic alloy consisting of Ir, Os, Re and Ru with variable W content. The rest of the W presumably condenses as the oxide WO_2 and is in another phase. Evidence showing the existence of a metal phase consisting of micrometer-sized "nuggets" was discovered in the melilite of a Ca-Al-rich Type A inclusion by Wark and Lovering (1976). They

studied ten nuggets and found variable proportions of the following metals in each nugget: Fe (~10 percent), Ni (~1 percent, Mo (~23 percent), Ru (~20 percent), W (~1 percent), Os (~15 percent), Ir (~10 percent), Pt (~25 percent). In particular, the W content ranged from <0.5-2 percent; the Ir content from <0.5-21 percent. In this work the Ir values ranged from 0.42 ppm (Inclusion A-2) to 20 ppm (Inclusion B-30). If Ir is totally present in these nuggets, then the variability of Ir abundances can be directly related to the quantity of nuggets in each inclusion. This may not be the case as shown from the following calculation: the nuggets ranged in diameter from 0.5 to 3 μm (Wark and Lovering, 1976). For calculation purposes the entire nugget is assumed to be a sphere of Ir metal; a 3 μm nugget thus weighs 3.18×10^{-4} μg. The Ir abundance of inclusion B-30 is 20 ppm which is equivalent to 0.26 μg of Ir. To have 0.26 μg of Ir contributed entirely by nuggets, 820 pure Ir nuggets would be needed! Since the nuggets are not pure Ir and since the largest diameter nugget was used, 820 is clearly a lower limit of the nuggets needed to produce the Ir abundances in Inclusion B-30. Even the lowest Ir content observed (0.42 ppm in Inclusion A-2 which corresponds to 0.0082 μg) requires 26 pure Ir nuggets. Therefore, considering their relative rarity, it does not seem possible that the Ir concentration, as well

as that of Os, Re and Ru which correlate with Ir, can be controlled by the metallic alloy nuggets.

Formation of REE Patterns

The Allende inclusion REE patterns are highly fractionated into irregular patterns, especially in Groups II and III. These new REE patterns were very surprising when first observed (Tanaka and Masuda, 1973), since all other REE patterns ever studied had exhibited flat or smoothly fractionated patterns when normalized to chondrites (ex. Haskin et al., 1966). Smooth REE patterns are expected because the REE (excluding Eu) are chemically extremely coherent. Their main difference is a decrease in ionic radii with increasing mass and atomic number due to the lanthanide contraction. Due to its occasional divalent character, the Eu is sometimes frationated from the other REE which can only be trivalent. This is the well known positive or negative Eu anomaly.

Because of their similar properties, the REE have been used as indicators of differentiation in igneous rocks. Due to their size differences, the REE can be fractionated into different mineral lattices when crystallizing from a melt or during partial melting. The tendency of the REE to be taken up by different minerals may be quantitatively measured through the use of partition coefficients where the coefficient is the ratio of concentration of element

in solid to concentration of the element in the equilibrium melt (Schnetzler and Philpotts, 1968). Thus the smooth REE fractionations can be directly related to the partition coefficients which are directly related to the sizes of the REE as compared to the crystallizing mineral.

Group I Inclusions

The coarse-grained inclusions have mineralogies and textures that indicate solidification from a melt. Pyroxene and melilite separates from these inclusions show complementary patterns (Mason and Martin, 1974), but the overall flat bulk REE pattern of the inclusions is not dependent upon whether or not equilibrium is established between the minerals (Nagasawa et al., 1976). This supports their hypothesis (Nagasawa et al., 1976) that the bulk composition of the coarse-grained inclusions was fixed early with subsequent melting and crystallization of pyroxene and melilite in a closed system. Thus, the overall bulk pattern is not crystallochemically controlled, although the patterns exhibited by the constituent minerals are controlled. This model must be constrained to fit the oxygen isotope anomalies found in mineral separates of coarse-grained inclusions (Onuma et al., 1974). Thus complete melting cannot have taken place since that would result in homogenization of the oxygen isotopes. Nagasawa et al. (1976) suggested that since melilite is not a stable phase

but spinel and pyroxene are stable at the liquidus temperature of a Ca-Al rich melt (Seitz and Kushiro, 1974), small grains of extrasolar spinel and pyroxene survived as nucleating agents for larger grains of spinel and pyroxene. Therefore, the oxygen anomalies between melilite and pyroxene are attributed to small amounts of pre-existing pyroxene and melilite which formed later (Nagasawa et al., 1976). Grossman and Ganapathy (1976b) explain the uniform enrichment of the REE and other refractory elements in the coarse grained inclusions by condensing five percent of the total condensable material with nearly 100 percent of the refractory trace elements such as the REE, Zr, Hf, etc.

The Group I inclusion A-2 does not have the normal unfractionated pattern. The elements Gd to Er and Lu are depleted relative to the rest of the REE pattern (Fig. 3). Europium, which may have a small positive enrichment in the conventional sense, has the same relative abundance as Tm and Yb. As mentioned before, B-32 dark can be considered a two component system: one part being composed of bulk-Allende material and the other part consisting of a pattern of heavy REE (Fig. 15). The B-32 dark pattern with matrix subtracted and the pattern of A-2 are complements of each other. When they are combined, a pattern similar to the other Group I inclusions is obtained, except for depletions of Er and Lu. The oxides of Er and Lu are the least

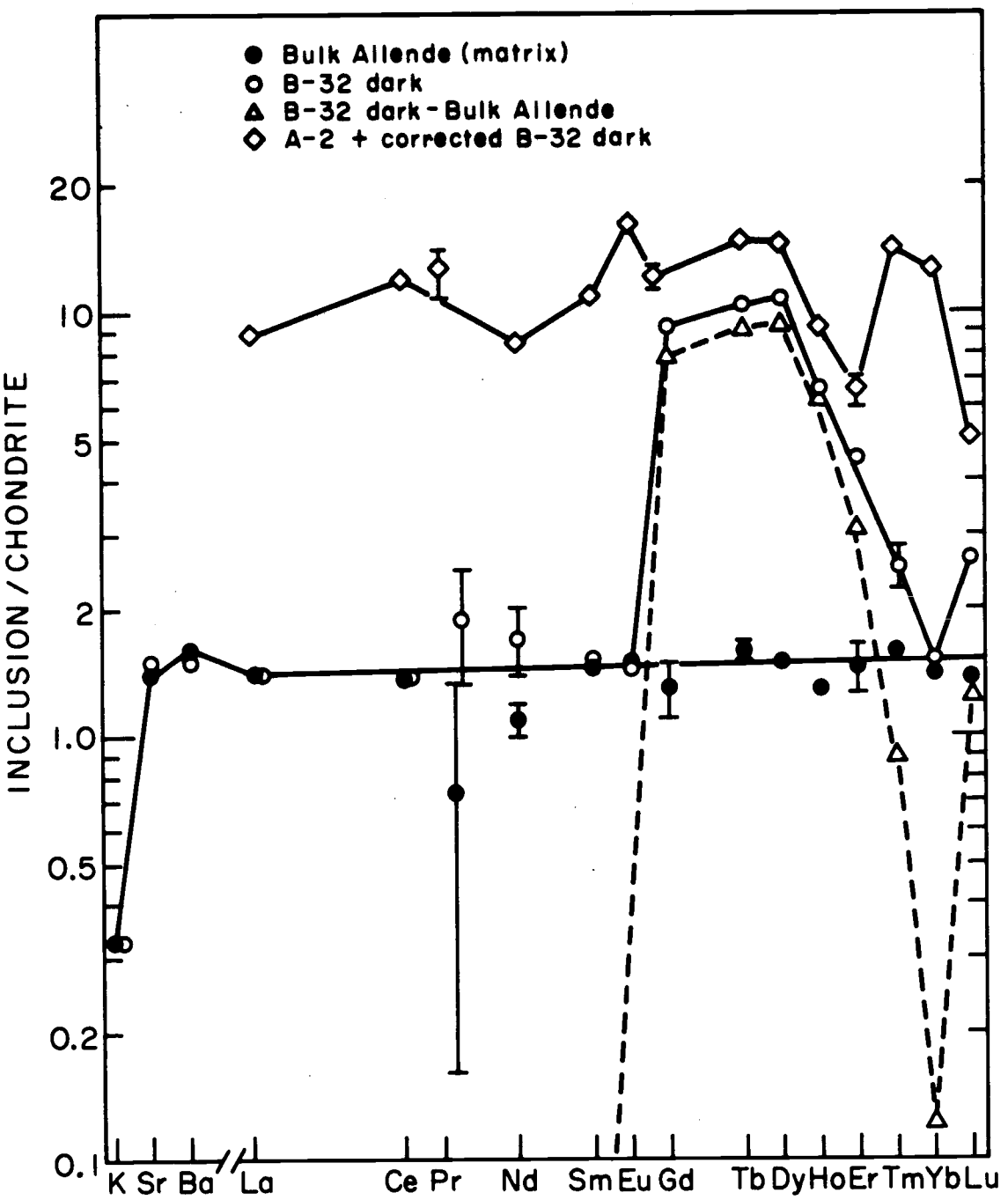

Figure 15. REE in B-32 dark can be considered a two-component system of matrix and intermediate REE. The REE of B-32 dark minus matrix contribution are combined with the REE of A-2 to obtain a pattern similar to normal Group I inclusions, except that the most refractory REE (Lu and Er) are still depleted.

volatile of all the REE; if they condensed first and were lost, a pattern such as seen in Fig. 15 could result.

Group III Inclusions

The Group III inclusions including B-30 show varying intensities of Eu and Yb depletions (Fig. 16, taken from Boynton, 1976). Note that for each analysis the Eu and Yb are depleted to similar degrees. These patterns can be best explained by the thermodynamic equilibrium calculations of Boynton (1975). He considered the REE condensation from a gas to solid to be thermodynamically controlled, rather than size or crystal controlled. When small amounts of La have condensed, the REE pattern shows strong depletions of Eu and Yb. If this fraction is then isolated from the gas, a pattern such as shown by inclusion B-30 should be observed. However, the thermodynamic calculations do not predict similar degrees of Eu and Yb depletions.

The inclusion Cl-S2, tentatively classified as Group I, has an alkali content similar to the Group III inclusions. It exhibits a normal REE pattern (Group I type) except for the depleted Ce. This pattern is not predicted from thermodynamic equilibrium calculations. An obvious interpretation of the Ce anomaly probably involves the oxidized state of Ce^{+4} relative to the normal trivalent state of the adjacent REE. However, the highly reducing environment of the early solar nebula, from which the

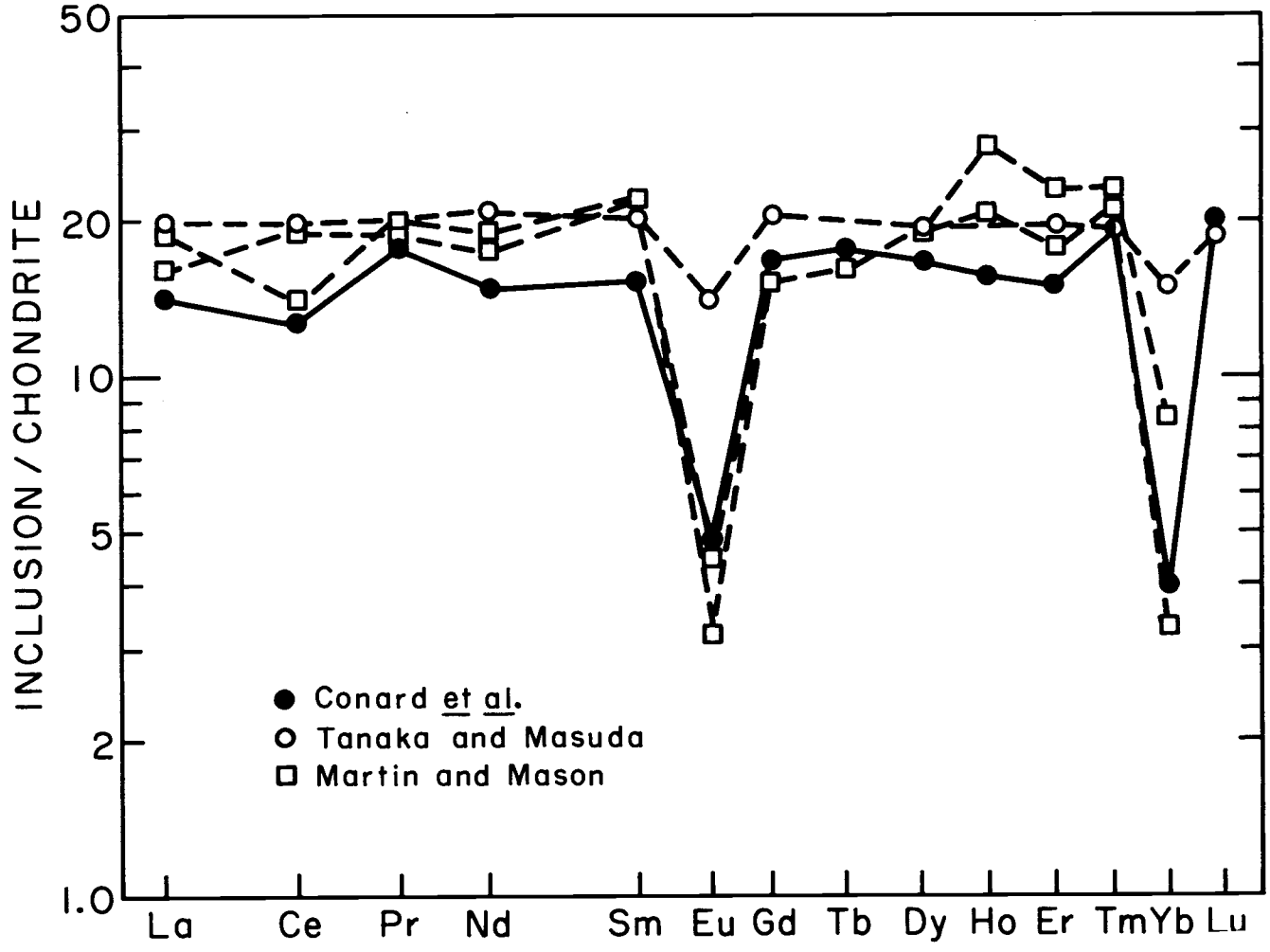

Figure 16. All Group III inclusions that have been analyzed show similar REE patterns but with different Eu and Yb content. From Boynton (1976).

Allende inclusions were formed, presents a formidable obstacle to the postulated Ce^{+4}.

Group II Inclusions

The REE patterns exhibited by the Group II inclusions (Fig. 17, taken from Boynton, 1976) can also be explained by the thermodynamic calculations of Boynton (1975). Here again the relative Eu and Yb are surprisingly the same for each inclusion. The Eu abundance is depleted in each inclusion but relative to its neighbor Lu, Yb is enriched. The condensation may be considered to be a three step process: 1) some REE are condensed and removed from the gas; 2) more REE are condensed and removed from the gas (this is the Group II inclusion fraction); and 3) the remaining REE in the gas condense.

The activities of the condensed REE oxides are unity if they crystallize as pure crystalline solids. The activities are less than unity if the trace REE condense in solid solution with a major phase. The solid solution condensation also allows the REE to condense at higher temperatures than if they were condensing as pure oxides. The following calculations (suggested by Boynton, private communication) assume the REE to be in one major phase and consider the condensation of REE into perovskite at 1650° (condensation temperature of perovskite given by Grossman, 1972). Boynton's equations are all normalized relative to

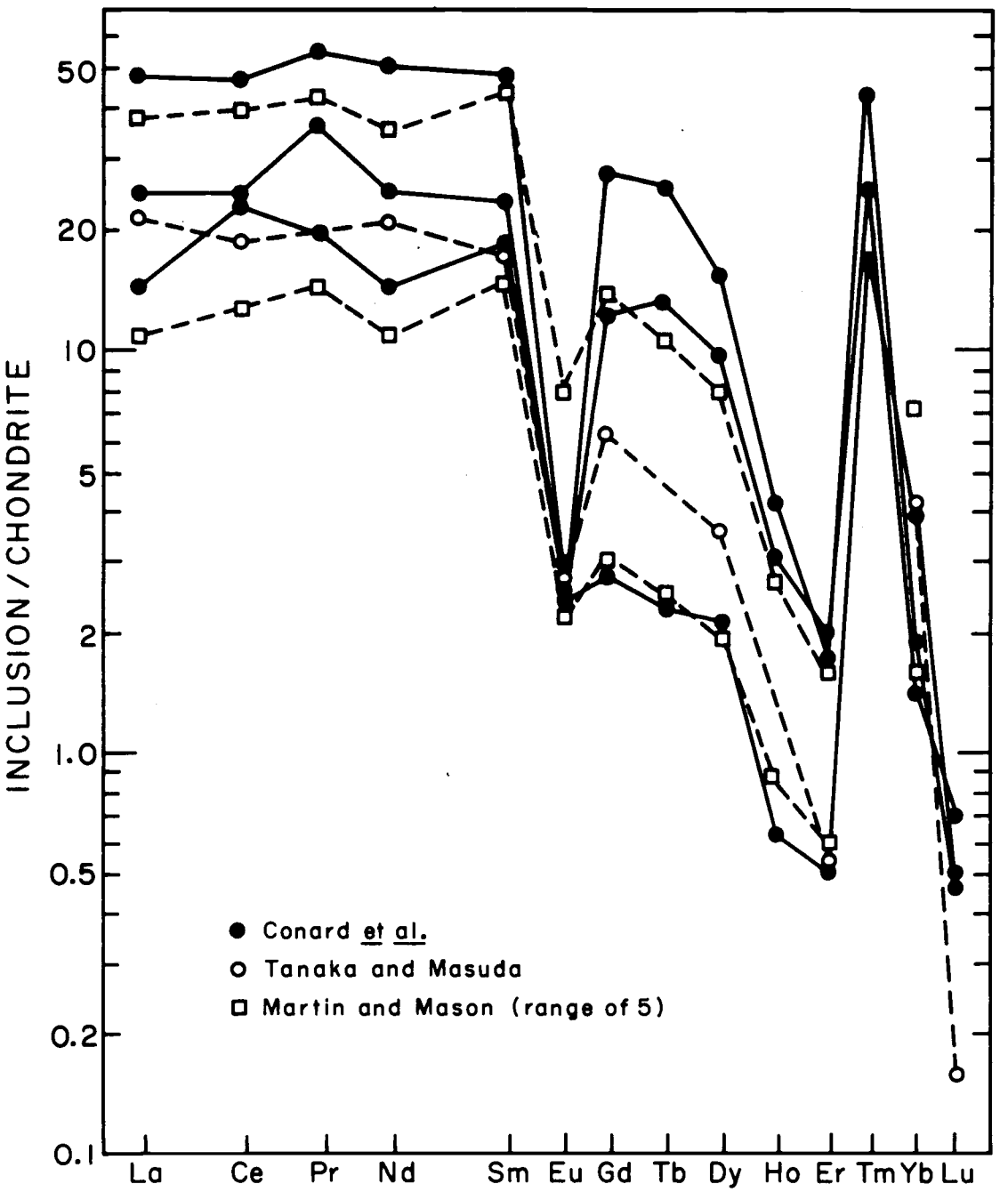

Figure 17. Detailed analyses of all Group II inclusions show similar fractionations with Tm enriched similar to the light REE. Absolute REE content varies over a factor of five. From Boynton (1976).

La, so that ratios are calculated. The relative activity coefficients can be calculated from eq. (9) of Boynton (1975):

$$\frac{x_{EO_{1.5}}/A_E}{x_{LaO_{1.5}}/A_{La}} = \frac{\gamma_{LaO_{1.5}}}{\gamma_{EO_{1.5}}} D_E \frac{1 - F_E}{1 - F_{La}} \qquad (1)$$

$x_{EO_{1.5}}$ = mole fraction of the element E in solid solution.

A_E = solar abundance of E.

γ_E = activity coefficient of E.

D_E = relative solid/gas distribution coefficient of E.

$1 - F_E$ = fraction of E remaining in the gas phase.

For Sm = E, the relative distribution coefficient D_{Sm} is defined as

$$D_{Sm} = \frac{(K_{Sm})^{1/2}}{(K_{La})^{1/2}} \cdot \frac{F_{SmO}}{F_{LaO}} \qquad (2)$$

K_{Sm} is the equilibrium constant for the reaction, $2SmO_{(g)} + H_2O_{(g)} = Sm_2O_3 + H_{2(g)}$ and F_{SmO} is the fraction of the total gaseous Sm present as the monoxide. The fraction of Sm condensed from the gas is

$$x_{SmO_{1.5}}/A_{Sm} = F_{Sm} \qquad (3)$$

Thus, substituting eq. (3) into eq. (1) and rearranging, the following equation for calculating relative

activity coefficients is obtained:

$$\gamma_{Sm} = \gamma_{La} D_{Sm} \frac{(1 - F_{Sm})}{F_{Sm}} \frac{F_{La}}{(1 - F_{La})} \qquad (4)$$

Here, F_{La} is the fraction of La in the gas that first condenses and is lost; $(1 - F_{La})$ represents the fraction of the gas that later condenses into the inclusions. The activity coefficients are not necessarily the same for each sample; therefore, these are calculated for each inclusion that is considered. It is assumed that the La available in the inclusion is 80 percent of the total La available in the system. Since relative activity coefficients are used, only the slope of the curve (γ_E vs ionic radii) is of interest. Thus $(1 - F_{La}) = 80$ percent is quite arbitrary and another value for $(1 - F_{La})$ would be just as convenient.

The Gd, Er, and Lu abundances in the inclusions (normalized to chondrites) are normalized to La = 0.80 and listed in Table 18. Using D_E (reproduced in Table 18; taken from Boynton, 1975) and substituting into eq. (4), the activity coefficients for Gd, Er, and Lu are calculated. On a plot of γ_E vs REE ionic radii a best fit straight line is drawn through the points γ_{Lu}, γ_{Er} and γ_{Gd} and extended so that γ's for the light REE could also be read from the graph. Perovskite shows no preference for La over Nd, i.e., the distribution coefficients are equal (Borodin and Barinsky, 1960). Thus the activity coefficient plot is modified to reflect the behavior of the light REE in

Table 18. Relative activity coefficients for the REE in three Group II Allende inclusions.

		B-32W				B-29				I-3			
	D[a]	X chond[b]	$(1-F_E)^c$	γ'^d	γ^e	X chond[b]	$(1-F_E)$	γ'	γ	X chond	$(1-F_E)$	γ'	γ
La	1	44.4	0.80		1.0	23.2	0.80		1.0	13.7	0.80		1.0
Ce	1.6	43.5			1.0	22.1			1.0	21.5			1.0
Pr	2.6	49.6			1.0	33.1			1.0	18.2			1.0
Nd	0.75	45.3			1.0	22.2			1.1	12.7			1.2
Sm	1.3	46.7			1.3	23.0			1.9	18.5			2.7
Eu	0.0014	2.6			1.6	2.94			2.5	2.6			4.4
Gd	65	31.2	0.56	21	1.8	13.8	0.476	15	3.5	3.1	0.18	3.6	7.0
Tb	200	26.2			2.3	13.6			6.5	2.3			11
Dy	350	16.6			2.6	10.5			8.8	2.2			30
Ho	380	4.2			3.0	3.1			12	0.64			48
Er	4300	2.1	0.038	43	3.5	2.45	0.085	98.6	16	0.65	0.038	42.8	78
Tm	245	42.5			4.0	24.4			23	16.9			130
Yb	0.54	1.86			4.6	1.41			31	3.9			205
Lu	32,000	0.44	0.0080	65	5.2	0.65	0.022	180	42	0.38	0.022	180	330

[a] D from Boynton (1975. D_{Tm} from Boynton (private communication).

[b] Times abundances in ordinary chondrites.

[c] Normalized using La = 0.80.

[d] γ' calculated from eq. (4), see text.

[e] γ from Fig. 16.

perovskite: a horizontal line intersecting with the $\gamma_{Gd} - \gamma_{Lu}$ line is drawn from La to Nd. The constructed plot is then displaced so that γ_{La} to γ_{Nd} is unity. Relative γ_E can be read directly from the graph (Fig. 18). These γ's are uncertain by a factor of three to five due to uncertainties in the D values which are attributed to uncertainties in the thermodynamic data (Boynton, private communication).

Now that activity coefficients have been calculated, condensation curves may be calculated for the inclusions, assuming small fractions of La have condensed. Eq. (4) is rearranged:

$$F_E = \frac{1}{1 + \frac{(1 - F_{La})}{F_{La}} \frac{\gamma_E}{\gamma_{La}} \frac{}{D_E}} \qquad (5)$$

The total amount of REE present in the system is not known; for this calculation a value of 55X chondrites is chosen. The value of this number is not particularly critical as long as it is higher than the abundances of REE in any of the inclusions that have been analyzed. If $(1 - F_E) \times 55$ is now calculated, the REE pattern in the inclusions should agree with the observed patterns if the model is valid. The pattern is much too high; therefore, a second step in the condensation sequence is needed. For a second step, it will be assumed that the inclusions do not condense all of the remaining REE in the gas but only a fraction of them.

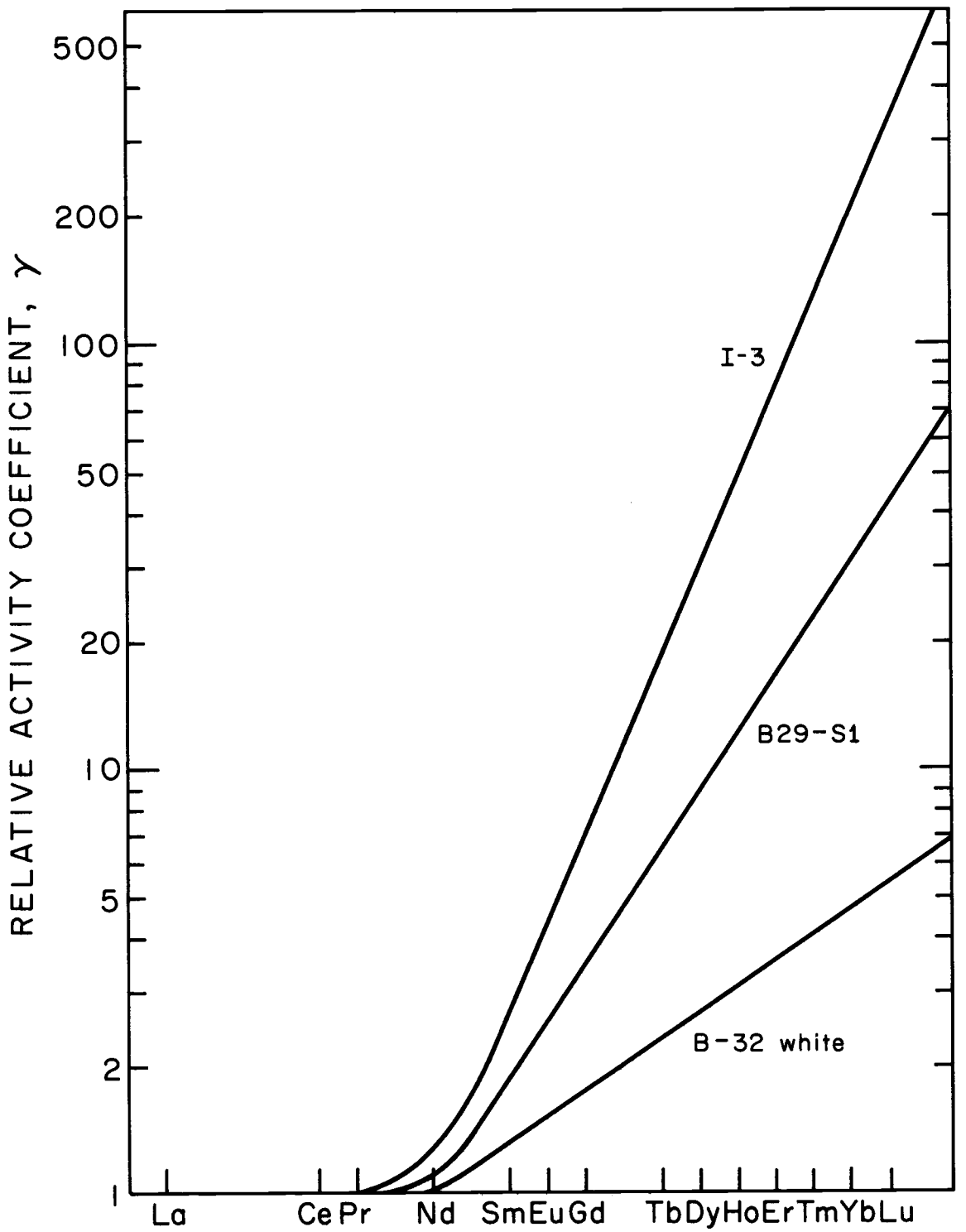

Figure 18. Relative activity coefficients for calculating REE in the Group II Allende inclusions.

A second condensation calculation is needed; the following equation is used:

$$F'_E = \frac{1}{1 + \frac{(1 - F'_{La})}{F'_{La}} \frac{\gamma_E}{\gamma_{La}} \frac{}{D_E}} \qquad (6)$$

In this equation, the fractions of REE in the inclusions are represented by F'_E since the REE are now being condensed out of the gas instead of remaining behind as in the first condensation calculation. The value of F'_{La} chosen here is dependent upon the value chosen for 100 percent REE (in this case 55X chondrites) and upon the value chosen for $(1 - F_{La})$.

To summarize, the value of an element is calculated by

$$H = F'_E \cdot (1 - F_E) \cdot 55 \qquad (7)$$

where $(1 - F_E)$ is calculated from the first step, F'_E is calculated from the second step and 55 is the assumed value given to the total abundance of the REE.

If all the REE are normalized to calculate activity coefficients, and these same activity coefficients used to calculate the theoretical abundances, perfect agreement would be obtained because the argument is circular. The circular argument is avoided here, since the normalized REE used to calculate activity coefficients (Lu, Er, and Gd) are not directly used but are used to draw a best fit straight line among them to obtain a slope for the line.

The activity coefficients (γ) are then arbitrarily normalized to La = 1. The calculated γ's of Lu, Er, and Gd obtained from the inclusions are not really essential; they are just used to make the guess easier as to what the slope of γ should be. Since the γ's are arbitrary, the proper slope of the line could be obtained via trial and error methods without ever using the inclusion abundances, but this would take considerably more time and patience.

Numbers obtained from the above calculations are given in Table 19 for B-32 white, B-29, and I-3. The calculated abundances are compared to the measured abundances in Figs. 19, 20 and 21 for B-32 white, B-29, and I-3, respectively. Agreement between the calculated and experimental values is surprisingly good in most cases considering the simple nature of the calculation. The obvious disagreements with the experimental values in B-32 white are noted for Eu where the calculated value is a factor of 10X too low and Yb which is 10X too high. Smaller disagreements are also noted for Ho which is 4X too high and for Tm which is almost 2X too low. The same type of disagreement in sample B-29 is also noted for the Eu and Ho calculations. In this case, however, the calculated values of Yb and Tm agree well with the measured numbers. For inclusion I-3, it is noted that the calculated values outline the general trend of the pattern. In addition to the Eu and Ho disagreements,

Table 19. Calculated theoretical REE patterns for three Group II Allende inclusions.

	B-32 white			B-29			I-3		
	$(1-F_E)$	F_E'	H	$(1-F_E)$	F_E'	H	$(1-F_E)$	F_E'	H
La	0.98	0.80	43.1	0.91	0.50	25.0	0.40	0.60	13.2
Ce	0.978	0.86	46.5	0.863	0.615	29.2	0.294	0.706	11.4
Pr	0.950	0.91	47	0.795	0.722	31.6	0.204	0.796	8.9
Nd	0.985	0.75	40.6	0.937	0.405	20.9	0.516	0.484	13.7
Sm	0.980	0.80	43.1	0.937	0.406	20.9	0.581	0.419	13.4
Eu	1.0	0.0037	0.20	1.0	0.00056	0.031	1.0	0.00049	0.027
Gd	0.56	0.994	30.6	0.346	0.950	18.1	0.067	0.933	3.44
Tb	0.36	0.997	19.7	0.244	0.969	13.0	0.035	0.965	1.84
Dy	0.27	0.998	14.8	0.203	0.975	10.9	0.054	0.946	2.81
Ho	0.29	0.998	15.9	0.242	0.969	12.9	0.078	0.922	3.94
Er	0.039	1.0	2.14	0.036	0.996	1.97	0.012	0.988	0.65
Tm	0.45	0.996	24.6	0.476	0.918	24.0	0.261	0.739	10.6
Yb	0.998	0.315	17.2	0.998	0.0177	0.97	0.996	0.0039	0.21
Lu	0.0082	1.0	0.45	0.013	0.999	0.714	0.0068	0.9932	0.371

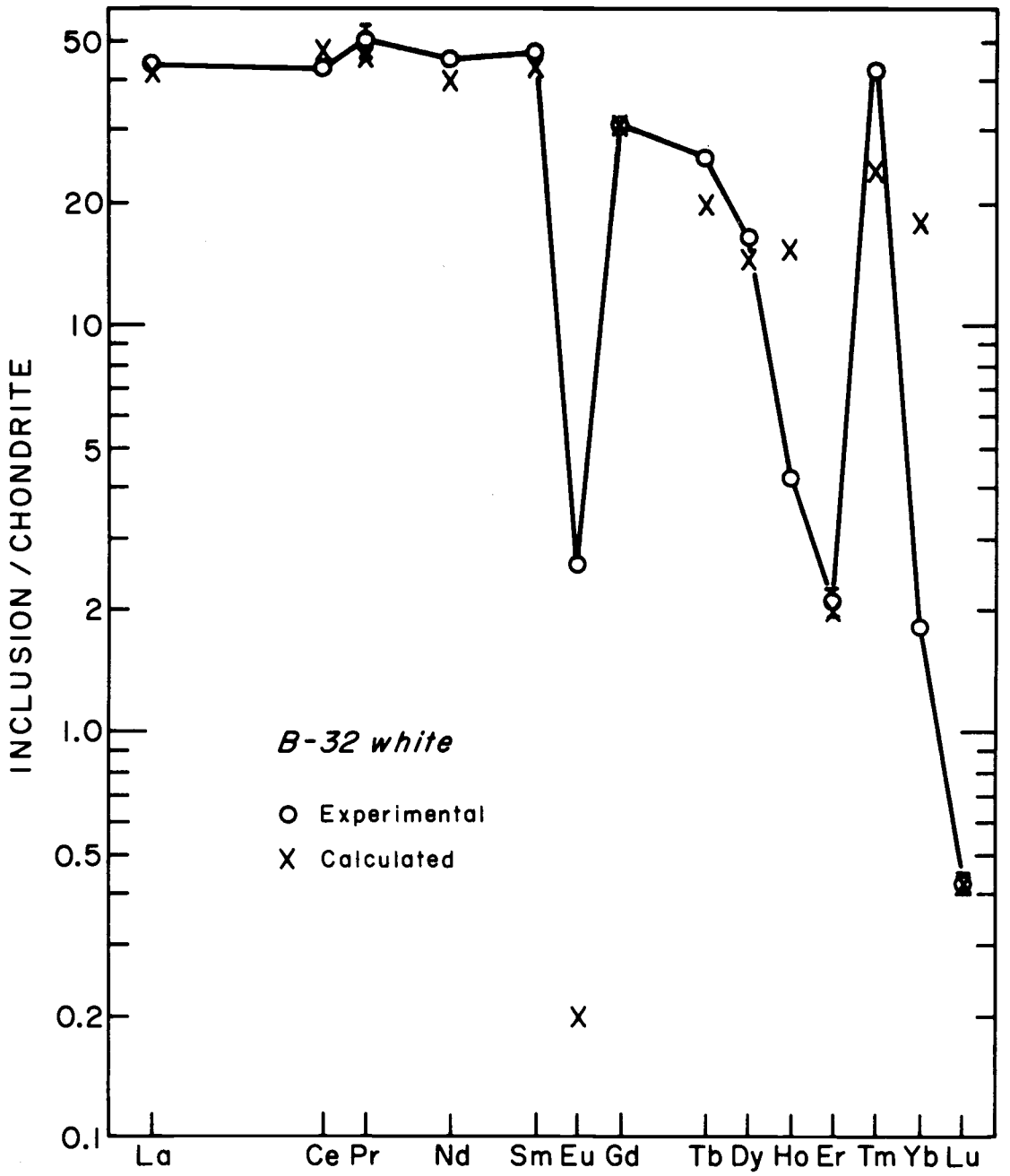

Figure 19. Experimental and calculated REE patterns for the Allende Group II inclusion B-32 white.

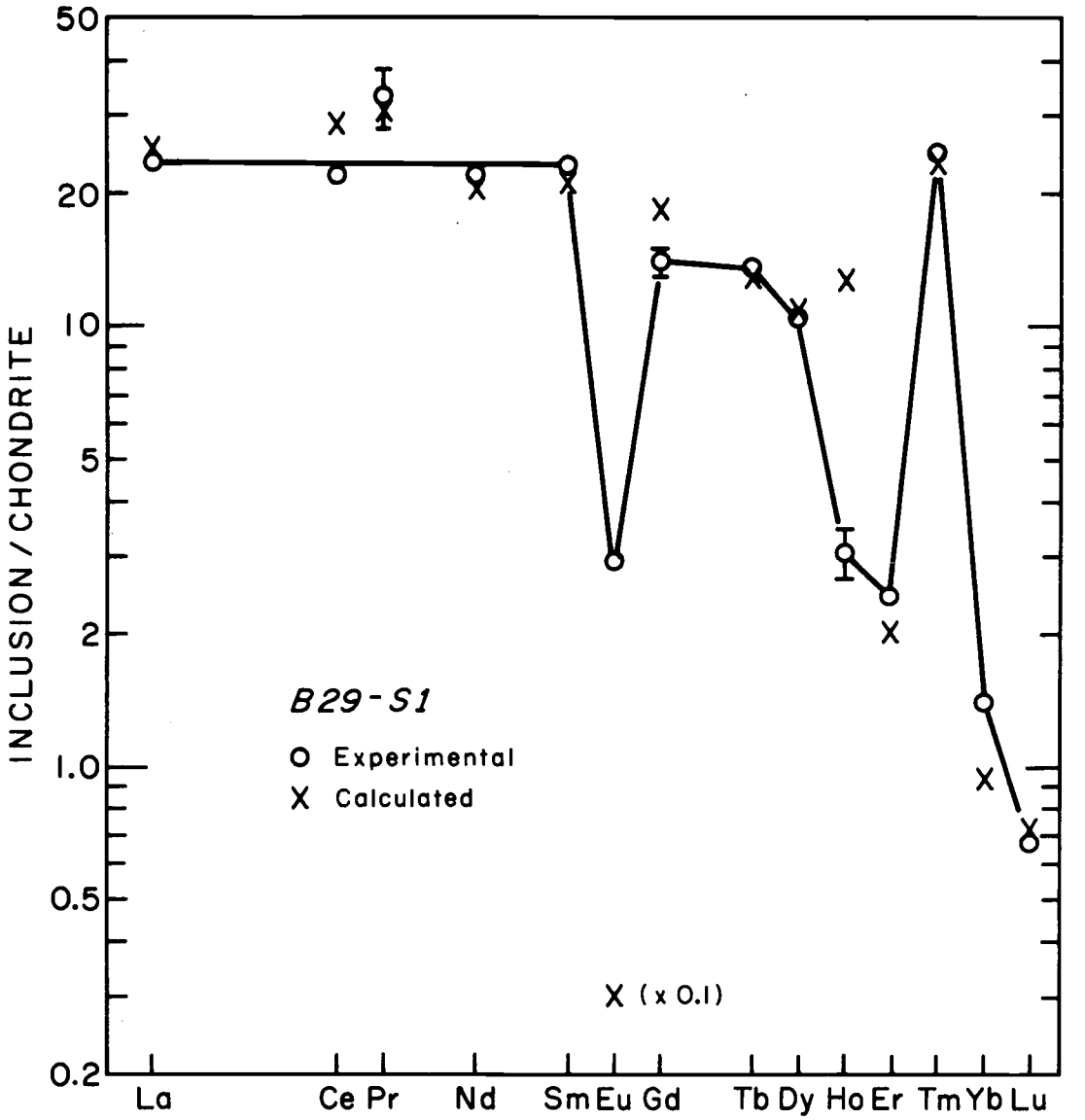

Figure 20. Experimental and calculated REE patterns for the Allende Group II inclusion B29-S1.

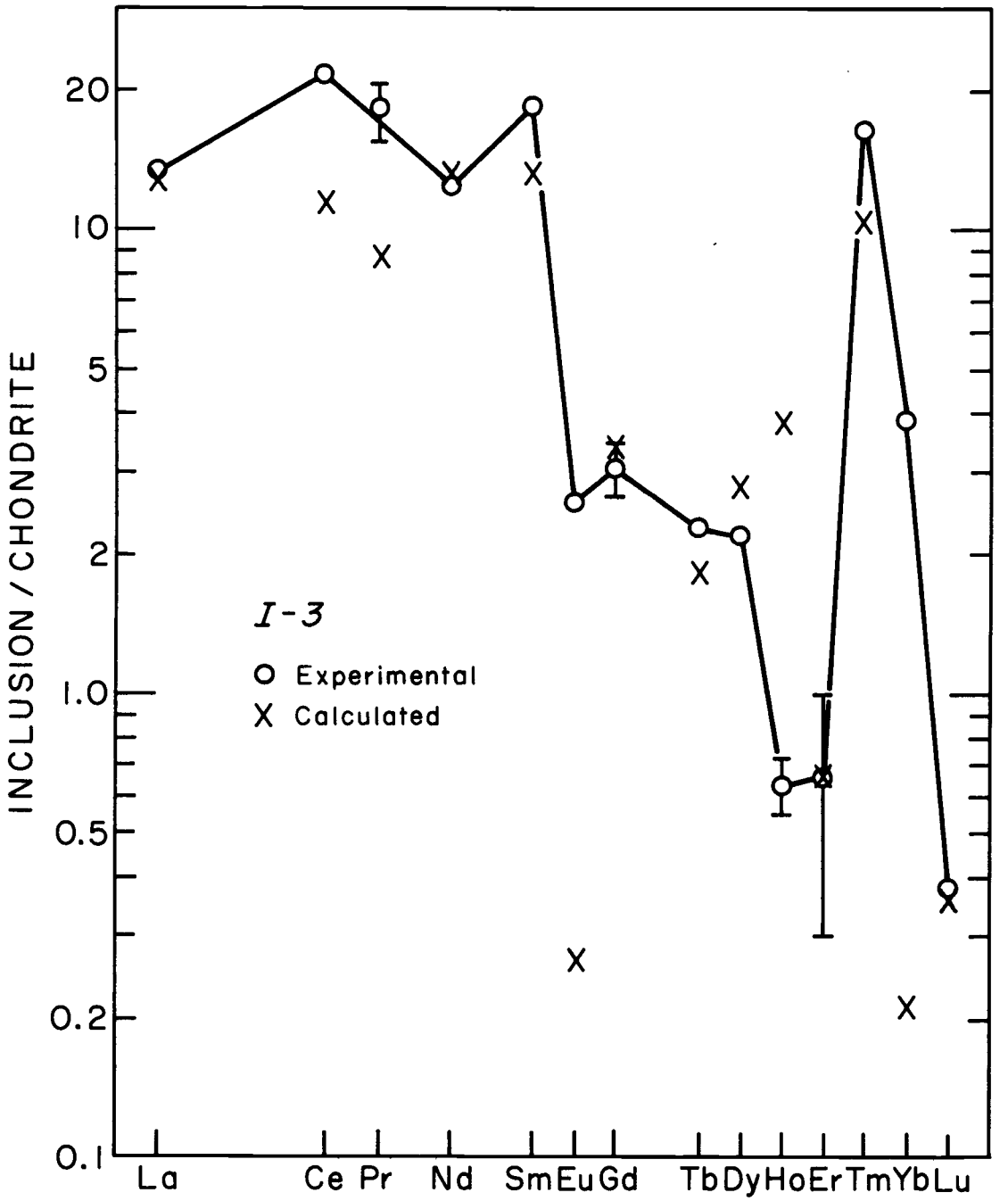

Figure 21. Experimental and calculated REE patterns for the Allende Group II inclusion I-3.

Yb is 20X too low and the zig-zag pattern of the light REE is not reproduced in detail.

What is different about the calculation of I-3 as compared to B-29 or B-32 white? The activity coefficient curve of I-3 is by far the steepest of the three inclusions. Probably more important is the large fraction of gas assumed lost before the inclusions condensed. To make the calculation of I-3 work as well as it does, 60 percent of the total REE available has to be lost before I-3 condenses. This is certainly a much larger fraction of REE that are lost compared to the two percent and nine percent REE losses for B-32 white or B-29, respectively. Apparently the calculation is not valid when a large fraction of the REE are considered lost as appears to be the case for I-3. Thermodynamic equilibrium is probably not the only contributor to this REE pattern; instead a more complex sequence of events must have occurred to form I-3.

For the B-29 and B-32 white inclusions, it was pointed out that the calculated Ho values were too high by a factor of 4X in both cases. In addition, Ho in I-3 is 6X too high. The systematically high Ho values are probably due to the uncertainties in the activity coefficients caused by the uncertainties in the thermodynamic data and are within the uncertainty of the D values. The calculated Eu is too low by factors of 10X (B-32 white) and 100X (B-29); however, these discrepancies should not be considered a

serious failure of the model considering the complex nature of Eu. At 1650°K only 34 percent of the total Eu is present as gaseous EuO (Boynton, 1975). The D coefficient is calculated considering the Eu-EuO fractionation; but if some Eu condensed at the same time as the EuO, the inclusion would contain more Eu than the calculation predicts, which is experimentally observed.

The calculated Yb is 9X too high in B-32 white, 18X too low in I-3, and approximately agrees with the observed abundance in B-29. The D coefficient is calculated for YbO condensing to Yb_2O_3, when actually $>10^5$ of the Yb is present in the atomic state rather than the monoxide (Boynton, 1975). Therefore, it is probably accidental that the Yb calculation for B-29 yields the experimental number.

The theoretical curve for I-3 predicts both Eu and Yb to be much lower in abundance than experimentally observed. This suggests the addition of a component enriched in Eu and Yb such as that proposed to be lost during the formation of the REE pattern of inclusion B-30.

Therefore, the thermodynamic model appears to be a first approximation for interpretation of the sharply fractionated REE patterns observed for Group II inclusions.

Although the normalized abundances of Eu and Yb in Groups II and III vary from inclusion to inclusion, within every inclusion the Eu and Yb are very similar. This is also the case for the Group I inclusion A-2 which has a

fractionated pattern and Cl-S2 which has a negative Ce anomaly. This observation suggests covariance of Eu and Yb as divalent ions; however, the ratio of Yb(II)/Yb(III) $\approx 10^{-6}$ at 1360°K (Boynton, 1975) which argues against the presence of divalent Yb.

The elements Eu and Yb are the most volatile of all the REE. A speculation of what may have occurred to cause their covariance is as follows: The Group II inclusions (without Eu and Yb) condensed and started to gravitationally settle from the gas so that they are not now in equilibrium with the entire gaseous volume. A fraction of the gas that is not in contact with the inclusions is swept away. The remaining REE in the gas condense into the Group II inclusions. Relative to the rest of the REE, Eu and Yb are depleted, although the entire Eu and Yb in the fraction of gas that was not blown away condensed into the Group II inclusions (Boynton, private communication). This model is not without its problems since the other elements of higher volatility than Eu and Yb would also be expected to have similar enrichments as Eu and Yb and this is not the case.

Sr Data

An important constraint in any theory of how these REE patterns were formed is the common degree of enrichment or depletion of Eu and Sr. It is immaterial what type of inclusion is being considered; the Eu and Sr abundances are

covariant and nearly equal on a chondritic normalized basis. This is particularly striking in the high-alkali inclusions which have large negative Eu depletions.

Traditionally, divalent Eu is associated with Sr due to their similarities in ionic size and charge. The selective partitioning of Eu^{+2} from the other REE is accomplished by minerals with a high affinity for Eu (such as plagioclase) crystallizing from a melt. In the low alkali inclusions, there is evidence of recrystallization; thus Eu and Sr could be preferentially taken up by the Ca-bearing mineral melilite which may be playing the same role as anorthite in plagioclase crystallization. An intriguing question concerns the entry of Sr in the inclusion. It is suggested that both Sr^{2+} and Eu^{2+} reside in the same mineral.

The high alkali (fine grained) inclusions show no evidence of ever having been molten (Grossman et al., 1975) so explanation using crystallization from a melt cannot be used. From thermodynamic equilibrium calculations similar to those used from W, the condensation temperature of the pure crystalline oxides can be calculated. The following equilibria were considered using a total pressure of 10^{-3} atm and solar elemental abundances:

Condensation Reaction	$T_{condensation}$ (°K)
$Sr_g + H_2O_g = SrO_s + H_2$	1195°
$2\ Eu_g + 3\ H_2O_g = Eu_2O_{3s} + 3\ H_2$	1127°

$$2\ EuO_g + H_2O_g = Eu_2O_{3s} + H_2 \qquad 1140°$$

$$Eu_g + H_2O_g = EuO_s + H_2 \qquad 1079°$$

Thermodynamic data was taken from Hultgren et al. (1973), Brewer and Rosenblatt (1969), Gschneider et al. (1973), JANAF Tables (1961), and Handbook of Chemistry and Physics (1970-1971).

The calculation for Sr is only an approximation since the free energy for the reaction $Sr_g + 1/2\ O_{2\ g} = SrO_c$ was calculated from coefficients for the free-energy equation (Handbook of Chemistry and Physics, 1970-1971) that were extended approximately 500°C below the valid temperature range.

There is less than 120° difference in the condensation temperatures of Sr and Eu. In a slowly cooling equilibrium condensation this difference would be large enough to preclude the simultaneous condensation of Sr and Eu. However, in a nonequilibrium rapid cooling situation, the 120° difference in condensation temperatures is probably not significant.

Since the condensation temperatures of the pure oxides of Eu and Sr are so low, it is more likely that they condensed at a higher temperature in solid solution with a major mineral phase. It has already been shown that Eu does not condense entirely as Eu_2O_3 in the high alkali inclusions. The theoretical estimate of Eu abundances in the high alkali inclusions is 10 to 100 times lower than the

experimental abundances indicating that another source of Eu may possibly be contributing to the total Eu content in these inclusions. Since 66 percent of Eu is present in the atomic state and since Eu and Sr are similarly enriched, it is suggested that Eu and Sr are co-condensing as divalent ions into a common mineral phase, possibly melilite which has an affinity for Eu over the trivalent REE.

Sm-Nd Fractionation

A new method of Sm-Nd age dating has been suggested by Lugmair (1974) which may be adapted to systems with fractionated Sm/Nd ratios; i.e. non-chondritic. Because of this fractionation restriction, the method would not be applicable to inclusions B29-S1 or B-32 which have chondritic Sm/Nd ratios. Inclusions A-2, C1-S2, and I-3 with ratios of about 1.4 could be likely candidates for this type of age dating, assuming there is still a portion of these inclusions that have not undergone destructive analysis.

Olivine Aggregate

Inclusion I-8 is tentatively classified as an olivine aggregate based upon its Fe content and similarity to the bulk Allende which is mostly olivine (see discussion in the mineralogy section). Unfortunately, the activation for short lived radionuclide generation was not carried out on

this sample so most of the major element data (especially Mg and Al) are not available.

Very little analyses have been done on olivine aggregates or chondrules. Major element data for a dark inclusion and a Type c chondrule published by Clarke et al. (1970) constitute the first analyses of these inclusions. Tanaka and Masuda (1973) analyzed Al, Ca and REE in a mixture of three olivine chondrules; Martin and Mason (1974) analyzed three olivine inclusions for major and trace element (REE) concentrations but did not specify if they were chondrules or aggregates. The mineralogy of olivine aggregates is extensively discussed in Grossman and Steele (1976) and a trace element study of an olivine aggregate mistakenly thought to be a Ca-Al rich fine grained inclusion appears in Grossman and Ganapathy (1976b). The available data for olivine inclusions is compared in Table 20. It is obvious that the olivine inclusions are extremely variable in composition. The FeO composition of I-8 (about 27 percent) is comparable to the dark inclusion in Clarke et al. (1970) and to the bulk Allende. The FeO composition of the other inclusions in Table 20 is about nine percent.

The REE abundances vary over two orders of magnitude. The composition of I-8 is similar to the olivine chondrules of Tanaka and Masuda (1973) and to the lower limit of the range defined by Martin and Mason (1974). Tanaka et al.

Table 20. Comparison of elemental content of Allende olivine chondrules and aggregates with the Bulk Allende.

	I-8 (This work)	Bulk Allende	Clarke et al. (1970)		Tanaka and Masuda (1973)[a]	Martin and Mason (1974)		Tanaka et al. (1975)[b]	Grossman and Ganapathy (1976b)[c]
			Dark inclusion	Type c chondrule		Range	Average		
TiO_2 %		0.17±0.03	0.13	0.12		0.17-0.30	0.22		
Al_2O_3		2.9±0.1	2.56	17.8	2.95	3.4-9.4	5.7	0.62	
FeO	23.1±0.4	31.3±0.3	31.4?	8.8		9.6-11.0	10.5		9.23±0.05
MgO		26.6±0.4	23.91	15.2		23.5 36.6	31.8		
CaO	3.7±0.3	2.3±0.2	3.0	5.3	2.71	2.7-8.3	4.7	0.180	1.29±0.07
Na_2O	1.06±0.02	0.46±0.01	0.34	10.6		0.45-2.7	1.5		
K ppm	1000±200	235±6	<83	4980		250-1660	750		
Sc	12.4±0.1	10.7±0.5							9.45±0.01
Cr	2300±100	3550±200	3830	1368					1800±10
Co	385±10	680±20							11.1±0.1
Ni	10200±600	13700±500							
Zn	35±10	108±8							104±2
Rb						1.1-20	6.9	0.67	
Sr	18.6±0.6	15.0±0.4				13-20	18	2.44	
Ba		6±2						18.0	
La	0.51±0.03	0.48±0.02			0.648	0.79-1.9	1.2	0.021	1.79±0.04
Ce	1.4±0.3	1.16±0.06			1.64	2.5 4.8	4.0	0.32	5.2±0.2
Pr	<0.25	0.09±0.07				0.32-0.72	0.45		
Nd	1.0±0.2	0.71±0.09			1.18	1.6-3.1	2.1	0.029	
Sm	0.296±0.003	0.286±0.004			0.379	0.49-1.1	0.73	0.0098	1.13±0.01
Eu	0.124±0.003	0.110±0.001			0.140	0.13-0.19	0.16	0.0082	0.065±0.006
Gd	0.3±0.1	0.33±0.06			0.500	0.46-1.1	0.75	0.0122	
Tb	0.079±0.006	0.077±0.004				0.08-0.17	0.12		0.18±0.04
Dy	0.55±0.01	0.46±0.01			0.618	0.53-0.92	0.75	0.0140	0.7±0.5
Ho	0.121±0.005	0.101±0.003				0.13-0.19	0.16		
Er	0.44±0.02	0.29±0.04			0.398	0.38-0.60	0.47	0.0098	
Tm	0.09±0.01	0.051±0.004				<0.2	<0.2		
Yb	0.34±0.01	0.315±0.009			0.406	0.47-0.70	0.60	0.0097	0.15±0.03
Lu	0.050±0.001	0.046±0.001			0.0600			0.00152	
Ta		0.13±0.04							0.13±0.02
Ir	0.84±0.05	0.78±0.06							0.004±0.001
Au	0.57±0.03	0.118±0.006							0.009±0.002

[a] Mixture of three olivine chondrules

[b] Olivine chondrule.

[c] Olivine aggregate.

(1975) found a giant olivine inclusion that is about 40X lower than the other published REE values for olivine inclusions. The olivine inclusion measured by Grossman and Ganapathy (1976b) has REE similar to the upper limits found by Martin and Mason (1974) except for Yb which is a factor of three smaller than their lower limit.

Not enough detailed analyses have been done to attempt to define any patterns or trends in olivine inclusions. It is also probably not valid to compare olivine chondrules and olivine aggregates as has been done above. The variability of the olivine is reflected in the major element compositions; the presence of varying amounts of Al_2O_3, CaO and the alkalis is due to the common accessory minerals nepheline, sodalite, and other Ca-Al rich phases (Grossman and Steele, 1976).

From the above discussion, it is evident that inclusion I-8 is not very similar to olivine inclusions and aggregates analyzed by other workers. It may be of particular importance however, since it possibly contains a true Tm positive anomaly (Fig. 3). It is difficult to understand why this anomaly should be present. The normalized Tm abundance is 1.7X higher than its neighbor Yb on the light REE. The Tm has a large counting statistics error (~20 percent) associated with it; 2σ from the experimentally determined abundance would place the lower limit of Tm along the line defined by the other REE. Thus, this

positive anomaly may be statistical fluctuation. The anomaly, if it is true, is not predicted by equilibrium thermodynamics, nor is it expected from crystal control relations. Since Tm can only be trivalent, it should follow the other trivalent REE in any melting or crystallizing process.

SUMMARY AND CONCLUSIONS

The differences in mineralogy and trace element content between each group of Ca-Al rich inclusions indicate differences in their chemical histories. Group II is much more enriched in volatiles, the light REE and Ta than is Group I, while Group III has intermediate concentrations. Refractories other than the light REE and Ta are highest in the Group I inclusions, decreasing from Group I to III to II. Thus it appears that Group I inclusions were formed by a higher temperature process than Group II or III adding support to Martin's (1976) or Grossman and Ganapathy's (1976b) theories of condensation.

The siderophile elements Ir and Re are linearly correlated along a line defined by cosmic ratios and probably are combined as an alloy. Tungsten which is usually thought of as siderophile in meteorites is 99 percent WO in the gaseous phase and would condense as WO_2 at 1380°K according to equilibrium thermodynamic calculations. Although W gas condenses to W metal at a higher temperature (1885°K at 10^{-3} atm from Grossman, 1973) than WO condenses to WO_2, there is so much more WO that in a slightly non-equilibrium situation, WO_2 would be the expected condensate.

The REE determinations allowed the Ca-Al rich inclusions to be classified according to the scheme of Martin and Mason (1974). A variety of REE patterns were observed:

1) the flat 10-12X chondrites pattern of Group I inclusions. Also included in this group were inclusion A-2 which has a fractionated pattern with depleted Gd to Er and Lu and the inclusion Cl-S2 which has a pronounced Ce depletion (the first such observed); 2) the flat 10X chondrites pattern with depleted Eu and Yb characteristic of Group III; 3) the flat light REE (10-40X chondrites) with highly fractionated heavy REE but with normal Tm enrichments characteristic of Group II inclusions. Groups I and II inclusions are the most common variety so far observed in Allende high Ca-Al inclusions; Group III is relatively uncommon. The equilibrium thermodynamic calculations of Boynton (1975) provide an explanation for the REE pattern shown by Group III inclusions. Thermodyanmics also provide a method for theoretically calculating the REE patterns observed in Group II inclusions.

An important observation concerning the REE patterns is that all the fractionated patterns have nearly equal normalized chondritic ratios for Eu and Yb, and that all the patterns have equal normalized chondritic ratios for Eu and Sr. The similarity of Eu and Sr suggests divalent Eu residing in the same phase as the Sr; the similarity of Eu and Yb also suggests divalent Yb although this is highly unlikely from thermodynamic calculations. Understanding why Eu and Yb are covariant is important in understanding the history and formation of these inclusions.

The inclusion I-8 which was tentatively identified as an olivine aggregate may possess a REE pattern with a true Tm positive anomaly. This strange pattern is difficult to understand and no adequate explanation for it is offered.

The inclusions failed to describe an isochron when age-dating was performed on them (Gray et al., 1973), implying that none have survived from their time of formation in an entirely unaltered state. The alteration was mild however because anomalous Mg and O isotopic ratios have been discovered (Lee and Papanastassiou, 1974; Onuma, 1974) which would have been homogonized in a stress situation.

The data obtained in this work do not show that any one proposed condensation scheme found in the literature is unambiguously the best explanation. However, those proposed by Martin (1976) or Grossman and Ganapathy (1976b) appear to explain best the observed features of the inclusions. There are myriads of information still hidden in these tiny bodies; future analyses of Allende inclusions and inclusions found in other C-3 and C-2 meteorites, particularly using mineral separates, may some day reveal the secrets of their formation.

BIBLIOGRAPHY

Anders, E. 1971. How well do we know cosmic abundances? Geochim. Cosmochim. Acta 35:516-522.

Amiruddin, A. and W.D. Ehman. 1962. Tungsten abundances in meteoritic and terrestrial materials. Geochim. Cosmochim. Acta 26:1011-1026.

Borodin, L.S., and R.L. Barinskii. 1960. Rare earths in perovskites (Knopites) from massifs of ultrabasic alkalic rocks. Geochemistry 4:343-351.

Blander, M. and L.H. Fuchs. 1975. Calcium-aluminum-rich inclusions in the Allende meteorite: Evidence for a liquid origin. Geochim. Cosmochim. Acta 39:1605-1619.

Boynton, W.V. 1975. Fractionation in the solar nebula: Condensation of yttrium and the rare earth elements. Geochim. Cosmochim. Acta 39:569-584.

Boynton, W.V. 1976. In preparation.

Boynton, W.V., R.L. Conard, D.B. Curtis, and R.A. Schmitt. 1976. The precise determination of the fourteen rare-earth elements and barium and strontium by radiochemical neutron activation analysis (in preparation).

Brewer, L. and G.M. Rosenblatt. 1969. Dissociation energies and free energy functions of gaseous monoxides. In Advances in High Temperature Chemistry (Editor, L. Eyring), Vol. II, Academic Press, pp. 1-83.

Cameron, A.G.W. 1968. A new table of abundances of the elements in the solar system. In Origin and Distribution of the Elements (Editor, L.H. Ahrens), Pergamon Press, pp. 125-143.

Chou, C.L., P.A. Baedecker, and J.T. Wasson. 1976. Allende inclusions: Volatile-element distribution and evidence for incomplete volatilization of presolar solids. Geochim. Cosmochim. Acta 40:85-94.

Clarke, R.S. Jr., E. Jarosewich, B. Mason, J. Nelen, M. Gomez, and J.R. Hyde. 1970. The Allende Mexico meteorite shower. Smithson. Contrib. Earth Sci., No. 5.

Clayton, R.N., L. Grossman, and T. Mayeda. 1973. A component of primitive nuclear composition in carbonaceous meteorites. Science 182:485-488.

Conard, R.L., R.A. Schmitt, and W.V. Boynton. 1975. Rare-earth and other elemental abundances in Allende inclusions (abstract). Meteoritics 10:384-387.

Curtis, D.B. 1974. Chemical investigations of minerals from L-6 chondritic meteorites. Ph.D. Thesis. Oregon State University.

Emery, J.F., J.E. Strain, G.D. O'Kelley, and W.S. Lyon. 1969. Non-destructive neutron activation analysis of the Allende meteorite. Radiochem. Radioanal. Let. 1:137-141.

Filby, R.H., A.I. Davis, K.R. Shah, G.G. Wainscott, W.A. Haller and W.A. Cassatt. 1970. Gamma Ray Energy Tables for Neutron Activation Analysis. Washington State University.

Flanagan, F.J. 1973. 1972 values for international geochemical reference samples. Geochim. Cosmochim. Acta 37:1189-1200.

Ganapathy, R. and L. Grossman. 1976. Chemical characteristics of high-temperature condensates (abstract). Lunar Science VII:278-280.

Geilman, W. and W. Gehauhr. 1953. Zur fallung der alkalimetalle als tetraphenylborbindungen. Z. Anal. Chem. 139:161-181.

Gray, C.M., D.A. Papanastassiou, and G.J. Wasserburg. 1973. The identification of early condensates from the solar nebula. Icarus 20:213-239.

Grossman, L. 1972. Condensation in the primitive solar nebula. Geochim. Cosmochim. Acta 36:597-619.

Grossman, L. 1973. Refractory trace elements in Ca-Al-rich inclusions in the Allende meteorite. Geochim. Cosmochim. Acta 37:1119-1140.

Grossman, L. 1974. Chemical fractionation in the solar nebula. In Proceedings of the Soviet-American Conference on the Cosmochemistry of the Moon and Planets, in press.

Grossman, L. 1975. Petrography and mineral chemistry of Ca-rich inclusions in the Allende meteorite. Geochim. Cosmochim. Acta 39:433-454.

Grossman, L. and S.P. Clark, Jr. 1973. High-temperature condensates in chondrites and the environment in which they formed. Geochim. Cosmochim. Acta 37:635-649.

Grossman, L., R.M. Fruland and D.S. McKay. 1975. Scanning electron microscopy of a pink inclusion from the Allende meteorite. Geophys. Res. Lett. 2:37-40.

Grossman, L. and R. Ganapathy. 1976a. Trace elements in the Allende meteorite - 1. Coarse-grained, Ca-rich inclusions. Geochim. Cosmochim. Acta 40:331-344.

Grossman, L. and R. Ganapathy. 1976b. Trace elements in the Allende meteorite - 2. Fine-grained, Ca-rich inclusions. Geochim. Cosmochim. Acta, in press.

Grossman, L. and R. Ganapathy. 1975. Volatile elements and high-temperature condensation (abstract). Lunar Science VI:318-320.

Grossman, L. and J.W. Larimer. 1974. Early chemical history of the solar system. Rev. Geophys. Space Phys. 12:71-101.

Grossman, L. and I.A. Steele. 1976. Amoeboid olivine aggregates in the Allende meteorite. Geochim. Cosmochim. Acta 40:149-155.

Gschneider, K.A., N. Kippenhan and O.D. McMasters. 1973. Thermochemistry of the rare earths. Part I. Rare earth oxides. Report IS-RIC-6, Rare-Earth Information Center, Ames, Iowa.

Handbook of Chemistry and Physics. 1970-1971. Editor: R.C. Weast. Chemical Rubber Company, Cleveland, Ohio.

Handbook of Elemental Abundances in Meteorites. 1971. Editor: B. Mason. Gordon and Breach.

Haskin, L., F. Frey, R.A. Schmitt, and R.H. Smith. 1966. Meteoritic, solar, and terrestrial rare earth distributions. In Physics and Chemistry of the Earth (Editors: L.H. Ahrens, F. Press, S.K. Runcorn and H.C. Urey), Vol. 7, pp. 167-321. Pergamon Press.

Hultgren, R., P.H. Desai, D.T. Hawkins, M. Gleiser, K. Kelley and D.D. Wagman. 1973. Selected Values of the Thermodynamic Properties of the Elements. American Society for Metals, Metals Park, Ohio.

JANAF Thermochemical Tables. 1961 and later. Compiled by the Thermal Research Lab., Dow Chemical Company, Midland, Michigan.

JANAF Thermochemical Tables. 1967. Second Addendum. Compiled by the Thermal Research Lab., Dow Chemical Company, Midland, Michigan.

Keays, R.R., R. Ganapathy, J.C. Laul, U. Krähenbühl and J.W. Morgan. 1974. The simultaneous determination of 20 trace elements in terrestrial, lunar, and meteoritic material by radiochemical neutron activation analysis. Anal. Chim. Acta 72:1-29.

King, E.A. Jr., E. Schonfeld, K.A. Richardson and J.S. Eldridge. 1969. Meteorite fall at Pueblito de Allende, Chihuaha, Mexico: Preliminary information. Science 163:928-929.

Krähenbühl, U., J. Morgan, R. Ganapathy and E. Anders. 1973. Abundance of 17 trace elements in carbonaceous chondrites. Geochim. Cosmochim. Acta 37:1353-1370.

Kurat, G., G. Hoinkes and K. Fredriksson. 1975. Zoned Ca-Al-rich chondrule in Bali: New evidence against the primordial condensation model. Earth Planet. Sci. Lett. 26:140-144.

Larimer, J.W. 1967. Chemical fractionations in meteorites - I. Condensation of the elements. Geochim. Cosmochim. Acta 31:1215-1238.

Laul, J.C. and R.A. Schmitt. 1975. Dunite 72417: A chemical study and interpretation. Proc. 6th Lunar Sci. Conf., Geochim. Cosmochim. Acta Suppl. 6:1321-1354.

Lee, T. and D.A. Papanastassiou. 1974. Mg isotopic anomalies in the Allende meteorite and correlation with O and Sr effects. Geophys. Res. Lett. 1:225-228.

Lord, H.C. III. 1965. Molecular equilibria and condensation in a solar nebula and cool stellar atmospheres. Icarus 4:279-288.

Lugmair, G.W. 1974. Sm-Nd ages: A new dating method (abstract). Meteoritics 9:369.

Lugmair, G.W., N.B. Scheinen and K. Marti. 1975. Sm-Nd age of Apollo 17 basalt 75075: Two-stage igneous processes in mare basalt genesis (abstract). Lunar Science VI:531-533.

Martin, P.M. 1976. The formation of Allende inclusions. Preprint.

Martin, P. and B. Mason. 1974. Major and trace elements in the Allende meteorite. Nature 249:333-334.

Marvin, U.B., J.A. Wood and J.S. Dickey, Jr. 1970. Ca-Al rich phases in the Allende meteorite. Earth Planet. Sci. Lett. 7:346-350.

Mason, B. and L.G. Berry. 1968. Elements of Mineralogy, W.H. Freeman and Company, pp. 77-82, 281.

Mason, B. and P. Martin. 1974. Minor and trace element distribution in melilite and pyroxene from the Allende meteorite. Earth Planet. Sci. Lett. 22:141-144.

Masuda, A., N. Nakamura and T. Tanaka. 1973. Fine structures of mutually normalized rare earth patterns of chondrites. Geochim. Cosmochim. Acta 37:239-248.

Morgan, J.W., T.V. Rebagay, D.L. Showalter, R.A. Nadkarni, D.E. Gillum, D.M. McKoan, and W.D. Ehmann. 1969. Allende meteorite: Some major and trace element abundances by neutron activation analysis. Nature 224:789-791.

Nagasawa, H. 1971. Partitioning of Eu and Sr between coexisting plagioclase and K-feldspar. Earth Planet. Sci. Lett. 13:139-144.

Nagasawa, H., D.P. Blanchard, J.A. Philpotts and N. Onuma. 1976. Trace element distribution in mineral separates of the Allende inclusions and their genetic implications. Preprint.

Nakamura, N. 1974. Determination of REE, Ba, Fe, Mg, Na and K in carbonaceous and ordinary chondrites. Geochim. Cosmochim. Acta 38:757-775.

Onuma, N., T. Tanaka and A. Masuda. 1974. Rare-earth abundances in two mineral separates with distinct oxygen isotopic composition from an Allende inclusion (abstract). Meteoritics 9:387-388.

Schmitt, R.A., R.H. Smith and D.A. Olehy. 1964. Rare-earth, yttrium, and scandium abundances in meteorite and terrestrial matter. II. Geochim. Cosmochim. Acta 28:67.

Schnetzler, C.C. and J.A. Philpotts. 1968. Partition coefficients of rare-earth elements and barium between igneous matrix material and rock-forming-mineral phenocrysts - I. In Origin and Distribution of the Elements (editor: L.H. Ahrens), pp. 928-938. Pergamon Press.

Seitz, M.G. and I. Kushiro. 1974. Melting relations of the Allende meteorite. Science 183:954-957.

Showalter, D.L., H. Wakita, R.H. Smith and R.A. Schmitt. 1971. Abundance of the 14 REE and 12 other major, minor and trace elements in Allende Meteorite Reference Material (AMRM). Submitted to Smithson. Contrib. Earth Sci.

Tanaka, T. and A. Masuda. 1973. Rare-earth elements in matrix, inclusions, and chondrules of the Allende meteorite. Icarus 19:523-530.

Tanaka, T., N. Nakamura, A. Masuda and N. Onuma. 1975. Giant olivine chondrule as a possible later-stage product in the nebula. Nature 256:27-28.

Wakita, H., and R.A. Schmitt. 1970. Rare-earth and other elemental abundances in the Allende meteorite. Nature 227:478-479.

Wakita, H., R.A. Schmitt and P. Rey. 1970. Elemental abundances of major, minor and trace elements in Apollo 11 lunar rocks, soil and core samples. In Proc. Apollo 11 Lunar Sci. Conf. Geochim. Cosmochim. Acta Suppl. I:1685-1664, Pergamon.

Wakita, H. and D. Zellmer. 1970. Unpublished work.

Wänke, H., H. Baddenhausen, H. Palme and B. Spettel. 1974. On the chemistry of the Allende inclusions and their origin as high temperature condensates. Earth Planet. Sci. Lett. 23:1-7.

Wark, D.A. and J.F. Lovering. 1976. Refractory/Platinum metal grains in Allende calcium-aluminum-rich clasts (CARC's): Possible exotic-pre-solar material? (abstract). Lunar Science VII:912-914.

Whittaker, E.J.W. and R. Muntus. 1970. Ionic radii for use in geochemistry. Geochim. Cosmochim. Acta 34: 945-956.

APPENDIX

RADIOCHEMICAL PROCEDURE

The radiochemical procedure developed by Boynton et al. (1976) allows for the separation of K, Ba, and Sr individually and the REE as a group. The method of Laul and Schmitt (1975) was used for K determinations. The basic procedure is outlined in Appendix Figure 1. Details of the chemistry are as follows.

Carriers and REE Standard

As in most basic radiochemical procedures, inactive carriers (mg quantities of the elements of interest) are added to the sample before separations are carried out. The carriers are pipetted into nickel crucibles and dried prior to the radiochemical analysis. A list of the carriers used here is provided in Appendix Table 1.

The mixed REE carrier was designed by W.V. Boynton in order to minimize error in yield determinations via reactivation. Thus, only a small concentration of elements with very large cross sections and short half lives (ex. Eu and Dy) are used. The natural abundances of Nd and Yb contain only about five percent ^{148}Nd and thirteen percent ^{176}Yb. To enhance the counting statistics for ^{149}Nd and ^{177}Yb, enriched Nd (95.44 percent ^{148}Nd) and Yb (96.43 percent ^{176}Yb) are added to the carrier solution. (Enriched isotopes were obtained from the Oak Ridge National Laboratory.) To

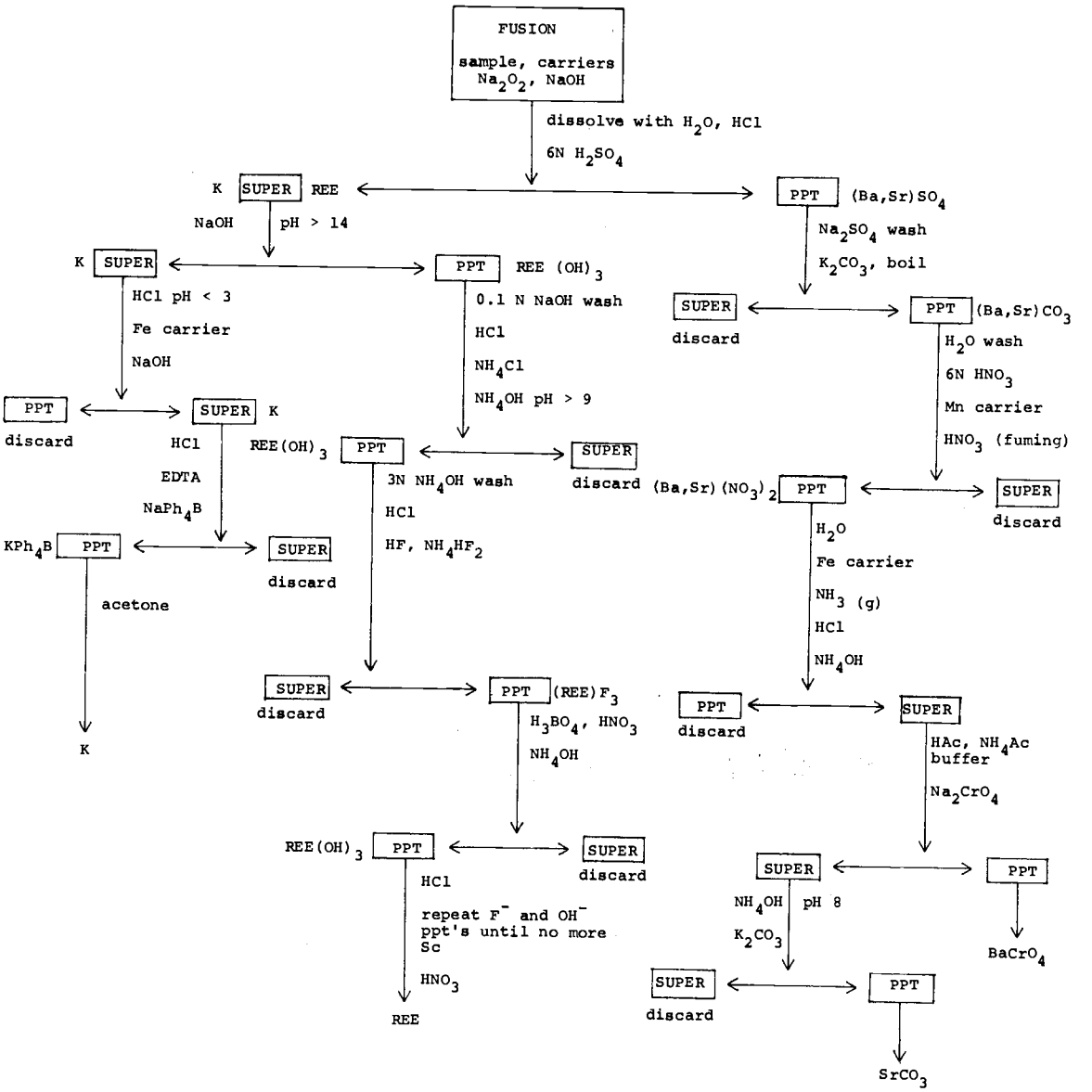

Appendix Figure 1. Flow chart for the RNAA of REE, Ba, Sr, and K.

Appendix Table 1. Inactive carrier solutions used for RNAA.

Element	Amount	Concentration (mg/ml)
Ba	5 ml	10 mg Ba
Sr	5 ml	10 mg Sr
K, Rb, Cs (Mixed)	1 ml	5 mg K
		2 mg Rb, Cs
		0.002 μc ^{137}Cs
REE (Mixed)	4 ml	4 mg La
		4 mg Ce
		4 mg Nd + 0.5 mg ^{148}Nd
		0.1 mg ^{152}Sm
		0.04 mg Eu
		0.4 mg Tb
		0.05 mg Dy
		2 mg Ho
		0.5 mg Er
		1 mg Tm
		1 mg Yb + 1 mg ^{176}Yb
		0.5 mg Lu

reduce the contribution of 23.5 m ^{155}Sm (E_γ = 104 keV) to the peak of 46.8 h ^{153}Sm (E_γ = 103.3 keV) an enriched Sm isotope (^{152}Sm = 98.29 percent) is used instead of the natural Sm. A suggestion for future preparation of the carrier solution is to double the Er concentration from 0.5 mg/ml to 1.0 mg/ml to improve the counting statistics for that element.

The mixed REE standard (also designed by W.V. Boynton) has the individual elements present in approximately chondritic ratios (Appendix Table 2). Thus, its usefulness is maximized for chondritic REE patterns because both samples and standards will have nearly the same backgrounds.

Fusion

Samples and carriers (Appendix Table 1) are heated in a Ni crucible with about 8 g Na_2O_2 and 8-10 pellets of NaOH until completely molten. The crucibles should be dull red in color and the molten state should be maintained about three minutes to yield a good fusion. After about five minutes cooling, the melt is broken up with water and the crucibles rinsed with concentrated HCl to give a final volume of about 150 ml in a 400 ml beaker. Enough acid is added to completely dissolve the fusion melt (clear green solution).

Appendix Table 2. Concentration of individual REE in mixed REE standard (in 2N HNO_3).

Element	Concentration (µg/g)
La	6.20
Ce	18.9
Pr	2.66
Nd	10.3
Sm	3.17
Eu	0.782
Gd	4.64
Tb	0.94
Dy	4.69
Ho	1.86
Er	4.65
Tm	0.627
Yb	3.95
Lu	0.644

Barium and Strontium

An excess of 6M H_2SO_4 is used to precipitate Ba and Sr from the rest of the sample. The supernate is saved for K and REE chemistry. The precipitate should age about 15 minutes before pouring off the supernate to facilitate coagulation and increase the Ba-Sr yield. (Do not cool in an ice bath. If the sulfate cools too fast, an extremely fine white crystalline precipitate forms that is very difficult to centrifuge.) The sulfate precipitate is then washed with 1M Na_2SO_4 and then boiled with 40 ml of 50 percent K_2CO_3 for 10 or 15 minutes. The carbonate precipitate is washed twice with water, dissolved in a minimum of 6N HNO_3 and H_2O, and ten mg Mn holdback carrier is added. Barium and Sr are then precipitated as nitrates with fuming HNO_3. Allow the precipitate about ten minutes of aging time in an ice bath. The precipitate is dissolved in water (about 20 ml), 10 mg of Fe holdback carrier is added and $Fe(OH)_3$ is precipitated by bubbling in NH_3 gas. The precipitate is just dissolved with HCl and then just reprecipitated with 3N NH_4OH. After centrifuging, the supernate should be a clear to pale orange color. To the supernate add 6N ammonium acetate and 6N acetic acid in 2:1 ratio (about six ml total). The solution pH is about four. Add 1 ml of 1.5 M Na_2CrO_4, then heat for a few minutes to coagulate $Ba(CrO_4)$. The precipitate is washed with water, dissolved

in HNO_3, and transferred and sealed in a half dram polyvial for counting. The supernate from the preceding step is made basic (orange to yellow) with NH_4OH (pH = 7-8), 2 ml of 50 percent K_2CO_3 is added. Heat to precipitate $SrCO_3$. The $SrCO_3$ is washed with water, dissolved in HNO_3, transferred and sealed in a half dram polyvial for counting. Barium and Sr are counted using a 7.5 cm x 7.5 cm NaI(Tl) well detector. The 388-keV gamma ray of ^{87m}Sr ($t_{1/2}$ = 170 m) and the 166-keV gamma ray of ^{139}Ba ($t_{1/2}$ = 82.9 minutes) are used for determining activities. In some cases the 515-keV gamma ray of ^{85}Sr ($t_{1/2}$ = 64.0 d) and the 124.2 or 133.7 keV gamma ray of ^{131}Ba ($t_{1/2}$ = 12.0 d) can be counted. When this is done, it is best to use a Ge(Li) detector for the Ba counting because the NaI(Tl) will not resolve the various gamma ray energies of ^{131}Ba.

Rare Earth Elements

The supernate from the sulfate precipitation is brought to pH > 14 using NaOH pellets and 10N NaOH which causes the $REE(OH)_3$ to precipitate. The supernate is saved for K chemistry. The hydroxides are washed with 0.1N NaOH, dissolved in HCl and reprecipitated with NH_4OH (pH > 9, dark blue solution) to complex the Ni contributed by the crucibles. (If the NH_4OH precipitation is not sufficiently basic, not all the Ni will be complexed and the step may have to be repeated. An indication that this is

necessary is the presence of a green precipitate after the solution has been centrifuged and the supernate has been poured off.) The hydroxide is then washed with 3N NH_4OH; the wash solution should be very pale blue to clear in color. The final hydroxide precipitate (brown in color) is dissolved in a minimum amount of HCl and the REE are precipitated as fluorides with 2-3 drops of HF and about 1 ml of hot saturated NH_4HF_2 (prepared fresh). The fluorides are dissolved with 1 ml H_3BO_3 and one-half ml HNO_3, diluted to about 15 ml with water, and reprecipitated as $REE(OH)_3$ with NH_4OH. The $REE(OH)_3$ are dissolved in a minimum of HCl, diluted to about 15 ml with water, and again precipitated as the fluorides. The fluoride steps must be repeated until most of the Sc is removed. Scandium removal is aided if the solution is kept around pH 3-4 during the fluoride precipitation step. Scandium removal is checked with a Ge(Li) detector; usually six fluorides or fewer will be sufficient, depending upon the ratio of Sc to the REE. The final $REE(OH)_3$ precipitate is washed twice with water to insure that all boron is removed, dissolved with minimum HNO_3, diluted to 1 ml with water, and sealed in a half dram polyvial for counting. The REE are then counted as a group by using a high-resolution Ge(Li) detector as discussed in the experimental section. Table 6, page 22, lists the counting sequences and the REE that are calculated from each count.

Potassium

The supernate from the NaOH precipitation is acidified with HCl; methyl orange indicator and 10 mg Fe holdback carrier are added. Iron hydroxide is then precipitated with NaOH. The supernate is neutralized with HCl and acetic acid (blue to yellow) and adjusted to pH = 1. To complex interferents, 0.5 g of EDTA is added. An excess of solid sodium tetraphenylborate is used to precipitate K; an ice bath is used for better yields and to coagulate the precipitate. The K-tetraphenylborate compound is filtered, washed with water to remove Na and dissolved in acetone. (The wash solution should be a tetraphenylborate solution rather than pure water.) The K solution is placed in a two dram polyvial for counting. Care must be taken during this procedure not to contaminate the K solution with NH_4^+ since NH_4^+ will also precipitate with Na-tetraphenylborate. Potassium is then counted on a Ge(Li) detector, using the 1525-keV gamma ray of ^{42}K ($t_{½}$ = 12.4 h) for determining activities. In some cases, it is also possible to count for Rb and Cs after the K has decayed away. The Rb and Cs radionuclides measured are 18.6 d ^{86}Rb (E_γ = 1078 keV) and 2.05 y ^{134}Cs (E_γ = 605 keV).

Yields

The K yield is obtained from the ^{137}Cs tracer contained in the alkali carrier solution. Barium, Sr, and the REE yields are determined by reactivation by using comparators made up by pipetting 1 ml each of the carrier solutions used in the RNAA. For Ba and Sr the yield is determined by again counting ^{87m}Sr and ^{139}Ba on a NaI(Tl) detector after an activiation of two minutes at a flux of 1 x 10^{12} $n/cm^2/sec$ (100 KW in the OSU TRIGA Reactor rabbit terminal). Yields for the REE are determined from the radionuclides listed in Table 6, page 22. The activation for REE yields is a two minute irradiation at a flux of 5 x 10^{12} $n/cm^2/sec$ (500 KW in the OSU TRIGA Reactor rabbit terminal). Usually the overall REE yield curve is flat, when this is the case Ce can be interpolated between La and Nd and only one count is necessary. When the light REE are depleted, i.e. fractionated relative to the heavy REE, then Ce should be counted because the depletion from La to Sm is not a smooth function of ionic radii. Yields for Pr, Gd, Tb, and Tm are determined by interpolation although Tb and Tm could be counted in a very late count.